

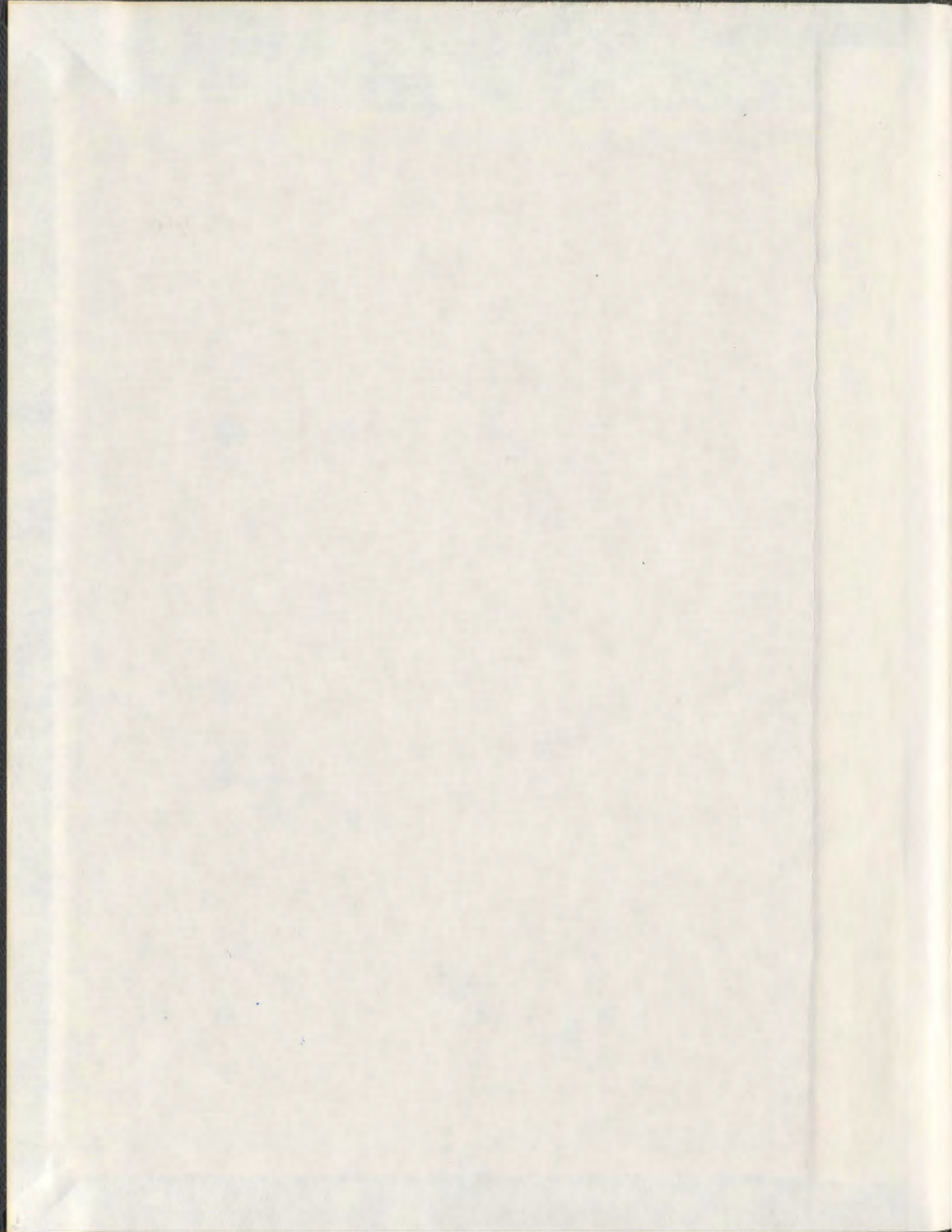
IMPROVEMENT AND INVESTIGATION OF SAMPLE
PREPARATION FOR MATRIX-ASSISTED LASER
DESORPTION/IONIZATION OF PROTEINS

CENTRE FOR NEWFOUNDLAND STUDIES

TOTAL OF 10 PAGES ONLY
MAY BE XEROXED

(Without Author's Permission)

FAN XIANG



001311



INFORMATION TO USERS

This manuscript has been reproduced from the microfilm master. UMI films the text directly from the original or copy submitted. Thus, some thesis and dissertation copies are in typewriter face, while others may be from any type of computer printer.

The quality of this reproduction is dependent upon the quality of the copy submitted. Broken or indistinct print, colored or poor quality illustrations and photographs, print bleedthrough, substandard margins, and improper alignment can adversely affect reproduction.

In the unlikely event that the author did not send UMI a complete manuscript and there are missing pages, these will be noted. Also, if unauthorized copyright material had to be removed, a note will indicate the deletion.

Oversize materials (e.g., maps, drawings, charts) are reproduced by sectioning the original, beginning at the upper left-hand corner and continuing from left to right in equal sections with small overlaps. Each original is also photographed in one exposure and is included in reduced form at the back of the book.

Photographs included in the original manuscript have been reproduced xerographically in this copy. Higher quality 6" x 9" black and white photographic prints are available for any photographs or illustrations appearing in this copy for an additional charge. Contact UMI directly to order.

UMI

**A Bell & Howell Information Company
300 North Zeeb Road, Ann Arbor, MI 48106-1346 USA
313:761-4700 800:521-0600**

**IMPROVEMENT AND INVESTIGATION OF SAMPLE
PREPARATION FOR MATRIX-ASSISTED LASER
DESORPTION/IONIZATION OF PROTEINS**

By

©Fan Xiang

M. Sc., Memorial University of Newfoundland

**A THESIS SUBMITTED TO THE SCHOOL OF GRADUATE
STUDIES IN PARTIAL FULFILMENT OF THE
REQUIREMENTS FOR THE DEGREE OF
DOCTOR OF PHILOSOPHY**

**DEPARTMENT OF PHYSICS & PHYSICAL OCEANOGRAPHY
MEMORIAL UNIVERSITY OF NEWFOUNDLAND**

JUNE, 1997

ST. JOHN'S

NEWFOUNDLAND

Abstract

Since the introduction of Matrix-Assisted Laser Desorption and Ionization (MALDI) in 1988 the application of MALDI mass spectrometry has become a vital research field. The method of analyte/matrix preparation plays a central role for achieving optimal performance in MALDI.

In the first part of this work, a new method of preparing the samples to increase contaminant tolerance is described. While the solvent composition and matrices used in the “dried droplet” method have changed since MALDI was introduced, there has been little fundamental change in this protocol. The “dried droplet” method for MALDI MS is a simple one step process, but high concentrations of nonvolatile liquid, such as glycerol, urea, DMSO and other protein stabilizers, can reduce or eliminate the intensity of protein ion signals. Instead of using the one step process, we developed a three step process. The examples presented in this part of this thesis illustrate how analyses were improved as a result of the new sample preparation procedure. The sample films produced by the new method adhere firmly to the substrate, allowing easier washing of the film compared to the dried-droplet deposits. The films were more uniform than dried-droplet deposits with respect to ion production. The presence of non-proteinaceous material at high concentrations in the solution did not seriously affect ion production from these films.

The basic difference between laser desorption/ionization and matrix-assisted laser desorption/ionization is that the laser radiation is directly absorbed by the analyte in the former case, while the matrix dominates energy absorption and the formation

of ions in the latter. In the second part of this work, the influence of matrix concentration on analyte ion yield and the mass resolution of the molecular ion signals were investigated. MALDI time-of-flight mass spectra of protein mixed at different concentrations in each of gentisic acid, *trans*- α -cyano-4-hydroxycinnamic acid and sinapic acid matrices, were obtained. The results showed that the intensities of the analyte ion peaks increase gradually with an increase in concentration of matrix in solution and then decrease slightly as the matrix concentration continues to increase. The analysis of the spectra also showed that the molecular ion peaks are broadened, and the mass resolution decreases, as the matrix concentration increases. A proposed interpretation of these results is given based on two categories of matrix concentration effects: a physical effect involving energy deposition and redistribution processes, and a chemical effect involving co-crystallization of the matrix and analyte followed by photochemical ionization.

Poor crystallization of a MALDI sample has a negative effect on its ability to generate ions. In the last part of this work a strategy was demonstrated to alleviate this problem. Certain amounts of impurities (or additives), present in solution during crystallization, have a pronounced effect on the crystallization process, in particular on the morphology of the deposited crystals. The technique of controlling crystal growth by additives was also discussed. The crystallization of gentisic acid mixed with its isomers and other benzoic acid derivatives was then investigated. The performance of the resulting crystals in MALDI MS was evaluated. The results showed that the admixture of gentisic acid with 2,3-dihydroxybenzoic acid or 3-amino-2,5,6-trifluorobenzoic acid homogenized the crystal morphology, and consequently improved the MALDI MS performance.

Acknowledgments

It is my great pleasure to thank all those who have contributed to this dissertation. I wish to thank Dr. R. C. Beavis for offering the right amount of supervision at the right time. Thanks are also due to Dr. M. Morrow and Dr. R. Helleur for their participation in my Supervisory Committee. I am grateful to Dr. J. de Bruyn for his remarkable service as Graduate Officer in the Department of Physics.

This work has been funded by the Natural Science and Engineering Research Council of Canada (NSERC) through grants awarded to Dr. R. C. Beavis. Financial assistance from the School of Graduate Studies and the Department of Physics, in the form of Graduate Fellowship and Teaching Assistantship, is also acknowledged.

Particularly, I would like to sincerely take this opportunity of acknowledging my indebtedness to my wife, Liya, for the valuable assistance and encouragement she gave me during the preparation of this work, and my son, Junyang, for his understanding and patience over the last three years when I tried to explain “M A L D I” to him.

Table of Contents

Abstract	i
Acknowledgments	iii
List of Tables	vi
List of Figures	xiv
1 Introduction	1
1.1 Development of Desorption Methods	1
1.2 Previous Work on MALDI	5
1.3 Summary of This Work	9
2 Experimental Apparatus	12
2.1 Laser Ion Source and TOF Instrument	12
2.2 Ion Detection	18
3 Polycrystalline Film Method of Sample Preparation	20
3.1 Conventional Method of Sample Preparation and its Disadvantages .	20
3.2 New Method of Sample Preparation	24
3.3 Experimental Results	27
3.4 Discussion	36
4 Effects on MALDI Performance of Protein/Matrix Molar Ratio	40
4.1 Phenomenological Description of Laser-Induced Thermal Desorption .	40

4.2	Experiment and Results	46
4.3	Discussion	59
5	Influence of Matrix Additives on MALDI	63
5.1	Influence of Additives on the Growth of a Crystal	63
5.2	Experimental and Results	68
5.3	Discussion	87
6	Summary	100
	Bibliography	104
	Appendix	114

List of Tables

4.1	Summary of matrix solution concentrations	48
5.1	List of additives used in the experiment	70
5.2	The crystal data for 2,4DHB and 2,5DHB	72
5.3	Properties of UV absorption of dihydroxybenzoic acids	99

List of Figures

2.1	Principle of time of flight mass spectrometry.	13
2.2	Instrumental arrangement.	14
2.3	The ion source assembly.	15
2.4	Fresnel reflection attenuator.	17
3.1	Flowchart showing the dried-droplet method of sample preparation. .	22
3.2	Flowchart showing the polycrystalline film method of sample preparation.	25
3.3	Photomicrographs (magnification: 250x) showing the three stages of preparation of a polycrystalline film of sinapic acid. (a) The dried droplet deposit formed using Solution A. (b) The same deposit after smearing with a glass microscope slide. (c) The same deposit after growing a film using a Solution B consisting of 2:1 (water):(acetonitrile) saturated with sinapic acid.	29
3.4	A scanning electron micrograph (magnification: $10^4\times$) of an 4-HCCA polycrystalline film. The scale is indicated on the micrograph. Solution B was 2:1 (aqueous 0.1% trifluoroacetic acid):(acetonitrile)(v/v) saturated with the matrix.	30

- 3.5 A laser desorption TOF mass spectrum of horse skeletal muscle myoglobin (mol. mass = 16951 u) taken from an 4-HCCA polycrystalline film. The singly and doubly charged ion species are shown. Solution B was 2:1 (aqueous 0.1 % trifluoroacetic acid):(acetonitrile)(v/v) containing 0.5 μ M myoglobin. This spectrum represents the sum of transients recorded for 30 consecutive laser shots. 31
- 3.6 A laser desorption TOF mass spectrum of horse skeletal muscle myoglobin (mol. mass = 16951 u) taken from an 4-HCCA polycrystalline film. The singly and doubly charged ion species are shown. Solution B was 5:3:2 (aqueous 0.1 % trifluoroacetic acid):(acetonitrile):(glycerol) (v/v/v) containing 0.5 μ M myoglobin. This spectrum represents the sum of transients recorded for 30 consecutive laser shots. 33
- 3.7 A laser desorption TOF mass spectrum of horse skeletal muscle myoglobin (mol. mass = 16951 u) taken from an 4-HCCA polycrystalline film. The singly and doubly charged ion species are shown. Solution B was 2:1 (aqueous 6 M urea):(acetonitrile)(v/v) containing 1.0 μ M myoglobin. This spectrum represents the sum of transients recorded for 30 consecutive laser shots. 34
- 3.8 A laser desorption TOF mass spectrum of horse skeletal muscle myoglobin (mol. mass = 16951 u) taken from an 4-HCCA polycrystalline film. The singly and doubly charged ion species are shown. Solution B was 2:1 (1 M NaCl):(acetonitrile)(v/v) containing 0.5 μ M myoglobin. This spectrum represents the sum of transients recorded for 30 consecutive laser shots. 35

4.1	The positive ion TOF mass spectra of horse skeletal muscle myoglobin (mol. mass = 16951 u) in solutions of 2,5DHB matrix of different concentration at fixed laser power. The amount of myoglobin in each sample was approximately 5 pmol. The singly and doubly charged ion species are shown. Each spectrum represents the sum of transients recorded for 20 consecutive laser shots.	50
4.2	The positive ion TOF mass spectra of horse skeletal muscle myoglobin (mol. mass = 16951 u) in solutions of 4HCCA matrix of different concentration at fixed laser power. The amount of myoglobin in each sample was approximately 5 pmol. The singly and doubly charged ion species are shown. Each spectrum represents the sum of transients recorded for 20 consecutive laser shots.	51
4.3	The positive ion TOF mass spectra of horse skeletal muscle myoglobin (mol. mass = 16951 u) in solutions of sinapinic acid matrix of different concentration at fixed laser power. The amount of myoglobin in each sample was approximately 5 pmol. The singly and doubly charged ion species are shown. Each spectrum represents the sum of transients recorded for 20 consecutive laser shots.	52
4.4	Plots of the ion yield of myoglobin versus the 2,5DHB to myoglobin molar ratio for singly (a) and doubly (b) charged molecular ions. The amount of myoglobin in each sample was fixed at approximately 5 pmol.	53
4.5	Plots of the ion yield of myoglobin versus the 4HCCA to myoglobin molar ratio for singly (a) and doubly (b) charged molecular ions. The amount of myoglobin in each sample was fixed at approximately 5 pmol.	54

4.6	Plots of the ion yield of myoglobin versus the sinapinic acid to myoglobin molar ratio for singly (a) and doubly (b) charged molecular ions. The amount of myoglobin in each sample was fixed at approximately 5 pmol.	55
4.7	Plots of the measured peak widths (FWHM) versus molar ratio of 2,5DHB to myoglobin for singly (a) and doubly (b) charged molecular ions. Spectra were obtained from 6-9 spots on each of the samples, then peak widths (FWHM) were measured for each of the spectra, and averaged.	56
4.8	Plots of the measured peak widths (FWHM) versus molar ratio of 4HCCA to myoglobin for singly (a) and doubly (b) charged molecular ions. Spectra were obtained from 6-9 spots on each of the samples, then peak widths (FWHM) were measured for each of the spectra, and averaged.	57
4.9	Plots of the measured peak widths (FWHM) versus molar ratio of sinapinic acid to myoglobin for singly (a) and doubly (b) charged molecular ions. Spectra were obtained from 6-9 spots on each of the samples, then peak widths (FWHM) were measured for each of the spectra, and averaged.	58
5.1	Molecular packing in benzamide as viewed along the a axis.	66
5.2	Chain formed by the hydrogen-bonds of benzamide. An additive benzoic acid molecule, which replaces a benzamide molecule, is shown. .	67

5.3	Photomicrograph showing crystals of 2,5-DHB prepared by dried droplet method at concentration of 10g/L. (a) Rim with crystal needles protruding towards the centre of the deposit (magnification: 85x) (b) Thin crystals in central region (magnification: 730x).	69
5.4	Photo microscope image demonstrating the crystal type of 2,3-DHB prepared by dried droplet method at a concentration of 10g/L (magnification: 85x).	73
5.5	Photo microscope image demonstrating the crystal type of 2,4-DHB prepared by dried droplet method at a concentration of 10g/L (magnification:85x).	74
5.6	Photo microscope image demonstrating the crystal type of 2,6-DHB prepared by dried droplet method at a concentration of 10g/L (magnification:85x).	75
5.7	Photomicrograph showing crystals of 3,4-DHB prepared by dried droplet method at a concentration of 10g/L. (a) Rim with crystal needles protruding towards the centre of the deposit (magnification: 85x) (b) Thin polycrystalline in central region (magnification: 730x).	76
5.8	Photomicrograph showing crystals of 3,5-DHB prepared by dried droplet method at a concentration of 10g/L. (a) Rim with crystal needles protruding towards the centre of the deposit (magnification: 85x) (b) Thin polycrystalline in central region (magnification: 730x).	77
5.9	Photomicrograph showing crystals of 2,3-DHB:2,5-DHB mixed in 1:1 (v:v) ratio, prepared by dried droplet method, (a) magnification: 55x, (b) magnification: 500x; (c) photo microscope image of crystals of 4HCCA with the same magnification as in (b), for comparison.	78

5.10	Photomicrograph showing crystals of 2,6-DHB:2,5-DHB mixed in 1:1 (v:v), prepared by dried droplet method, (a) magnification: 85x, (b) magnification: 730x.	79
5.11	Photomicrograph showing crystals of 2,4-DHB:2,5-DHB mixed in 1:1 (v:v), prepared by dried droplet method, (a) magnification: 85x, (b) magnification: 730x.	80
5.12	Photomicrograph showing crystals of 3,4-DHB:2,5-DHB mixed in 1:1 (v:v), prepared by dried droplet method, (a) magnification: 85x, (b) magnification: 730x.	81
5.13	Photomicrograph showing crystals of 3,5-DHB:2,5-DHB mixed in 1:1 (v:v), prepared by dried droplet method, (a) magnification: 85x, (b) magnification: 730x.	82
5.14	A laser desorption TOF mass spectrum of horse skeletal muscle myoglobin (mol. mass = 16951 u) taken from 2,3-DHB:2,5-DHB. The singly and doubly charged ion species are shown. Sample solution was prepared as a mixture of 1:10 (v:v), 10 μ M myoglobin:co-matrix at 10g/L. 1 μ L of sample solution was dropped on the probe tip. This spectrum represents the sum of transients recorded for 20 consecutive laser shots.	84
5.15	Laser desorption TOF mass spectra of bovine insulin(mol. mass = 5733.5 u) taken from (a) 2,3-DHB:2,5-DHB, (b) neat 2,5-DHB. The matrix adduct peak of the singly charged molecular ion is apparent for neat 2,5-DHB.	85

5.16	A laser desorption TOF mass spectrum of horse skeletal muscle myoglobin (mol. mass = 16951 u) taken from 2,3-DHB:2,5-DHB. The singly and doubly charged ion species are shown. Sample solution was prepared as a mixture of 1:20 (v:v), 10 μ M myoglobin:co-matrix at 10g/L. 1 μ L of sample solution was dropped on the probe tip. Amount of myoglobin in dried sample was 0.5 picomole. This spectrum represents the sum of transients recorded for 20 consecutive laser shots.	86
5.17	A laser desorption TOF mass spectrum of horse skeletal muscle myoglobin (mol. mass = 16951 u) taken from the rim of a 2,4-DHB:2,5-DHB deposit. The singly and doubly charged ion species are shown. Sample solution was prepared as a mixture of 1:10 (v:v), 10 μ M myoglobin:co-matrix at 10g/L. 1 μ L of sample solution was dropped on the probe tip. This spectrum represents the sum of transients recorded for 20 consecutive laser shots.	88
5.18	A laser desorption TOF mass spectrum of horse skeletal muscle myoglobin (mol. mass = 16951 u) taken from the rim of a 2,6-DHB:2,5-DHB deposit. The singly and doubly charged ion species are shown. Sample solution was prepared as a mixture of 1:10 (v:v), 10 μ M myoglobin:co-matrix at 10g/L. 1 μ L of sample solution was dropped on the probe tip. This spectrum represents the sum of transients recorded for 20 consecutive laser shots.	89
5.19	Photo microscope image demonstrating the crystal type of 4A3MB prepared by the dried droplet method at a concentration of 10g/L (magnification: 85x).	90

5.20	Photo microscope image demonstrating the crystal type of 4ATFB prepared by the dried droplet method at a concentration of 10g/L (magnification: 85x).	91
5.21	Photo microscope image demonstrating the crystal type of 4A3MB:2,5-DHB prepared by the dried droplet method at a concentration of 10g/L (magnification: 85x).	92
5.22	Photomicrographs showing crystals of 3ATFB:2,5-DHB (v:v), v=solution volume, mixed at different ratios. (a) 1:5, (b) 2:5, (c) 3:5, (d) 4:5, (e) 5:5 (magnification: 55x) and (f) 5:5 (magnification: 500x).	93
5.23	A laser desorption TOF mass spectrum of horse skeletal muscle myoglobin (mol. mass = 16951 u) taken from the mixture of 3ATFB:2,5-DHB at 5:5 ratio. The singly, doubly and triply charged ion species are shown. Sample solution was prepared as a mixture of 1:10 (v:v), 10 μ M myoglobin:co-matrix at 10g/L. 0.5 μ L of sample solution was dropped on the probe tip. This spectrum represents the sum of transients recorded for 10 consecutive laser shots.	94
5.24	Projection of 2,5-DHB crystal structure, showing dimers stacked along b axis.	97
6.1	Transmission of light through a microscope cover-slip.	115
6.2	Plot of transmittance versus incident angle for TE wave.	118
6.3	Plot of transmittance versus incident angle for TM wave.	119

Chapter 1

Introduction

In this chapter a short overview describing recent developments of desorption methods in mass spectrometry is given. In particular, research related to Matrix-Assisted Laser Desorption and Ionization (MALDI) is discussed. Then a summary of the present work is given.

1.1 Development of Desorption Methods

Mass spectral analysis is one of the most powerful analytical methods characterized by both high sensitivity and high information content. Mass spectrometry provides information to the analytical chemist concerning atomic composition and molecular structure of an unknown compound, or the concentration of a target analyte present in complex matrices. Mass spectrometry also continues to provide a valuable experimental approach for physical and physical-organic chemists interested in the energetics of gaseous ions and their interactions with neutral molecules, surfaces, electromagnetic radiation, etc. Formerly, samples for a mass spectrometer had to be supplied in the gas phase to allow ionization to take place. Several options are possible. In the easiest case, the sample is a gas or has sufficient vapour pressure at room temperature. Thermally stable samples can be heated and evaporated in the vacuum of the mass spectrometer's ion source. With the growing demand for the

detection and structure determination of ever larger and more complex molecules in biochemical analysis, conventional desorption and ionization methods in mass spectrometry exhibit increasing difficulties with these larger molecules because of the involatility and instability of such materials.

The first significant improvement in MS ion sources for large molecules was the discovery of Plasma Desorption Mass Spectrometry (PDMS) by Torgerson and Macfarlane [1]. In a PDMS ion source, a sample is deposited on a thin metal foil. A 10 μCi ^{252}Cf source is placed behind the sample foil. In each fission event, two collinear fission fragments with an energy of 80 to 120 MeV are created. One fragment hits the start detector and triggers the measurement, whereas the other penetrates the sample and causes desorption of a number of secondary ions. These ions could then be accelerated away from the surface and analyzed in a mass spectrometer. The simplicity, tolerance towards impurities, and sensitivity, made PDMS ideal for biopolymer analysis during the 1980's. However, the method was limited to a mass range of up to 45,000. this fact stimulated further exploration of desorption methods.

In the early 1980's fast atom bombardment mass spectrometry (FABMS), an offspring of secondary ion mass spectrometry (SIMS) with special sample preparation, was introduced by Barber et al [2]. As in PDMS, desorption/ionization of non-volatile biopolymers in FABMS is induced by primary particle impact. A focused beam of neutral atoms (Xe, Ar in 6 - 10 keV) was used in early experiments [3], and ions (Cs^+ up to 40 keV) were used in later developments [4]. Unlike in PDMS, stable ion currents lasting for minutes could be produced, but the use of a liquid matrix, such as a mixture of glycerol, water and an acid, is essential. An advantage of the liquid matrix is that analyte molecules at the surface are continually replenished from the interior of the sample droplet by diffusion and convection. Broad applicability to a wide variety of compounds of biochemical interest ($m/z < 25,000$ [5]), as well as facile

integration of the FAB ion source into common sector and quadrupole instruments, led to the great popularity of the ion source in many laboratories during the 1980's and early 1990's [6]. Resolution and sensitivity depend on the properties of analytes and the matrix constituents. The high background ion signal usually arises from the matrix liquid. The viscous matrix leads to ion suppression effects, e.g. more hydrophilic compounds tend to remain in the droplet interior whereas hydrophobic compounds tend to migrate to the surface of the droplet, suppressing the ionization of the more hydrophilic compounds. However, these suppression effects are much less serious for "continuous-flow-FAB", since the surface is continuously refreshed [3].

Instead of using energized particles as in PDMS and FABMS, a laser beam can be used for ion generation in mass spectrometric analysis. The historical development of the field has been strongly influenced by that of laser technology. In 1966 the design of a mass spectrometer, for ions generated from a surface with a Q-switched laser beam, was reported [7]. The rather poor quality of the results in these times was attributable to the limited performance of the lasers used in these studies. The laser desorption/ionization (LDI) technique was revived after Posthumus et al. [8] reported the production of cations from polar non-volatile molecules ($m/z < 1250$) by laser desorption in the source of a double focusing mass spectrometer. However, the effort to implement the LDI method for higher mass compounds was not successful. In laser desorption experiments the sample should have a high absorption coefficient at the laser wavelength. For commonly used UV lasers, this condition is not met for large numbers of important biopolymers. Also, the direct absorption of radiation by those analytes often leads to fragmentation and failure to obtain useful molecular mass information.

The idea of mixing analytes with a good absorber and limiting radiation damage to the analytes appears to have been demonstrated first by Tanaka et al. [9], who

mixed fine metal powder into glycerol as matrix and produced spectra of proteins ($m/z < 35,000$) with a pulsed UV laser, and by Karas and Hillenkamp [10] who used a solid matrix to obtain spectra of mellitin and other peptides. Hillenkamp's group did the initial research and made contributions that paved the way for the acceptance of the technique. Beavis and Chait entered the field early and have also made very important contributions, in particular by demonstrating the usefulness of a new class of matrices [11, 12, 13, 14]. Karas and Hillenkamp's technique, in which the analyte molecules are mixed with a suitable matrix in molar ratios of the order of 1:10000, and the resulting solid solution then excited by pulsed laser, has been widely adopted as standard practice for the analysis of biopolymers and is commonly referred to as matrix-assisted laser desorption/ionization (MALDI).

Since the introduction of MALDI in 1988 the application of MALDI mass spectrometry has become an important research field. Primary target analytes of this technique are peptides and proteins. In practice, MALDI has demonstrated a number of advantages over FAB. Ion production from high-molecular-weight polypeptides by MALDI extends well above the 5000 u limit commonly the case for FABMS measurements [15]. MALDI shows little discrimination between different peptides. FABMS tends to provide unstable or low ion currents for hydrophilic peptides whereas MALDI spectra show no deterioration for this important class of compounds. MALDI also shows detection limits of $<$ one picomole of analyte for peptides [16]. This sensitivity is clearly an asset in many areas of biochemical research where often only minute traces of the analyte are available. Protein molecular mass determinations are particularly straightforward with MALDI. Molecular weights of the largest proteins successfully analyzed are well above 200,000 u [17]. Prompt ion fragmentation occurs rarely for MALDI. The most intense peaks in the high-mass region of the spectra are protonated molecules, including singly, doubly and multiply charged ions. This

feature makes it easy to find the molecular masses of proteins. In addition to peptides and proteins, other classes of compounds, such as oligosaccharides [18], nucleic acids [19, 20], and synthetic polymers [21, 22], can be analyzed. The absolute sensitivity of such analyses was found to be similar to that reported for peptides [23]. The technique appears to be well-suited to analysis of complex mixtures such as enzymatic digests, [24, 25, 26, 27]. A combination of enzymatic digestion and MALDI can, therefore, contribute to protein sequence determination [28]. The application of MALDI to quantitative analysis has also been approached by a number of groups, as the result of improvements in sample preparation and instrumental protocols [29, 30, 31, 32].

1.2 Previous Work on MALDI

More than 1000 papers have been published on MALDI since its introduction in 1988. This section is an overview of that literature as it pertains to the topics discussed later. An important aspect of MALDI is the fact that the results depend entirely on the correct choice of matrix for a given laser wavelength. The first successful MALDI mass spectra of proteins were recorded by Hillenkamp's group [10] using nicotinic acid as the matrix, and by Tanaka et al. [9] using cobalt powder finely dispersed in glycerol. In the former case, the laser source was a frequency-quadrupled Nd:YAG laser radiating at 266 nm, whereas the latter investigation used an N_2 laser emitting at 337 nm. Beavis and Chait have systematically investigated various matrices, and found very good results for derivatives of aromatic carboxylic acids, such as 2-pyrazinecarboxylic acid, 4-hydroxy-3-methoxybenzoic acid (vanillic

acid), and *trans*-3,5-dimethoxy-4-hydroxycinnamic acid (sinapic acid) [11, 12]. Reviewing the performance of matrices discovered, they have suggested three criteria to be fulfilled by a useful matrix in MALDI, namely: low sublimation pressure; capacity to strongly absorb at the wavelength used; and miscibility of the matrix solution with aqueous analyte solutions. Many groups have tried to find better matrices for various analyte polymers. Karas and co-workers introduced 2,5-dihydroxybenzoic acid (2,5DHB) as a matrix [23]. This matrix not only offers good sensitivity for peptides and proteins, but also works well for carbohydrates [18] and glycolipids [33]. α -Cyano-4-hydroxycinnamic acid (4HCCA) was also shown to be a good matrix for protein analysis, with lower propensity for matrix adduct formation, by Beavis and Chait [34]. Zhao et al. [35] have demonstrated that nitrobenzyl alcohol on fibrous paper substrate is very useful for proteins. Though several other useful matrix compounds have been found, sinapic acid, 2,5DHB and 4HCCA seem to be currently popular matrices for solving most practical problems.

The characteristics of the laser radiation are also an important experimental factor for MALDI performance. The early work suggested that there was a threshold for production of protein ions as a function of laser irradiance in MALDI, and that the threshold value is 100 MW cm^{-2} using nicotinic acid [10]. Subsequent investigations have shown that the early measurement was in error, and that the true threshold is approximately 1 MW cm^{-2} [12, 14, 36, 37, 38]. A parameter that has proven to be less critical is the wavelength of the laser light. Many different pulsed lasers over the wavelength range 266 - 420 nm have been used to produce protein ions [39, 40]. The main constraint on the laser wavelength is that the laser light must be absorbed strongly by the matrix crystals, but not by analytes, in order to minimize unwanted photochemical reactions. Since absorption in the amino acid side-chains of proteins becomes important below 280 nm, nitrogen lasers (337 nm) and frequency-tripled

Nd:YAG lasers (355 nm) are currently favored over frequency-quadrupled Nd:YAG lasers (266 nm).

In order to provide information for the theoretical treatment of MALDI, the velocity distributions of the ions produced by MALDI have been measured by several groups. The main finding is that all the molecular ions ablated from the MALDI sample have about the same speed distribution, with an average speed of approximately 500 m/s and a distribution half-width of approximately 100 m/s [36, 41, 42]. The speed distribution is independent of molecular mass in the 1000 - 15,600 u range.

Sample preparation also has a significant effect on the MALDI ion production. As usually prepared by the "dried droplet" method, a droplet of a solution of matrix and analyte is deposited on a metal substrate and allowed to dry. This preparation often results in samples with a nonhomogeneous morphology, which contain a higher analyte concentration around the crystal edges. For this reason the MS intensity can vary widely with position of laser irradiation of the dried droplet. A systematic investigation of the effects of different drying techniques on the efficacy of the "dried droplet" method of sample preparation indicated that vacuum drying is faster, and provides better ion yields and resolution, in MALDI-TOF spectra [43]. An alternate fast evaporation method was introduced by Vorm et al. [44]. In this procedure, matrix solution was first applied to the probe tip of the mass spectrometer in a highly volatile solvent, e.g., acetone, to obtain a thin layer of the matrix. In a second step a drop of analyte solution was deposited on the layer. The resulting sample surfaces became much more homogeneous, and the spectra showed higher resolution when a reflectron was used. More recently, the influence of matrix solution composition and pH on MALDI-MS analysis of peptides and proteins was described by Cohen and Chait [45]. They prepared matrix solutions by adding 4HCCA to the organic solvent in different compositions. The acidity of these solutions, in the 1.1 - 3.0 pH range, was

controlled by the addition of water and acid. The results from the experiment showed that the analysis of proteins and high-mass peptides (> 3000 u) is best performed using higher acidity matrix solutions ($\text{pH} < 1.8$), and the analysis of small peptides (< 3000 u) is best carried out using matrix solutions of somewhat higher pH.

Despite the success of MALDI for ionization of large molecules, the theoretical description of its mechanism remains a subject of continuing debate. A detailed discussion of possible models and mechanisms for MALDI, proposed up to 1992/93, has been summarized by Sundqvist [46], and by Vertes and Gijbels [47].

Earlier attempts to deal with certain aspects of the MALDI process have mainly focused on the mechanism of energy transfer between the matrix molecules and the analyte molecules [48], and on the development of the expanding plume of matrix molecules [49]. Vertes et al. [50] have suggested that there is an obstacle in the energy transfer to the embedded guest molecules. This so-called energy transfer bottleneck is caused by mismatch between the guest - host interaction frequency and the internal vibrational frequencies of the guest molecules. Vertes has also used a one-dimensional hydrodynamic model to calculate the expansion and temperature of the expanding plume of matrix molecules [51] and suggested that, at the sublimation temperature, there is a phase transition causing a plume of ejected material. The generated plume, in turn, undergoes gas dynamic expansion and adiabatic cooling. The entrained large molecules are therefore also stabilized in the expansion.

Another approach has been taken by Johnson and co-workers [52, 53]. A pressure pulse model, originally formulated for fast heavy-ion-induced sputtering, was applied to the ejection process in MALDI. In the original model the penetrating primary particles deposit their kinetic energy into the solid and set up a pressure gradient. Upon exceeding a threshold value this pressure gradient drives the expansion of the surface layer leading to desorption. In the case of MALDI, as the laser light penetrates

the target, energy is deposited and a pressure gradient builds up. This model predicts the existence of a fluence threshold, and that the energy conversion efficiency will be higher as pulse length is reduced.

Although the proposed models are able to account for some features of the MALDI experiments, none of them has attempted to explain ion formation, a prerequisite for mass analysis and detection in mass spectrometry. They have also not addressed the differences in efficiency between matrices with similar phase transition temperatures and optical characteristics.

1.3 Summary of This Work

As mentioned in the previous section, the method of analyte/matrix preparation plays a crucial role in achieving optimal performance in MALDI. In the first part of this work a new method of preparing the sample to increase contaminant tolerance is described. While the solvent composition and matrices used in the “dried droplet” method have changed since MALDI was introduced, there has been no fundamental change in this protocol. This method for MALDI MS is a simple one step process, but high concentrations of nonvolatile solvents, such as glycerol, urea, DMSO and other protein stabilizers, can reduce or eliminate the intensity of protein ion signals. Instead of using the one step process, we have used a three-step process. A drop of matrix was initially deposited on a polished flat probe and dried, then crushed and smeared on the probe surface by using a glass slide. A second drop of a solution of a mixture of matrix and protein was then applied to the spot bearing the smeared matrix material. The resulting polycrystalline film adhered firmly to the probe surface, and could be then washed vigorously to remove contaminants. The examples presented in Chapter

3 illustrate how analyses were improved as a result of this new sample preparation procedure.

The basic difference between laser desorption/ionization and matrix-assisted laser desorption/ionization is that the laser radiation is directly absorbed by sample in the former, but the matrix dominates energy absorption and the formation of ions in the latter. Therefore, in the second part of this work (Chapter 4) the influence of matrix concentration on the analyte ion yield, and on the mass resolution of the molecular ion signals, was investigated. MALDI time-of-flight mass spectra of protein mixed with different concentrations of matrix solution, for each of 2,5DHB, 4HCCA and sinapic acid, were obtained. The results showed that the intensities of the analyte ion peaks increase gradually with an increase in the concentration of the matrix solution under fixed laser fluence, and then level out and decrease slightly as the concentration of matrix solution is further increased. Analysis of the spectra also showed that the molecular ion peaks are broadened, i.e. mass resolution decreases, as the matrix concentration increases. These results were compared with the observations made by other groups using different approaches. An interpretation of these results has been proposed, based on two categories of matrix concentration effects, namely, a physical effect characterized by energy deposition and redistribution processes, and a chemical effect characterized by co-crystallization of the matrix and analyte followed by subsequent photochemical ionization.

Another potential pitfall with MALDI is poor crystallisation, which is known to significantly affect ion production. In the last part of this work (Chapter 5) a strategy was attempted to alleviate this problem. Impurities (or additives) present in the matrix solution can have a pronounced effect on the crystallization process, in particular on the morphology of the deposited crystals. The technique of controlling crystal growth by the use of additives is discussed. Crystallization of 2,5DHB mixed with

its isomers and other benzoic acid derivatives are then reported. The performance of the resulting crystals in MALDI MS was evaluated. The results showed that mixtures of 2,5DHB with 2,3-dihydroxybenzoic acid or 3-amino-2,5,6-trifluorobenzoic acid improved the homogeneity of the resulting crystal morphology, and consequently improved the MALDI MS performance.

Chapter 2

Experimental Apparatus

To date, matrix-assisted laser desorption of biopolymers has been obtained mainly in combination with time-of-flight (TOF) instruments. This observation is connected to the fact that laser desorption and ionization of molecules usually comes about during a short laser pulse, $\tau_{pul} = 10^{-8}$ s, and the time-of-flight mass spectrometer makes it possible to record the whole mass spectrum of a sample following that pulse. The mass spectra studied in this thesis were obtained with a linear time-of-flight analyzer constructed in-house. The linear time-of-flight mass spectrometer was designed by Dr. Beavis and has been described elsewhere [54]. In this chapter an overview is given of the experimental apparatus as well as the ionization and light sources.

2.1 Laser Ion Source and TOF Instrument

Time-of-flight mass spectrometers are relatively simple, inexpensive instruments with high sensitivity and a wide mass range, comparing to scanning mass spectrometers. As shown in Figure 2.1, ions are formed in a short source region in the presence of an electrical field (E) that accelerates the ions into a longer, field-free drift region (L). Ideally, all ions enter the drift region with the same kinetic energy (KE)

$$KE = zeES \quad (2.1)$$

(where e is the charge on an electron, z is the number of charges and S is the distance of the ion acceleration), but they will have velocities (v) given by:

$$v^2 = \frac{2zeES}{m} \quad (2.2)$$

which depend on their mass (m). The time (t) required to traverse the drift region

$$t = \sqrt{\frac{m}{2zeES}} L \quad (2.3)$$

also depends on the mass of the ion, so that the time spectrum can be converted directly to a mass spectrum

$$\frac{m}{z} = 2eES \frac{t^2}{L^2}. \quad (2.4)$$

To obtain timing information, the time of ion formation must be known. Thus TOF mass spectrometers generally use pulsed ionization, which is appropriate to the nature of the MALDI process.

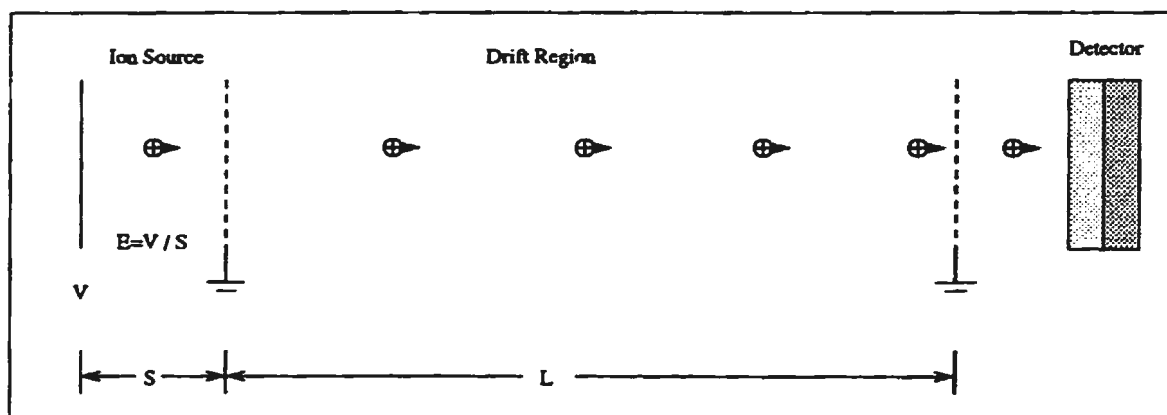


Figure 2.1: Principle of time of flight mass spectrometry.

A schematic drawing of the present apparatus is shown in Figure 2.2. The field-free region was constructed from 2.00" ID tubing and from a cube with openings on each of its 6 sides, using 3.37" conflat style flanges with copper gasket seals. The tube, cube and flanges are all made of 304 stainless steel, and were obtained from Huntington Mechanical Laboratories, Inc. (Georgetown, Ontario, Canada). One end of the tube was connected to a stainless steel vacuum housing (4.00" ID, 3-way tee), which was modified to serve as the detector chamber, using the flange. The other end was attached to the cube, which includes the ion source. The pumping system was an Edwards 100/300 Diffstak diffusion pump backed with an E2M8 roughing pump (Edwards High Vacuum, Burlington, Ontario, Canada). The diffusion pump was hung from the 3-way tee. An ion gauge mounted on the wall of the 3-way tee was controlled by a HP 5945A gauge controller. The total ion flight length was approximately one meter.

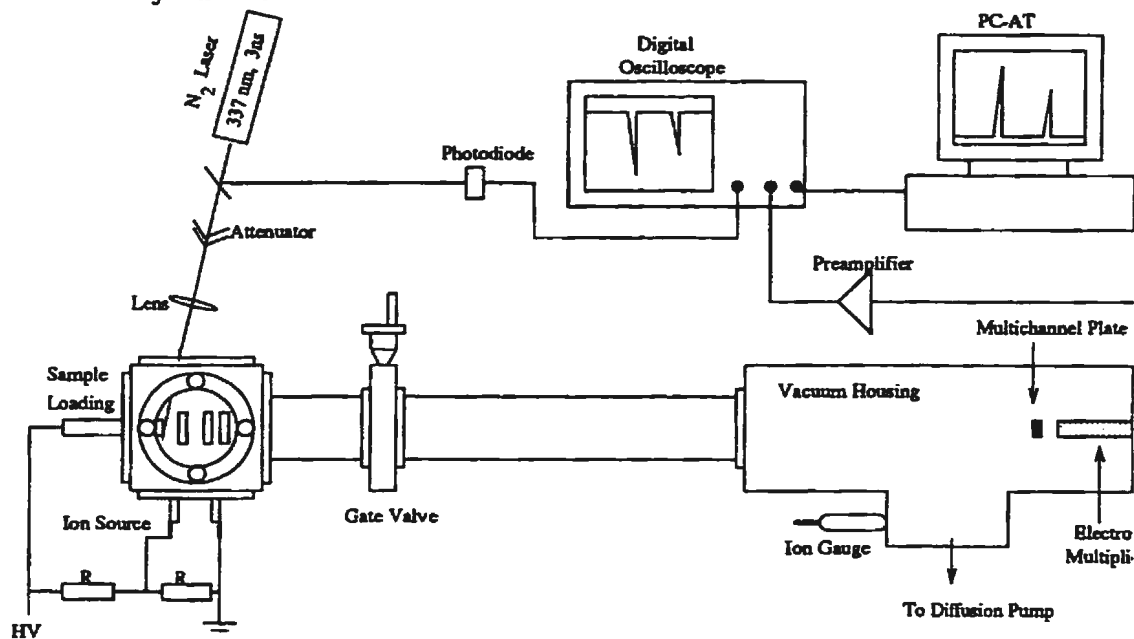


Figure 2.2: Instrumental arrangement.

One gate valve (Huntington GVA-200-v) was used near the ion source. The ion source could therefore be isolated from the flight tube by the gate valve. The ion source was designed using a ball-mounting scheme. In this scheme, the electrode system was assembled by stacking stainless steel rings alternating with 3/16" ceramic balls. A cross-sectional view of the ion source assembly is shown in Figure 2.3. Three balls were used between any two rings. There are three through holes in the rings to cradle the ceramic balls. The stack was then clamped with three threaded rods. This mounting arrangement ensured that the rings were accurately centered. The acceleration section consisted of two electric fields accelerating the ions in the same direction. The total accelerating voltage used in all experiments was +30 KV, with +30 and +15 KV on the sample stub and the first acceleration ring, respectively.

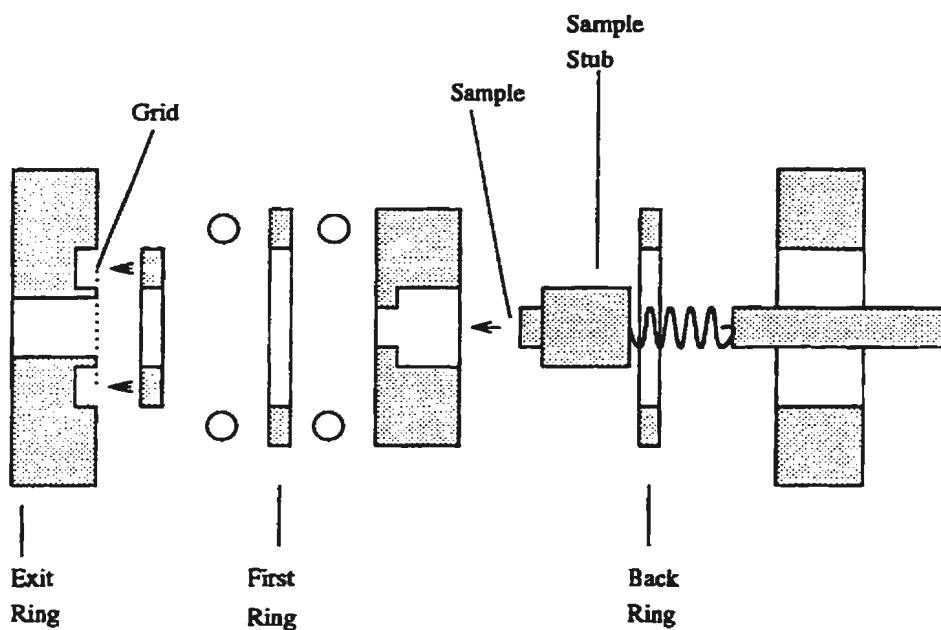


Figure 2.3: The ion source assembly.

The exit ring was held at ground potential. The ions were finally extracted through a high-transmission grid. A low ripple high voltage supply (Spellman Electronics, Hauppauge, NY, USA) produced the main acceleration voltage and a resistor chain mounted external to the ion source set the voltage on the first ring.

A nitrogen laser, emitting at 337 nm with 3 ns pulse width (LSI-337ND, Laser Science Inc.), was used for sample desorption/ionization in all experiments. The pulse energy of this laser was approximately 120 μJ , therefore a Fresnel reflection attenuator was used to control carefully the irradiance on the sample. A spatial filter was also used. It consisted of a $f=200$ mm silica convex lens, a 200 μm pin hole to improve the beam's homogeneity and a $f=100$ mm silica convex lens (Newport, Mississauga, Ontario, Canada). The light was finally focused by a 100 mm silica convex lens to a spot size of typically 100 μm in diameter on the sample, through a silica window mounted on the ion source cube. The laser incidence angle was approximately 70 degrees to the surface normal.

The Fresnel reflection attenuator was designed and constructed in-house. A schematic diagram of the attenuator is shown in Figure 2.4. Two sets of two circular microscope cover-slips mounted parallel in the end of two shafts produced the reflection. Each shaft had a gear mounted on it, and the two gears meshed so that turning either shaft drove the other. Both shafts were mounted on a plate with bearings. Turning one shaft rotated the other shaft in the opposite direction, thus opening up the angle between the pair of cover-slips. This arrangement allowed the operator to vary the attenuation caused by Fresnel reflection at different incidence angles, while minimizing the output's angular deviation. The calculation of transmittance dependence on laser incident angle for the attenuator is presented in the appendix. The property of the attenuator was initially evaluated by measuring a transmitted laser beam with a power meter. A regular calibration of the laser energy was not

necessary since the laser radiation was not a critical parameter for this work. Once proper laser power reached for each experiment, it was unchanged during few weeks through all of the samples to be run on that occasion.

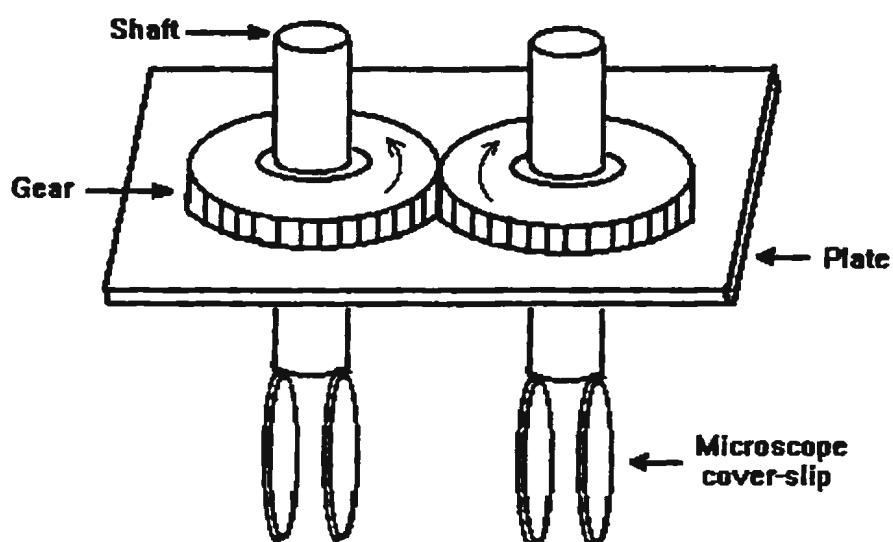


Figure 2.4: Fresnel reflection attenuator.

2.2 Ion Detection

Detection of relatively small ions, of masses up to several thousand atomic mass units, is straightforward using secondary electron multipliers (SEM) or multichannel plates (MCP). Larger ions require a higher acceleration potential to acquire high enough velocity for an efficient ion/electron or ion/ion conversion in the detector. In order to achieve suitable sensitivity the detector was constructed using a MCP/SEM-hybrid configuration, consisting of a 25 mm diameter multichannel plate (Hamamatsu F-1094-1) and a mesh dynode electron multiplier with a 25 mm diameter active area (Hamamatsu R2362, Hamamatsu Corp., Bridgewater, NY, USA). The channel plate was mounted approximately 3 mm in front of the electron multiplier. The side of the multichannel plate facing the ion beam was at ground potential. The back of the plate was at +1.1 kV. The potential difference between the rear surface of the multichannel plate and the first dynode of the electron multiplier was appropriately +20 V. The electrons emitted from the rear surface of the MCP in response to an ion striking its front surface gained adequate energy and struck the first dynode of the multiplier. The voltage across the dynode resistor chain was 2.0 kV. The output anode was connected to high voltage through a 1 M Ω pull-up resistor and the output was taken off the anode by two series of 50 nF capacitors (3 kV WDC). The output terminator resistance was 50 Ω .

The analog signal was preamplified and digitized by a digital oscilloscope (Tektronics 520, 500MS/s, 50,000 point record length option, Tektronix Canada Inc.,

Weston, Ontario). A high-speed optical detector (photodiode) intercepting a portion of the laser beam triggered the oscilloscope. An AT-type PC computer (Empac 386DX33) with the GPIB-II interface (AT-GPIB, National Instruments, Pointe-Claire, Quebec, Canada) was used for data acquisition. Each digitized record was transferred to the computer individually, where it was inverted, inspected to ensure that no overshoots were recorded, summed in a buffer, and displayed. The internal calibration was obtained by using the empirical equation $\sqrt{m/z} = at + b$, where the constants a and b were determined by two known masses that appear in standard mass spectra.

Chapter 3

Polycrystalline Film Method of Sample Preparation

The dried-droplet method, a popular procedure for preparing protein-doped matrix crystals for MALDI-MS, is a simple process. However, high concentrations of involatile solvents, strong detergents and some commonly-used protein stabilizers can reduce or eliminate the intensity of protein ion signals. In this chapter, a new method of preparing the sample probes to increase contaminant tolerance is described. The examples presented in this chapter illustrate how analyses are improved using this new sample preparation procedure.

3.1 Conventional Method of Sample Preparation and its Disadvantages

Matrix-assisted laser desorption was introduced in 1988 by Tanaka and co-workers [9] and Hillenkamp and co-workers [10]. In their original work, Tanaka dissolved the polypeptide of interest in glycerol and mixed the glycerol solution with a finely divided metal powder. A drop of this suspension was placed on a probe tip and intact protein ions were produced by a pulsed ultraviolet laser (a nitrogen gas laser, $\lambda = 337$ nm). Hillenkamp [10] mixed aqueous solutions of a protein and nicotinic acid. A drop of this mixture was dried, and irradiated by a frequency-quadrupled Nd:YAG laser, with a wavelength of 266 nm. The major difference between the results of the Tanaka method of sample preparation and the Hillenkamp method was sensitivity. Tanaka's

method required nanomoles of protein to prepare a sample for successful analysis. The Hillenkamp method required picomoles of protein, i.e. it was 1000 times more sensitive.

Progress in the past few years has been made with new matrix materials. The sample preparation procedure, however, has undergone very little change. Most of the matrices used today are aromatic organic acids, and the procedure for sample preparation may be summarized as follows. The first step is to make a saturated solution of the matrix material and mix the matrix solution (5-10 microliters) with a small volume (1-2 microliters) of a 10 μ mol protein solution. Both the protein and matrix material must be dissolved in the solvent, rather than suspended as finely divided solids. The optimum molar ratio of matrix to analyte in the final sample solution is between 1:1000 and 1:10,000. A droplet (0.5-2 microliters) of the resulting mixture is placed on the mass spectrometer's sample stage and dried at room temperature. As the solvent slowly evaporates, matrix crystals are formed and proteins are incorporated into the solid matrix crystals rather than being confined to their surface [23, 55, 56]. The above procedure is shown schematically in Figure 3.1. This procedure is now commonly referred to as the "dried-droplet" method, and is simple to perform, and effective.

Many biological samples are prepared or stored in solutions containing buffers and stabilizers. These solutions can consist of mixtures of many species, such as N-2-hydroxyethylpiperazine-N¹-2-ethanesulfonic acid (HEPES), dithiothreitol (DTT), dimethyl sulfoxide (DMSO), glycerol, urea and NaCl. These components can be present either to increase the solubility of the protein or to stabilize the protein's structure for long-time storage. Removal of the solution may be difficult if its presence is necessary to dissolve the protein. The concentrations of these additives can be quite high, e.g., 6 M urea is commonly used to enhance protein solubility in aqueous

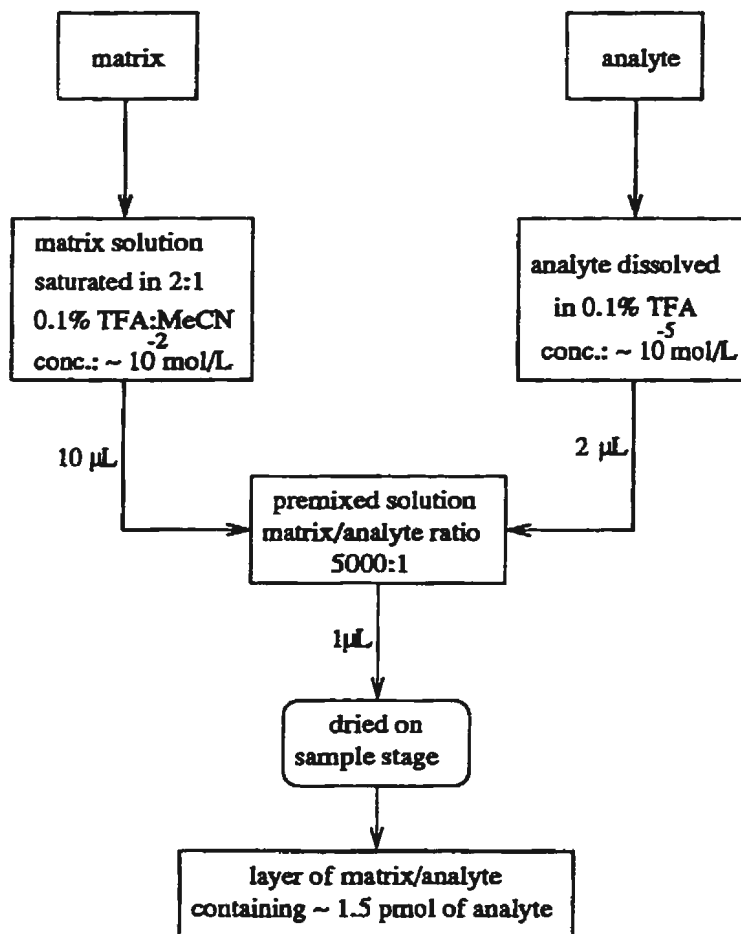


Figure 3.1: Flowchart showing the dried-droplet method of sample preparation.

solutions.

The presence of these buffers or stabilizers in the dried-droplet method is very detrimental to obtaining high quality MALDI mass spectra. They can be classified into two categories. Strong cationic detergents such as sodium dodecylsulfate (SDS) can cause problems even at extremely low levels. They completely suppress all protein signals if present at the concentrations normally used to promote protein solubility. Another class of detrimental contaminants is involatile liquid components such as glycerol. The dried-droplet method forms crystals at random seed sites throughout the solution as the solvent evaporates. These seed sites are either particulate matter accidentally introduced to the solvent or undissolved matrix crystal fragments. The solvent evaporation makes the surface of the droplet a preferred place for the formation of crystal nuclei. Observation by microscope shows that the microcrystals are formed at the air-liquid interface and then carried into the body of the solution by convection. If no involatile additive is present, these crystals adhere to the metal substrate, and the adhered crystals can be gently washed to etch away any highly soluble contaminants (such as salts). If involatile liquids such as glycerol are present, the crystals may either not form or remain coated with the glycerol, preventing attachment to the substrate. Even if crystals form and can be placed in the ion source, a coating of involatile liquid can abolish ion emission from the sample's surface when present in the final matrix/polypeptide solution at greater than 1% (v/v). Recognizing and solving these problems has been a challenge since MALDI was introduced. Sample preparation by growing large, protein-doped matrix crystals under more controlled conditions [54] has been shown to be effective for sample solutions containing low protein concentrations and high concentrations of involatile liquids or salts.

3.2 New Method of Sample Preparation

This section describes an alternate method of sample preparation [57], developed as a way of obtaining a more uniform and reproducible MALDI sample, and minimizing the effect of contaminants on ion emission. Two solutions containing the matrix were prepared. These are referred to below as solution A and solution B. All the solutions were prepared and used at room temperature (22^o C). Solutions were handled carefully, so as to minimize transfer of undissolved crystalline solid from one step to the next. In addition, fresh solutions were prepared every day, in order to prevent nucleation.

Figure 3.2 illustrates the proposed polycrystalline film method of sample preparation. Solution A contained the matrix alone. It was prepared using 0.3 ml of 2:1 (water):(acetonitrile) (v/v) or any appropriate solvent mixture. An excess of matrix was added to the solvent in a 0.5 ml Eppendorf tube and stirred for at least one minute with a vortex mixer. The tube was then placed in a bench-top centrifuge and spun to deposit undissolved matrix particles on the bottom of the tube. The supernatant was removed to another tube with a micropipet. Solution B contained matrix and analyte. The initial matrix solution was prepared by saturating 0.3 mL of a selected mixed solvent with matrix, and then removing excess matrix particles in the same manner as Solution A. Details of different solvent composition are shown in Section 3.3. An aliquot of this matrix-saturated solution was then mixed with a protein-containing solution to produce a final protein concentration of approximately 1 micromolar and a matrix/analyte ratio of 5,000:1. Any precipitation of the solute in either the protein-containing solution or the matrix-containing solution could lead to poor mass spectra. The substrate used was the mass spectrometer's sample stub;

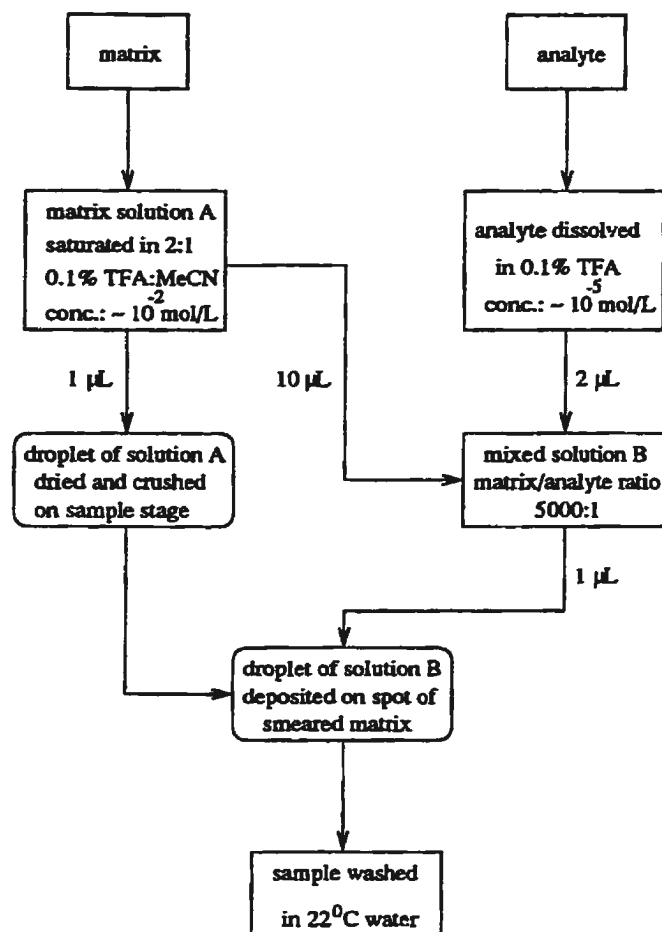


Figure 3.2: Flowchart showing the polycrystalline film method of sample preparation.

a stainless steel cylinder. The upper surface of the stub was polished with 400 grade finishing paper to remove machining marks but no special treatment was given to the surface. The stub was thoroughly cleaned with methanol and distilled water between each sample deposition. Brief washing of the surface of the sample stub in an ultrasonic bath was necessary to ensure that the previous sample was completely removed. As shown in Figure 3.2, a 0.5-1 microliter aliquot of Solution A was deposited on the surface and dried. The deposit formed was identical to that obtained by the dried-droplet deposit method, described above. A clean glass slide was then placed onto the dried deposit and pressed down onto the surface with an elastic rod, such as a pencil eraser. The glass slide was twisted several times to smear the deposit onto the surface. The crushed matrix could be brushed with a tissue or blown with air to remove any loose matrix particles. A 0.5-1 microliter aliquot of Solution B was then applied to the spot bearing the smeared matrix material. Within a few seconds an opaque film formed over the substrate's surface below the droplet, covering the metal. After about one minute, the probe tip was immersed in room temperature water to remove involatile liquid components and other contaminants. It is not necessary to let the droplet dry before washing: the film did not wash off easily. Excess water on the surface of the deposit was blotted with a tissue, and the sample was allowed to dry at room temperature.

It was noted that the aliquot of Solution B used to create the film must be free of particulate matter. Any particles of matrix present in this solution resulted in rapid nucleation of matrix crystals throughout the solution, interfering with the formation of the film. If Solution B was obviously cloudy, further centrifugation was necessary to clear the liquid. The sample preparation described above is referred to as the "polycrystalline film" method in the following sections.

Subsequent to its initial publication [57], a refinement of this method has been

discovered. In this refined method, the matrix is dissolved in isopropanol to a concentration of 1g/L. Several microliters of this solution are then spread out over the surface of the sample stage and dried rapidly with a stream of room temperature air. A very thin layer of fine crystals results from this treatment. This layer is then crushed by rubbing the surface with a paper lab wipe repeatedly and firmly. The drop of the sample and matrix in 2:1 water:acetonitrile is then applied as in the previous method. This alternate method is easier to perform on sample stages that are not perfectly flat.

A layer suitable for polycrystalline film formation can also be deposited by electropray. The matrix in this case is dissolved at 1g/L in methanol and electrosprayed onto the surface at a sufficiently low flow rate to prevent wetting of the surface. The resulting layer will form a polycrystalline layer when the second solution is applied to its surface.

3.3 Experimental Results

The following matrix materials were used in this study: *trans*-3,5-dimethoxy-4-hydroxycinnamic acid (sinapinic acid, SA) (Aldrich, lot#KY07201TV); *trans*-4-hydroxy-3-methoxycinnamic acid (ferulic acid, 4-FA) (Aldrich, lot#08522CY) [11]; *trans*- α -cyano-4-hydroxycinnamic acid (4-HCCA)(Sigma, lot#92H3649)[34] and *trans*-2-hydroxycinnamic acid (*o*-coumaric acid, oCA)(Sigma, lot#11H2505). All the matrices were purchased directly from commercial chemical suppliers and used without further purification. The protein used was horse skeletal muscle myoglobin (Sigma, catalog #M-0630, lot #61H7100). The materials were weighted on the bance and the molecule weight used for calculation of concentrations was as quoted on the lable of

the bottle. The solvents used were filtered, deionized water (produced using a Millipore cartridge system), acetonitrile (Fisher, reagent grade), urea (BDH, molecular biology grade) and glycerol (Fisher, reagent grade).

Photomicrographs illustrating the procedure for producing the polycrystalline films are shown in Figure 3.3. Figure 3.3(a) shows the initial dried-droplet deposit of sinapinic acid. The result was a carpet of micro-crystals of different sizes and orientations. The dominant crystal habits were thin tablets and long prisms. Figure 3.3(b) shows the same sample, after smearing the crystals with the glass slide.

Figure 3.3(c) is the polycrystalline film. At this scale, surface details of the film cannot be distinguished. Further magnification of the sample produced no further information: the surface appeared to be covered by unresolvable bright specks. Figure 3.4 is a scanning electron micrograph of a polycrystalline film produced using 4-HCCA. Under a light microscope, this film was indistinguishable from that shown in Figure 3.3(c). The film is composed of small crystals, with crystal dimensions less than one micrometer. Most of the crystals have dimensions of 200-400 nm. The crystals appear to be randomly oriented with respect to the substrate. The crystal habits are consistent with a monoclinic crystal structure.

Figure 3.5 is a mass spectrum of horse skeletal muscle myoglobin obtained from a 4-HCCA film. The solvent used for this spectrum did not contain any of the usual additives used in protein solutions. This spectrum is used for comparison with Figures 3.6-3.8. Myoglobin was chosen to illustrate protein ion production only because it has become a *de facto* standard for protein mass spectrometry. Other proteins have been tried, with similar results [58]. The sample did not show any strong variations in ion signal intensity as the laser was scanned across the surface of the film. This observation shows that the polycrystalline film method has a major advantage over the dried-droplet method. The dried-droplet method generally produces samples in

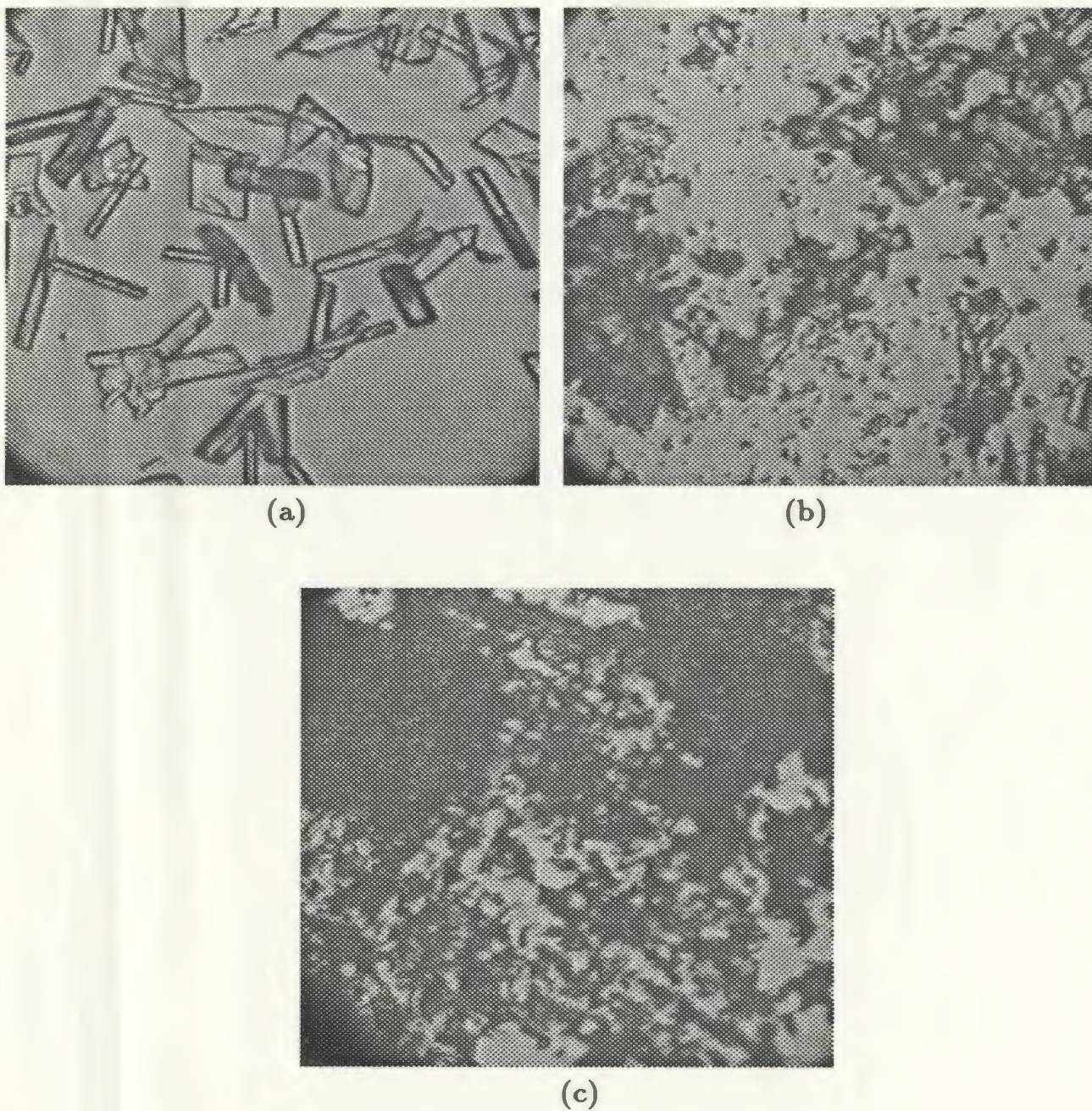


Figure 3.3: Photomicrographs (magnification: 250x) showing the three stages of preparation of a polycrystalline film of sinapic acid. (a) The dried droplet deposit formed using Solution A. (b) The same deposit after smearing with a glass microscope slide. (c) The same deposit after growing a film using a Solution B consisting of 2:1 (water):(acetonitrile) saturated with sinapic acid.

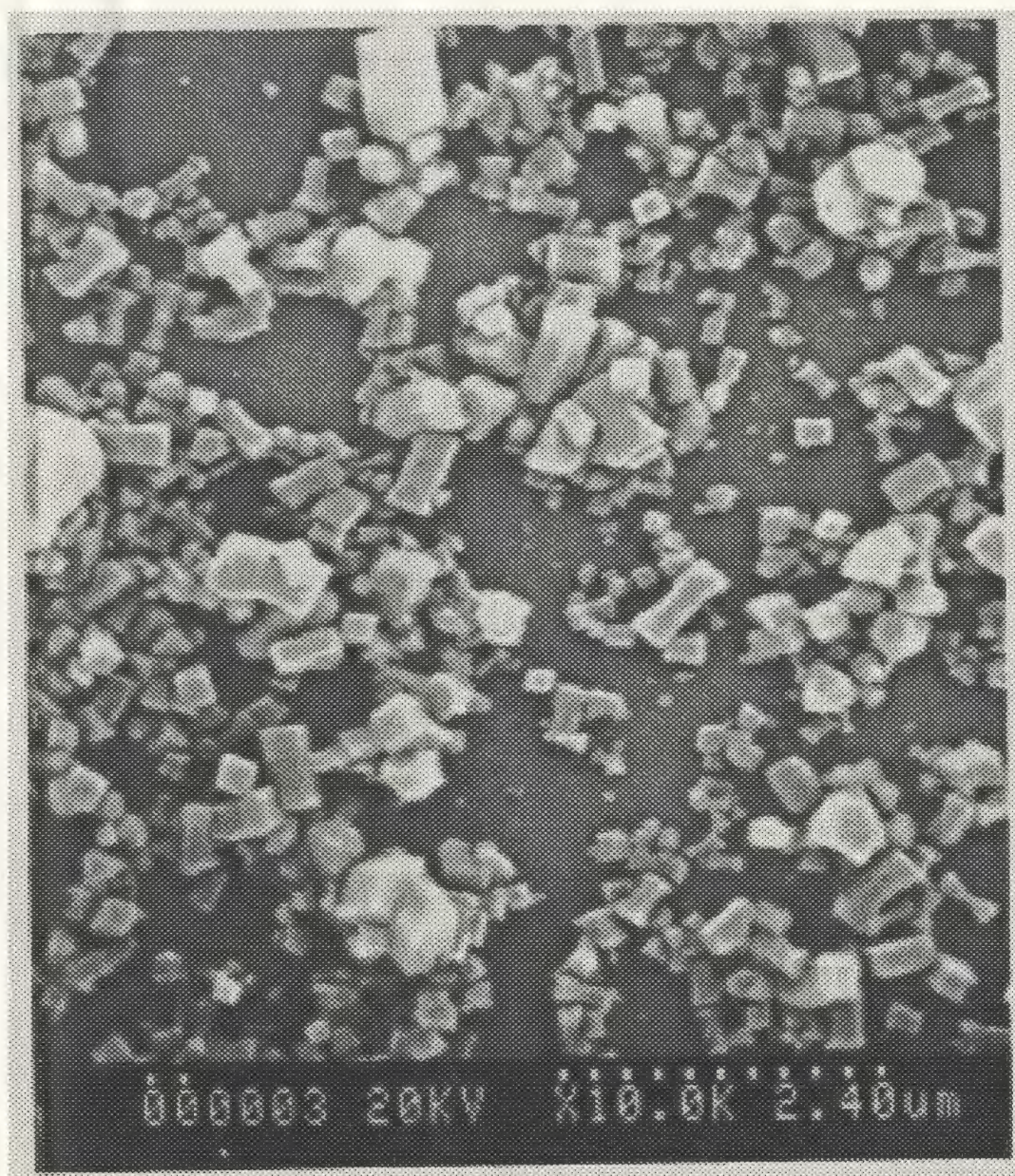


Figure 3.4: A scanning electron micrograph (magnification: $10^4\times$) of an 4-HCCA polycrystalline film. The scale is indicated on the micrograph. Solution B was 2:1 (aqueous 0.1% trifluoroacetic acid):(acetonitrile)(v/v) saturated with the matrix.

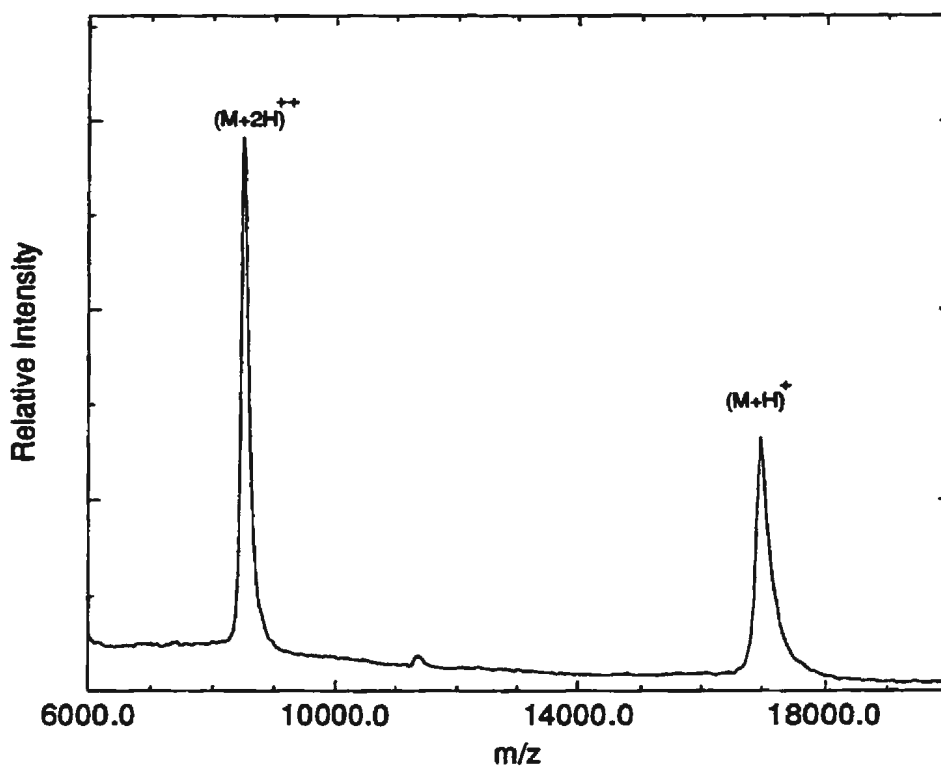


Figure 3.5: A laser desorption TOF mass spectrum of horse skeletal muscle myoglobin (mol. mass = 16951 u) taken from an 4-HCCA polycrystalline film. The singly and doubly charged ion species are shown. Solution B was 2:1 (aqueous 0.1 % trifluoroacetic acid):(acetonitrile)(v/v) containing 0.5 μ M myoglobin. This spectrum represents the sum of transients recorded for 30 consecutive laser shots.

which some parts of the deposit produce little or no analyte signal, while from other regions intense signals are produced. It should be noted that the ion production threshold behavior of these polycrystalline films was qualitatively different from that observed using the dried-droplet deposit method. Once threshold was reached, the protein analyte ion current from the film increased very rapidly with increased laser irradiance. The ion current increased more sharply than for dried-droplet deposits made from a similar solution. This strong dependence of ion-current on irradiance made it difficult to prevent saturation of the ion detection system.

Figure 3.6 was obtained with the same matrix as Figure 3.5, but using a Solution B containing 20% glycerol. It was noted that the traditional dried-droplet method applied to this solution B produced no protein ion signals. The polycrystalline film had the same morphology as the film shown in Figure 3.3c. The protein ion production characteristics of this film were identical with those of the film produced without any glycerol (Figure 3.5).

Figure 3.7 is a mass spectrum obtained from the same matrix, but with solution B composed of 2:1 (aqueous 6 M urea):(acetonitrile) (v/v). Again the dried-droplet method of this solution B produced no protein ion signals. The polycrystalline film produced strong signals over the entire surface of the film.

Figure 3.8 presents a mass spectrum obtained from the same matrix as Figure 3.5, but with Solution B composed of 2:1 (aqueous 1 M sodium chloride):(acetonitrile) (v/v). Once again, the presence of high concentrations of non-proteinaceous material in the solution did not seriously affect ion production.

Similar experiments were carried out using 3-indole(*trans*)acrylic acid, *trans*-sinapinic acid and 2,5-dihydroxybenzoic acid(2,5DHB) as matrices and myoglobin as analyte. The films produced by using 3-indole-(*trans*)acrylic acid and *trans*-sinapinic acid appeared similar to Figure 3.3c. They had similar properties with respect to

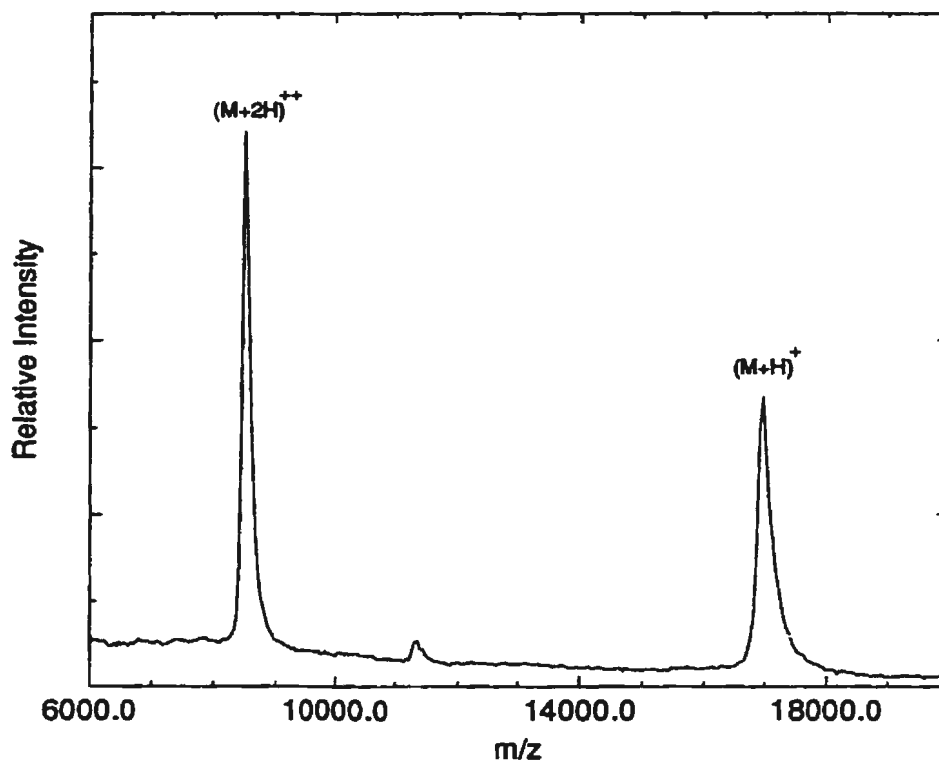


Figure 3.6: A laser desorption TOF mass spectrum of horse skeletal muscle myoglobin (mol. mass = 16951 u) taken from an 4-HCCA polycrystalline film. The singly and doubly charged ion species are shown. Solution B was 5:3:2 (aqueous 0.1 % trifluoroacetic acid):(acetonitrile):(glycerol) (v/v/v) containing 0.5 μ M myoglobin. This spectrum represents the sum of transients recorded for 30 consecutive laser shots.

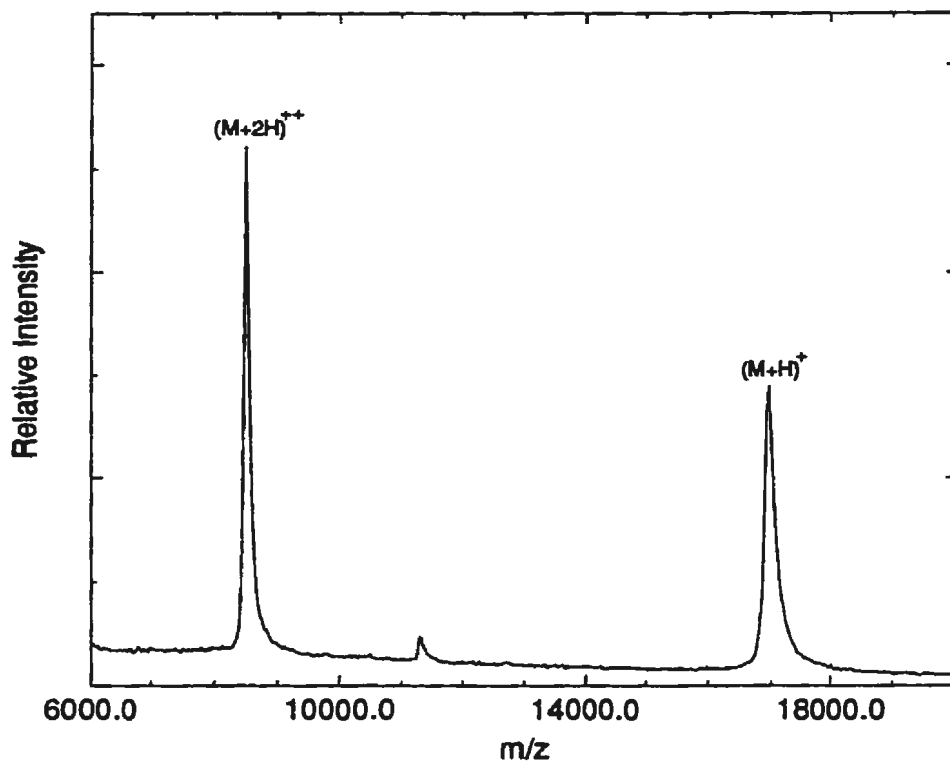


Figure 3.7: A laser desorption TOF mass spectrum of horse skeletal muscle myoglobin (mol. mass = 16951 u) taken from an 4-HCCA polycrystalline film. The singly and doubly charged ion species are shown. Solution B was 2:1 (aqueous 6 M urea):(acetonitrile)(v/v) containing 1.0 μ M myoglobin. This spectrum represents the sum of transients recorded for 30 consecutive laser shots.

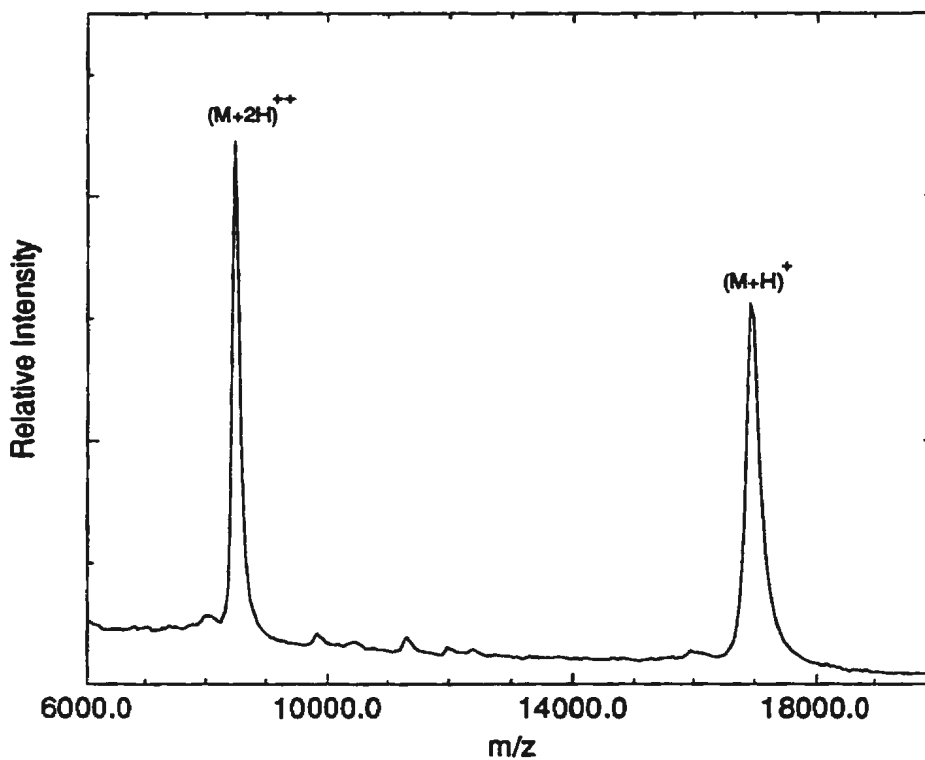


Figure 3.8: A laser desorption TOF mass spectrum of horse skeletal muscle myoglobin (mol. mass = 16951 u) taken from an 4-HCCA polycrystalline film. The singly and doubly charged ion species are shown. Solution B was 2:1 (1 M NaCl):(acetonitrile)(v/v) containing 0.5 μ M myoglobin. This spectrum represents the sum of transients recorded for 30 consecutive laser shots.

involatile liquid components and produced strong protein ion signals. These spectra are not shown here because they only repeat those shown in Figures 3.5-3.8. The polycrystalline film produced by using 2,5DHB showed different morphology from the other films. It was composed of small crystals, which were 4-5 times smaller than the crystals formed by the dried-droplet method, but were still distinguishable under an optical microscope. Careful observation showed that the smeared crystals from solution A were partially dissolved after the solution B was placed on the sample stage. Since 2,5 DHB is a highly water soluble matrix, it is easily washed off from the sample stage when the sample stage is immersed in water to remove involatile liquids and additives (Figure 3.2). Water soluble matrices, such as 2,5DHB, are therefore not suitable for polycrystalline film sample preparation.

A series of experiments was carried out to determine whether the nuclei formed by smearing the first deposit were acting as simple particulate nuclei or whether their crystal structure was important in film formation. A deposit of a particular matrix in Solution A was used as a base, and the second deposit of a different matrix in Solution B was placed on the base to see if film would grow. No films were formed using permutations of the matrices listed above. This result strongly suggests that a supersaturated solution nucleates much more readily when crystals of the solute are present. The effects produced by the presence of a seed crystal have been called secondary nucleation [59, 60]. If the smeared deposit was acting simply as a collection of particles, its chemical composition should not alter its efficacy in producing films.

3.4 Discussion

The results presented above suggested that the matrix has a special role in the

dried-droplet sample preparation method. Co-crystallization of matrix and analyte from matrix saturated solutions serves as an analyte purification step, since only the polypeptide molecules enter the crystal, excluding most other contaminants. Experiments involving growing polypeptide-doped sinapic acid crystals from solutions containing involatile liquids [54] provided a rationale for this purification process. This purification mechanism appears to work well over a broad range of analyte and contaminant concentrations [55, 56]. A laser-generated phase transition in the matrix crystals produces the MALDI effect [47].

In the dried-droplet method, matrix crystals begin to form as the most volatile solvent components evaporate. The most volatile component is typically an organic solvent such as methanol or acetonitrile. It is necessary that the matrix compound's solubility decreases as the volatile solvent evaporates. Crystallization continues as the droplet dries. The concentrations of the analyte and soluble contaminants increase as the droplet volume decreases, resulting in a highly concentrated solution as the last volatile solvent components disappear. It is this surface layer, grown at ill-defined analyte and contaminant concentrations, that is actually examined by the laser. Often the matrix can exclude the contaminants, or minimize their effects on the resulting surface layer, resulting in an analytically useful sample surface. Unfortunately, situations arise where highly concentrated contaminants interfere with matrix crystallization/analyte inclusion, resulting in low quality samples.

Based on the above discussion of dried-droplet sample preparation, it seems clear that it would be difficult to prepare truly reproducible samples from the dried-droplet method. The evaporation of solvent may cause trace contaminants to become important solutes during the growth of the surface layer of the sample crystals.

Much more reproducible results should be obtained from growing matrix crystals under near equilibrium conditions in a mother liquor containing both matrix and

analyte. Such a method of sample preparation, producing large matrix/protein crystals, is possible but is time consuming and uses larger amounts of analyte than the dried droplet method [23]. Experiments involving the growth of large matrix/protein crystals have shown that proteins can be preferentially extracted into matrix crystals from solutions containing high concentrations of glycerol or dimethylsulfoxide[54]. Crystals grown in this manner are useful samples if they are large enough to be easily washed prior to laser analysis.

Rapidly grown polycrystalline films, as described in this chapter, represent a different approach to creating a sample unaffected by evaporation of solvent in drying droplets. As opposed to slowly growing large crystals in nearly equilibrium conditions, the fabrication of polycrystalline films uses auxiliary seed sites to control a rapid crystallization process [61, 62]. Crystal nucleation at the air-liquid interface is replaced by secondary nucleation arising from the layer on the surface of the substrate. Microcrystals form inside the bulk solution, where solution concentrations change slowly. The film adheres to the surface, so the crystallization can be halted by washing off the droplet before its volume decreases significantly. The small size of crystals in the film means that the laser illuminates many crystals and crystal orientations at once, resulting in more uniform ion emission. The entire film can be considered as a single device, with ion emission characteristics that are the average of the ensemble of microcrystal structures and orientations. This is the most important feature of the polycrystalline film method compared to the dried droplet method. The films are much more uniform than dried-droplet deposits with respect to analyte ion production.

Another significant feature of the film growth protocol described above is its operational similarity to that of the dried-droplet method. Films that produce intense protein-ion currents can be grown in the presence of high concentrations of involatile

solvents without any pre-purification. These films adhere firmly to the substrate, allowing easier washing of the film compared to dried-droplet deposits.

The polycrystalline film method described in this chapter is the first successful approach to improve MALDI sample preparation. The method has been widely adopted in the field of MALDI applications. Many users have viewed this method as a major development in the study of MALDI.

Chapter 4

Effects on MALDI Performance of Protein/Matrix Molar Ratio

As mentioned above, sample preparation in MALDI involves co-crystallization of the analyte molecule with an excess of low mass, light-absorbing, organic molecules - the matrix. It has been demonstrated that a number of compounds from different chemical classes are suitable as matrices in MALDI. In this chapter the influence of initial matrix concentration on analyte ion yields and the mass resolution of the molecular ion signals are investigated. The results of the investigations are explained in terms of a proposed mechanism.

4.1 Phenomenological Description of Laser-Induced Thermal Desorption

To generate ions in MALDI, analytes must be desorbed and, at some point, ionized. Several recent papers have presented theoretical investigations on the process of molecules ablated from an energized matrix [47, 48, 52, 63, 64]. All these investigations have tried to answer the question: How can large molecules be transferred to the gas phase without fragmentation and degradation? Energy deposition and redistribution processes have been considered as a key factor in the description of MALDI mechanisms. The sequence of processes is proposed to be as follows: absorption of UV radiation by the crystal; rapid energy transfer into the lattice; thermal sublimation of the matrix; followed by a dense gas of matrix carrying the analyte

molecules embedded in it away from the surface. In this section a kinematic model for the above process is presented. The model is due to discussion in the book “Laser Beam Interactions with Materials” [65].

The temporal distribution of a laser pulse at the sample is not uniform in time, but approximates a Gaussian distribution function:

$$I(t) = I_0 \exp[-(t - t_0)^2/\tau_p^2] \quad (4.1)$$

where I_0 is the peak of the laser pulse irradiance (in Wcm^{-2}), t_0 is the time at peak power of the pulse and τ_p denotes for the halfwidth of the pulse.

The UV radiation falling on the crystal surface is absorbed in layers with a thickness of l , and results in electronic excitations in those layers. The thickness l can be related to the inverse of the absorption coefficient α . In nicotinic acid, for example, α is $4 \times 10^4 \text{ cm}^{-1}$, leading to a value for l between 0.1 to 1.0 μm . Through very fast internal conversion processes, the electronic excitation leads to internal vibrational excitation, and these internal vibrations are transferred to lattice vibrations. The characteristic time for this process ranges from 10^{-9} to 10^{-12} s [66].

If one assumes that the absorbed UV radiation energy of nanosecond laser pulses is instantaneously transformed to thermal molecular motion, the standard heat equation can be applied to describe the crystal heating dynamics of the matrix. Consider a homogeneous crystal in the form of a slab between the planes $z=0$ and $z=L$. The slab is assumed to be thermally insulated, so that no heat flow across the boundaries is allowed. The laser beam is incident onto the plane $z=0$. This situation can be described by

$$\frac{\partial T}{\partial t} = D \nabla^2 T + \frac{\alpha}{c_p \rho} I(t) e^{-\alpha z} \quad (4.2)$$

where $I(t)$ is the incident irradiance, D is the thermal diffusivity of the medium (in m^2s^{-1}), c_p is the specific heat of the medium (in $\text{Jkg}^{-1}\text{K}^{-1}$), α is the absorption

coefficient of the medium and ρ is the density of the medium (in kg m^{-3}). Assuming that all the absorbed energy is converted into heat and taking into account the fact that the heat has no time to penetrate into the sample during a laser pulse of length $\tau \leq 10^{-8}$ s, the temperature rise on the crystal surface ΔT can be evaluated by

$$\Delta T = \frac{\alpha \Phi}{c_p \rho} \quad (4.3)$$

where $\Phi = \int I(t)dt$ is the laser fluence (in J cm^{-2}). Equation (4.3) implies that the temperature change ΔT at a fixed laser power is proportional to the absorption coefficient α . The heat flow equation (4.2) can be solved by using a Green's function technique [67]. For the influence of a uniform penetrating light source with I_0 irradiance the rise of surface temperature, ΔT , at time t is [65]

$$\Delta T(t) = \frac{I_0}{K} \left\{ \frac{\delta}{\sqrt{\pi}} - \frac{1}{\alpha} \left[1 - \exp\left(\frac{\alpha\delta}{2}\right)^2 \text{erfc}\left(\frac{\alpha\delta}{2}\right) \right] \right\} \quad (4.4)$$

where the diffusion length $\delta = 2\sqrt{Dt}$ and the thermal diffusivity $D = K/c_p\rho$; here K , ρ and c_p are the thermal conductivity (in $\text{Wm}^{-1}\text{K}^{-1}$), the density and the specific heat of the material, respectively. The molecular desorption rate constant W , depends greatly on the temperature, as described by the Arrhenius law

$$W = \nu_l \exp[-E/k(T_0 + \Delta T)] \quad (4.5)$$

where $\nu_l = 10^{12} - 10^{14} \text{ s}^{-1}$ is the typical lattice vibration frequency, E is the binding energy of a molecule on the surface in the crystal and T_0 is the initial temperature. The rate of sublimation of the molecules from the heated layers is, therefore, given by

$$dN_g/dt = N_s W \quad (4.6)$$

where N_g is the number of molecules in the gas phase adjacent to the surface and N_s is the number of molecules on the surface, per unit area.

It has been shown experimentally that molecules can be desorbed intact and with relatively little internal energy at high heating rates, whereas they decompose at low heating rates [68]. Numerical calculations for the case of adenine crystals [66] and nicotinic acid [48] indicated that the rates required to desorb molecules without fragmentation are in excess of 10^8 K/s.

To explain the observation that guest molecules do not fragment and degrade, it was proposed [47, 48] that highly excited host molecules and lattice vibrations would undergo adiabatic cooling during sublimation and energy transfer to the guest molecules during sublimation would be low enough to prevent decomposition.

To treat energy redistribution between the matrix and analyte, the energy density of the incident irradiance, ρe , is partitioned in the following way [48]:

$$\rho e = (1 - x)H + L + xG + B \quad (4.7)$$

where H , L , G and B denote the energy density content of the host molecules, of the lattice and of the guest, and the energy density used for bond breaking, respectively; x is the volume fraction of the guest molecules. For easily comparing the discussion here to that in the literature, the energy density of the incident irradiance is notated as ρe , as used in the literature.

The area of the volume element heated by the laser is considered to be determined by the laser beam cross section. Its thickness is proportional to the inverse of the host absorption coefficient, α_H^{-1} . Therefore, the increase in energy density in this volume due to laser heating is given by:

$$\frac{d(\rho e)_{heat}}{dt} = \frac{\alpha_H + \alpha_G}{\sqrt{\pi}} I(t). \quad (4.8)$$

Here, $I(t)$, the laser irradiance, is expressed by Equation (4.1), and α_H and α_G are the effective absorption coefficients of the host and guest (weighted by their concentrations).

In the power density regime discussed above, there are two main mechanisms to cool the excited volume: phase transformation and heat conduction. In terms of the enthalpies of the possible phase transition processes, the two most effective cooling phase transitions are considered to be sublimation and evaporation.

The cooling rate, expressed by the phase transition enthalpy, ΔH_{phtr} , and temperature, T_{phtr} is written as [48]

$$\frac{d(\rho e)_{cool}}{dt} = \frac{\alpha_H p_0 \Delta H_{phtr}}{\sqrt{2\pi MRT}} \exp \left[\frac{\Delta H_{phtr}(T_L - T_{phtr})}{RT_L T_{phtr}} \right] \quad (4.9)$$

where p_0 is the ambient pressure; T_L is the lattice temperature and M is molecular mass.

In the kinetic equations for energy redistribution, the energy exchange terms are proportional to the energy differences and are given by

$$\frac{dH}{dt} = \frac{\alpha_H}{\alpha_H + \alpha_G} \frac{d(\rho e)_{heat}}{dt} - \alpha_{HL}(H - L) - \alpha_{HG}(H - G) - \alpha_{HB}H \quad (4.10)$$

$$\frac{dL}{dt} = \alpha_{HL}(H - L) - \alpha_{LG}(L - G) - \frac{d(\rho e)_{cool}}{dt} \quad (4.11)$$

$$\frac{dG}{dt} = \frac{\alpha_G}{\alpha_H + \alpha_G} \frac{d(\rho e)_{heat}}{dt} + \alpha_{HG}(H - G) + \alpha_{LG}(L - G) - \alpha_{GB}G \quad (4.12)$$

and

$$\frac{dB}{dt} = \alpha_{HB}H + \alpha_{GB}G. \quad (4.13)$$

Here, α_{HL} , α_{HG} , α_{HB} , α_{LG} , and α_{GB} are the host-lattice, host-guest, host-bond-breaking, lattice-guest, and guest-bond-breaking energy transfer coefficients, respectively. It is assumed that all of the processes except bond breaking are reversible.

The physical situation described by these equations can be explained as follows. The laser radiation electronically excites the host and, with a lower cross section, the

guest molecules. Fast internal conversion processes of the electronic excitation leads to internal vibrational excitation. At a given rate (α_{HL}) these internal vibrations are transferred to lattice vibrations and are also channeled directly to guest vibrations (α_{HG}). The lattice is cooled by the phase transformation and transfers energy to the guest molecules (α_{LG}). The guest heating rate is determined by direct light absorption and energy transfer from both the lattice and directly from the host molecules. Both the host and the guest molecules are subject to irreversible fragmentation, which consumes some part of the energy.

The energy transfer rate coefficients in Equations 4.10 - 4.13 are similar to those used for a guest molecule physisorbed on a host in Ref. [69]. The role of the physisorption bond in Ref. [69] is played here by hydrogen bonds and van der Waals interactions between the host and the guest molecules. The resulting energy transfer coefficients are given by:

$$\alpha_{HL} = \nu_H \exp(-\xi_{HL}) \quad (4.14)$$

$$\alpha_{HG} = \nu_H C_G \exp(-\xi_{HG}) \quad (4.15)$$

and

$$\alpha_{LG} = \nu_L C_G \exp(-\xi_{LG}). \quad (4.16)$$

Here C_G is the fractional volume concentration of guest molecules, $C_G = x/(1 - x)$, and ξ_{HL} , ξ_{HG} and ξ_{LG} are adiabaticity parameters [69]. It is the appearance of the guest concentration ratio, C_G , in Eqns (4.15) and (4.16) that leads to its role as a critical parameter. Too high a value of C_G leads to increased lattice/guest and host/guest molecular coupling.

Computational results [48] based on the above model suggest that the crucial kinetic competition is between cooling by sublimation of the host molecules and energy transfer to the guest molecules. The highest possible rate of sublimation

could be achieved by increasing the surface-to-volume ratio, using a host matrix with a low sublimation temperature and using a laser pulse short enough to promote volatilization instead of degradation. The rates of energy transfer to the guest could be reduced by using a subcritical concentration of the guest molecules, and using a matrix host molecule with poor frequency overlap with the frequencies of the guest molecule. In this chapter we investigate the empirical support for energy deposition and redistribution processes of MALDI mechanisms. While it is understood that the matrix plays an essential role in MALDI performance, a quantitative evaluation of matrix concentrations on MALDI performance has not been done. The present investigation focuses on the influence of matrix concentrations on both the analyte ion yield and the mass resolution. The significance of the investigation is to provide not only empirical tests of proposed MALDI mechanisms, but also to investigate how to optimize MALDI performance using proper ratios of matrix/analyte.

4.2 Experiment and Results

The matrix materials used in the present study, such as sinapinic acid, ferulic acid, α -cyano-4-hydroxycinnamic acid, were the same as that used in Chapter 3. In addition, 2,5-dihydroxybenzoic acid (gentisic acid, 2,5DHB) (lot# JY03202JX) [23], obtained from Aldrich Chemical Company, Inc, was used. All of the matrices were purchased from commercial chemical suppliers, and used without further purification. The protein used was horse skeletal muscle myoglobin. Deionized water was prepared with a Millipore cartridge system. Acetonitrile (MeCN) and ethanol were obtained from Fisher Scientific. Trifluoroacetic acid (TFA) was obtained from Sigma Chemical Co..

Appropriate amounts of matrix were dissolved in premixed solvents to give the different concentrations of matrix solutions. The solvent for sinapinic acid, ferulic acid and 4-HCCA was 2:1 (v/v) 0.1% aqueous TFA:MeCN, and was used to produce concentrations of matrix in solution from 10 mM to 200 mM. Gentisic acid was dissolved in 7:1 (v/v) pure ethanol:0.1% aqueous TFA, to give concentrations of matrix in solution from 25 mM to 175 mM. Myoglobin was dissolved in 0.1% aqueous TFA at a concentration of 10 μ M. MALDI sample preparation was performed in the following manner. The analyte solution was mixed with an equal volume of matrix solution. 1 μ L of mixture was deposited onto a stainless steel probe tip and stirred with the tip of a stainless steel tweezer until a layer covering the target was observed. The sample was then allowed to dry completely in air. The total quantity of myoglobin deposited on the target was approximately 5 pmol for all experiments. As compared with unstirred samples, which mainly dried to give irregular crystals distributed along the rim of a circular region for 2,5DHB and ferulic acid, the stirring procedure produced many smaller microcrystals uniformly distributed over the target surface, improving the reproducibility of mass spectra. In the case of 2,5 DHB, use of ethanol rather than MeCN also helped produce a homogeneous sample layer.

The mass spectrometer was operated in the linear mode with an ion acceleration voltage of 30 kV. The laser power was 30% above the threshold for each matrix and unchanged through all concentrations of the matrix. The mass spectra presented here have been accumulated over 20 laser pulses. The concentrations of matrix solutions studied in this chapter, and the molar ratios of matrix/protein in each sample, are summarized in Table 4.1. For each matrix, minimum and maximum concentrations of matrix in its solution, listed in the Table, correspond respectively to the limit of detection of analyte ions on MALDI and to the solubility limit at room temperature. Six typical TOF mass spectra of myoglobin mixed with the different concentrations

Table 4.1: Summary of matrix solution concentrations

4HCCA (mM)	Ferulic acid (mM)	Sinapinic acid (mM)	2,5DHB (mM)	Molar ratio of matrix/protein in sample
10	10			1000
			25	2500
30	30	30		3000
50	50	50	50	5000
70		70		7000
			75	7500
80				8000
100	100	100	100	10000
		140		14000
	150	150	150	15000
			175	17500
	200			20000

of matrix solution for each of 2,5DHB, 4HCCA, and sinapinic acid, are shown in Figures 4.1, 4.2, and 4.3, respectively. In all spectra, the major peaks observed correspond to the singly and doubly charged analyte molecular ions.

Figures 4.1 - 4.3 demonstrate that the intensities of the analyte ion peaks increase gradually with an increase in concentration of matrix solution using a fixed laser fluence, and then decrease slightly as the concentration of matrix solution continues to increase. This general trend is demonstrated more clearly in Figures 4.4, 4.5 and 4.6 for the different matrices by plotting the ion yield of analyte against the matrix to analyte molar ratio. Each point in Figures 4.4 - 4.6 represents an average of 6 - 9 replicate experiments on the same sample surface. Error bars indicating standard deviations are also shown. This investigation however, could not be extended to much lower matrix concentrations (<10 mM), as no analyte molecular ions were observed for the laser fluence available. Figures 4.4 and 4.6 show that the protein ion intensity increases with increasing matrix concentration in the sample and reaches a plateau around a molar ratio of $\sim 10^4$.

The effect of matrix concentration on the resolution of the mass spectrum was also investigated by measuring the full-width at half-maximum (FWHM) of the analyte molecular ion peaks. This investigation was motivated by the observation of unsymmetric myoglobin ion peaks, especially using 2,5DHB and sinapinic acid as matrices. Spectra were obtained from six - nine spots on each of the samples, then the mass resolutions (FWHM) were measured for each of the spectra and averaged for each of the concentrations of matrix solution. The results are presented in Figures 4.7, 4.8 and 4.9 for 2,5DHB, 4HCCA and sinapinic acid, respectively. These figures show that the molecular ion peaks were broadened, and the mass resolution correspondingly decreased, as the matrix concentration was increased. Similar observations have been made by Shannon Cornett *et al.* [70] for gramicidin D (≈ 1881 u) in a binary matrix,

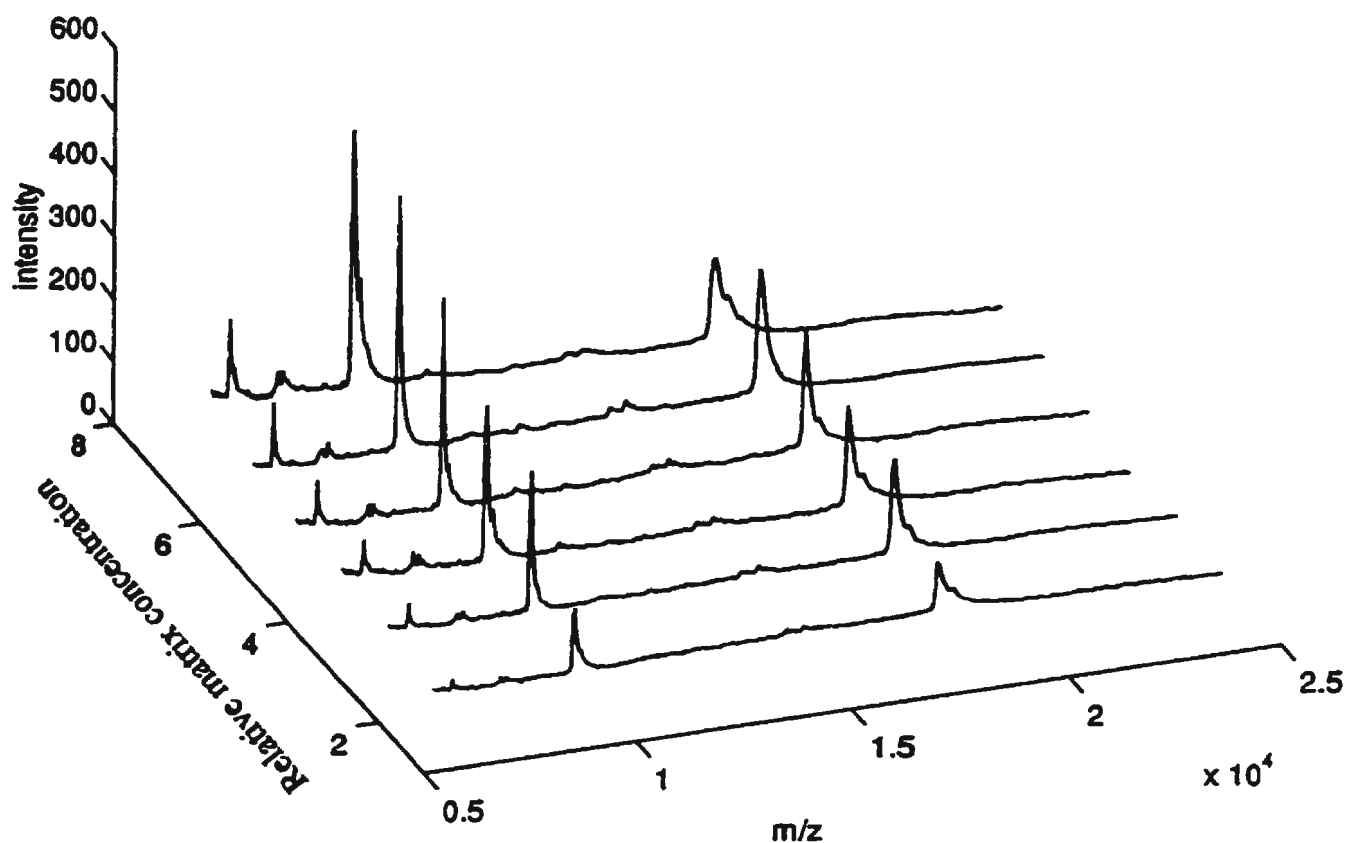


Figure 4.1: The positive ion TOF mass spectra of horse skeletal muscle myoglobin (mol. mass = 16951 u) in solutions of 2,5DHB matrix of different concentration at fixed laser power. The amount of myoglobin in each sample was approximately 5 pmol. The singly and doubly charged ion species are shown. Each spectrum represents the sum of transients recorded for 20 consecutive laser shots.

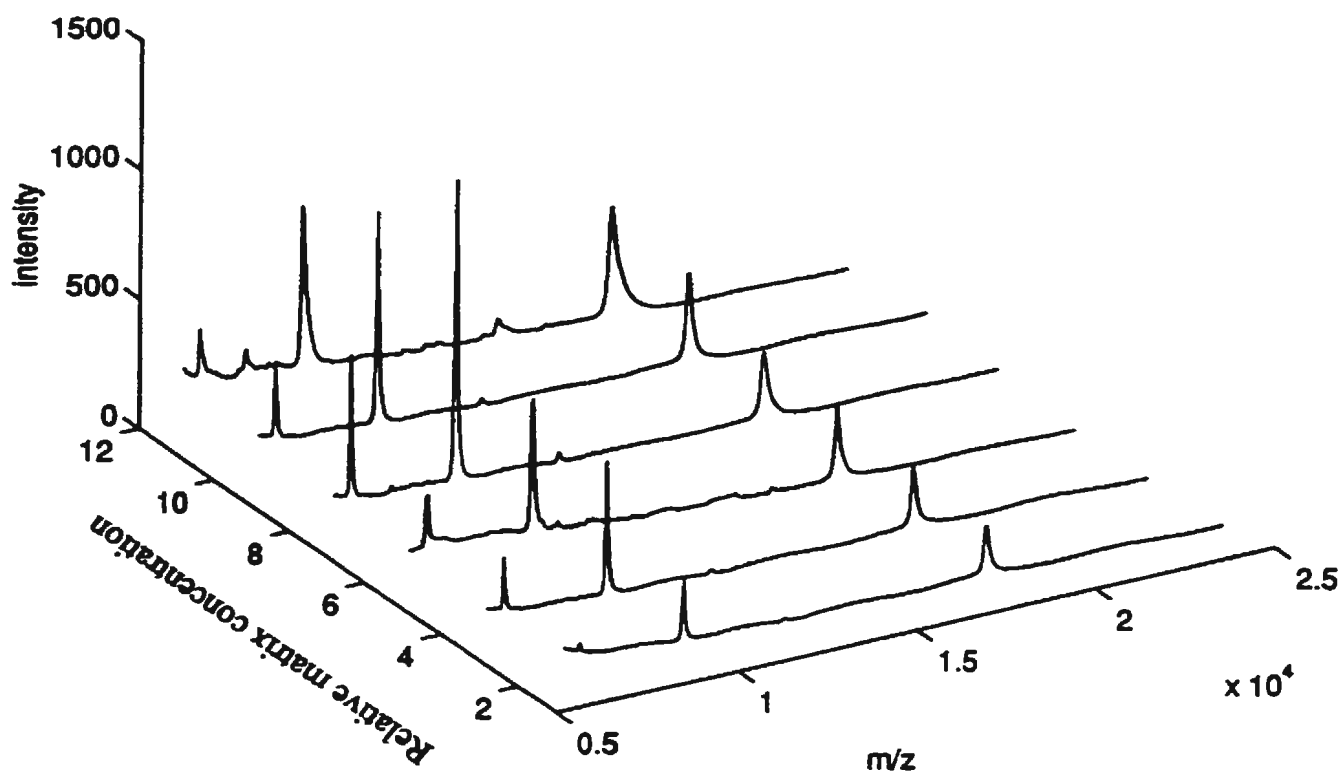


Figure 4.2: The positive ion TOF mass spectra of horse skeletal muscle myoglobin (mol. mass = 16951 u) in solutions of 4HCCA matrix of different concentration at fixed laser power. The amount of myoglobin in each sample was approximately 5 pmol. The singly and doubly charged ion species are shown. Each spectrum represents the sum of transients recorded for 20 consecutive laser shots.

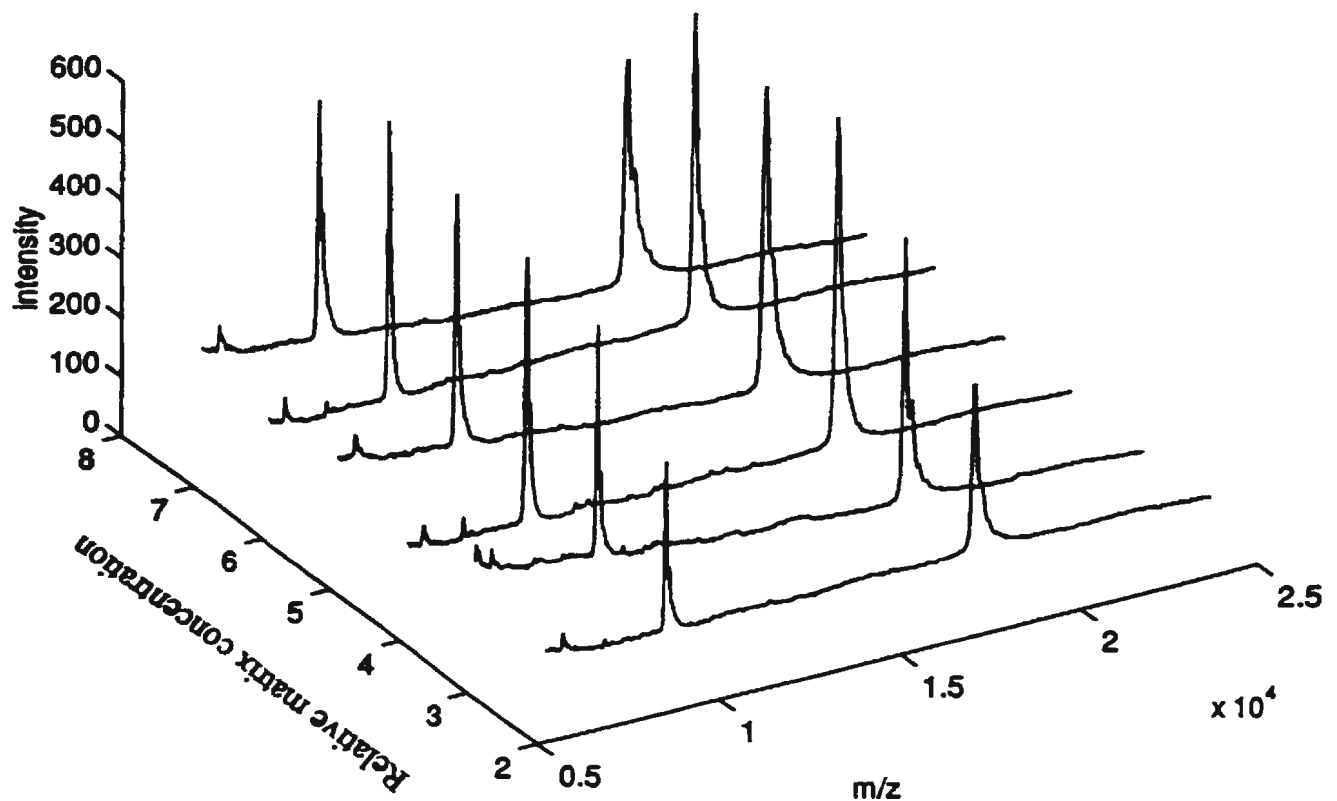
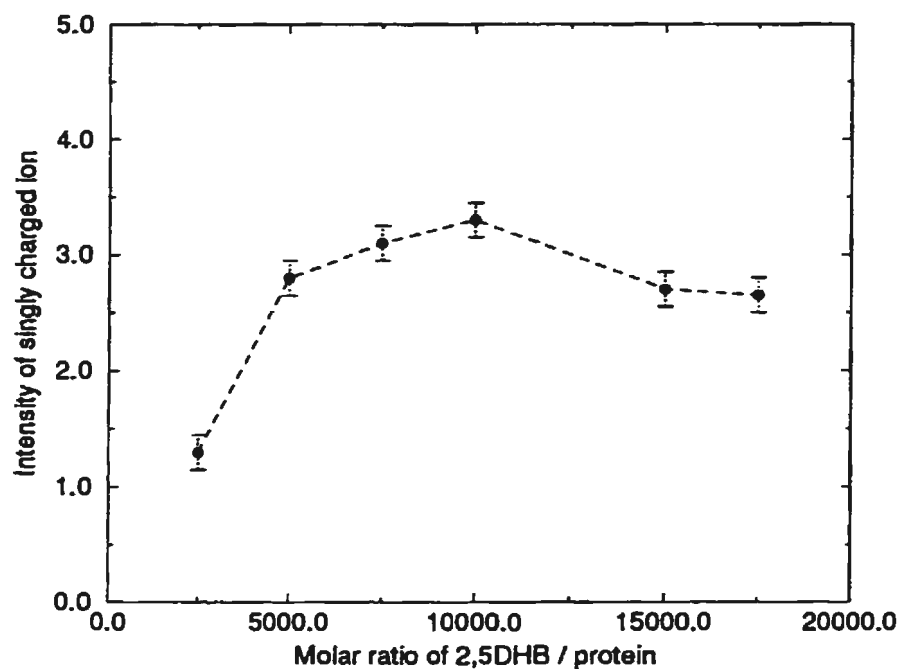
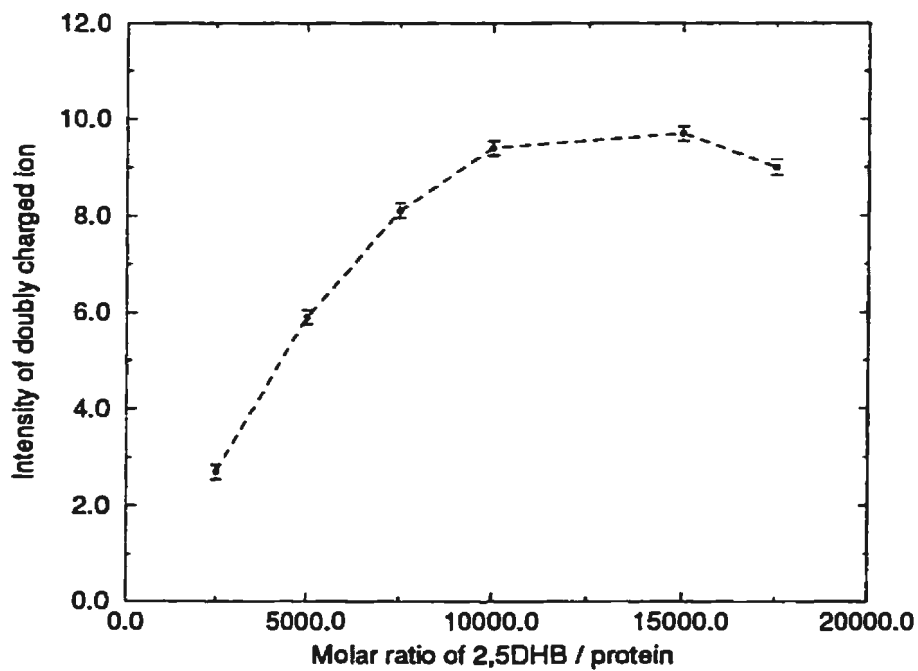


Figure 4.3: The positive ion TOF mass spectra of horse skeletal muscle myoglobin (mol. mass = 16951 u) in solutions of sinapinic acid matrix of different concentration at fixed laser power. The amount of myoglobin in each sample was approximately 5 pmol. The singly and doubly charged ion species are shown. Each spectrum represents the sum of transients recorded for 20 consecutive laser shots.

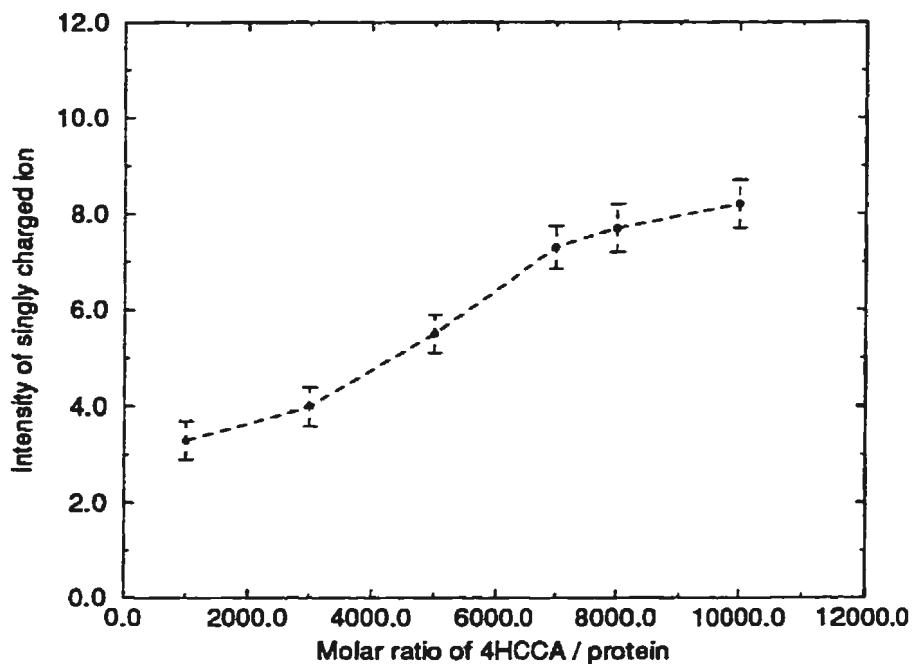


(a)

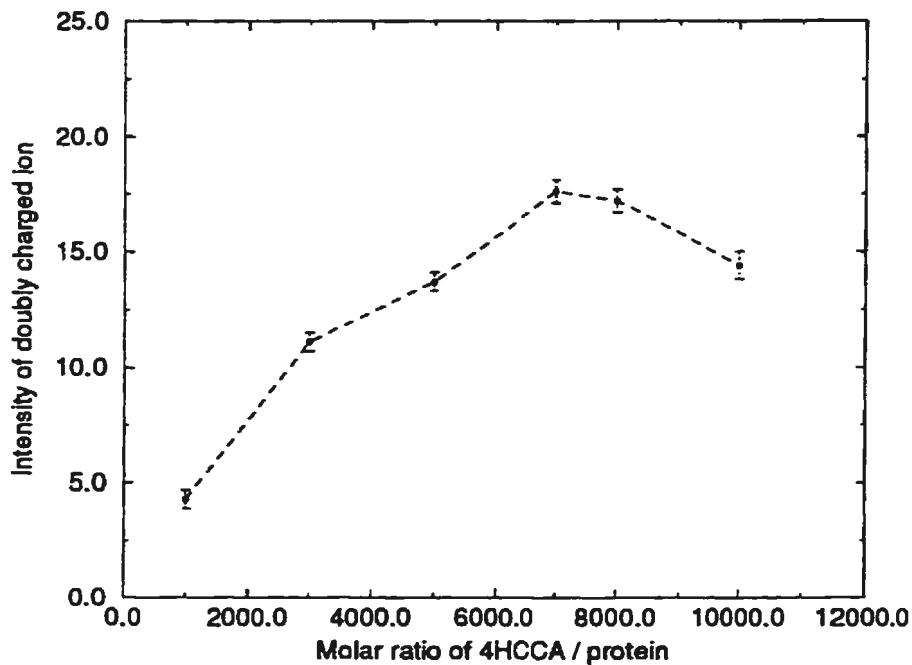


(b)

Figure 4.4: Plots of the ion yield of myoglobin versus the 2,5DHB to myoglobin molar ratio for singly (a) and doubly (b) charged molecular ions. The amount of myoglobin in each sample was fixed at approximately 5 pmol.

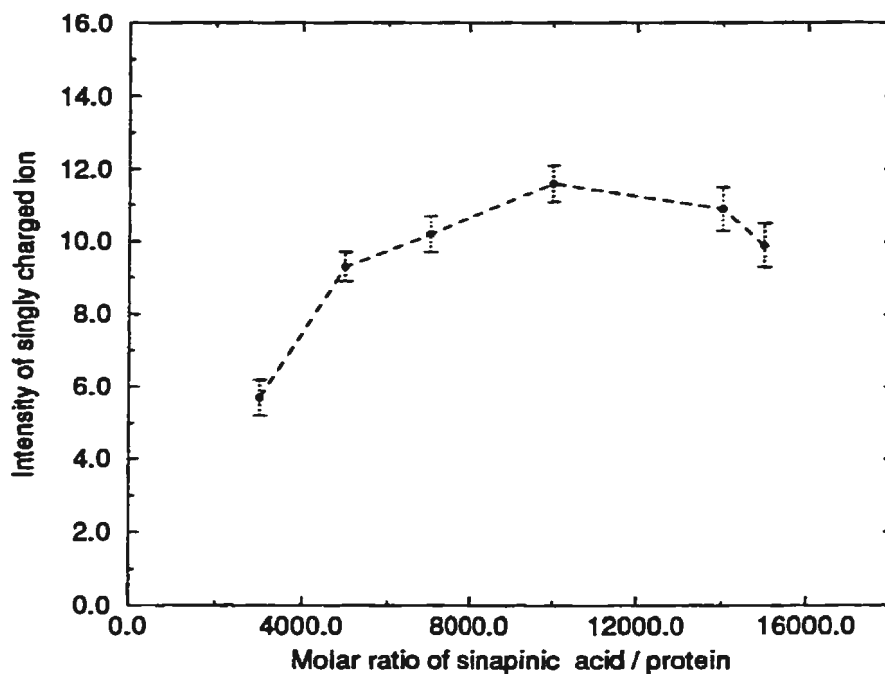


(a)

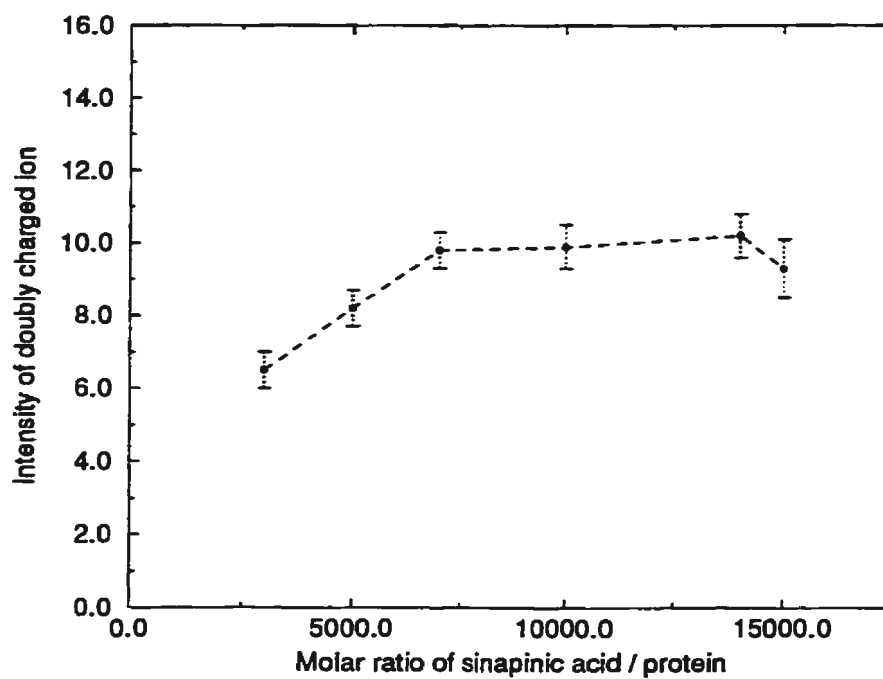


(b)

Figure 4.5: Plots of the ion yield of myoglobin versus the 4HCCA to myoglobin molar ratio for singly (a) and doubly (b) charged molecular ions. The amount of myoglobin in each sample was fixed at approximately 5 pmol.

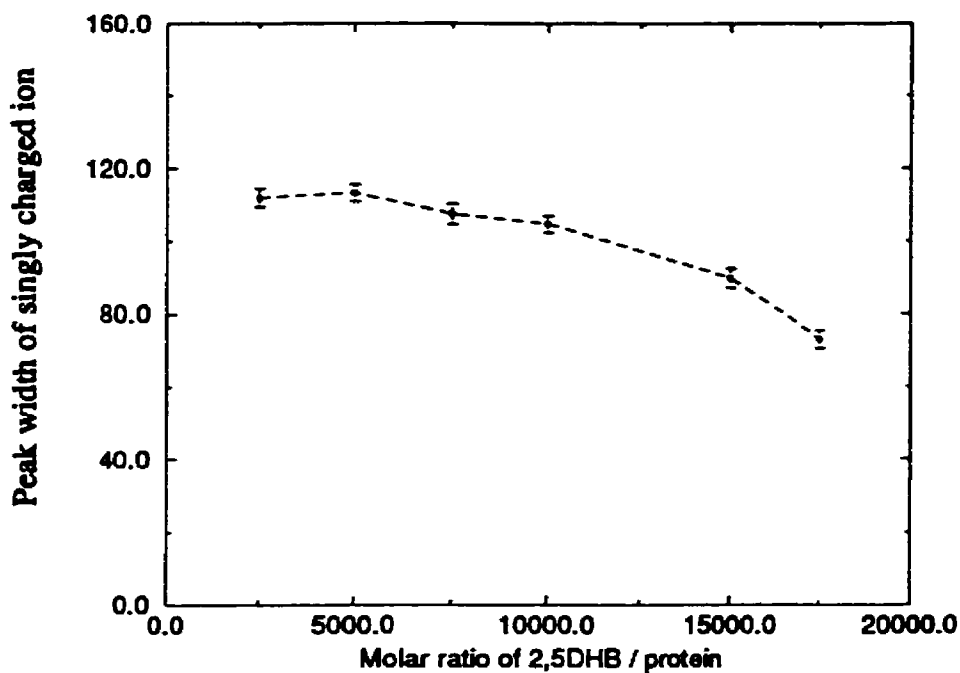


(a)

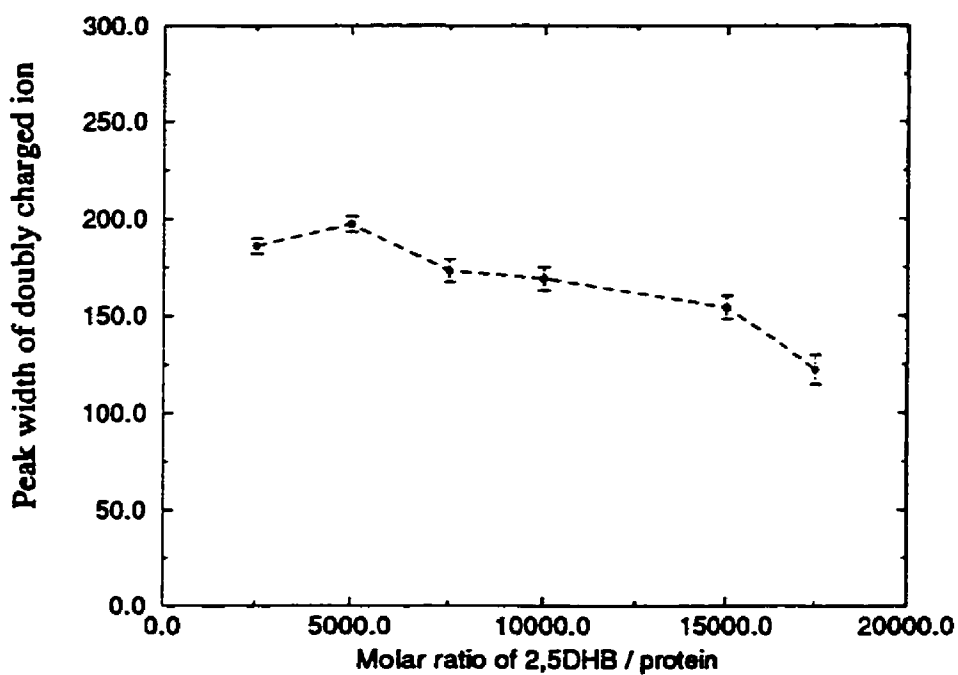


(b)

Figure 4.6: Plots of the ion yield of myoglobin versus the sinapinic acid to myoglobin molar ratio for singly (a) and doubly (b) charged molecular ions. The amount of myoglobin in each sample was fixed at approximately 5 pmol.

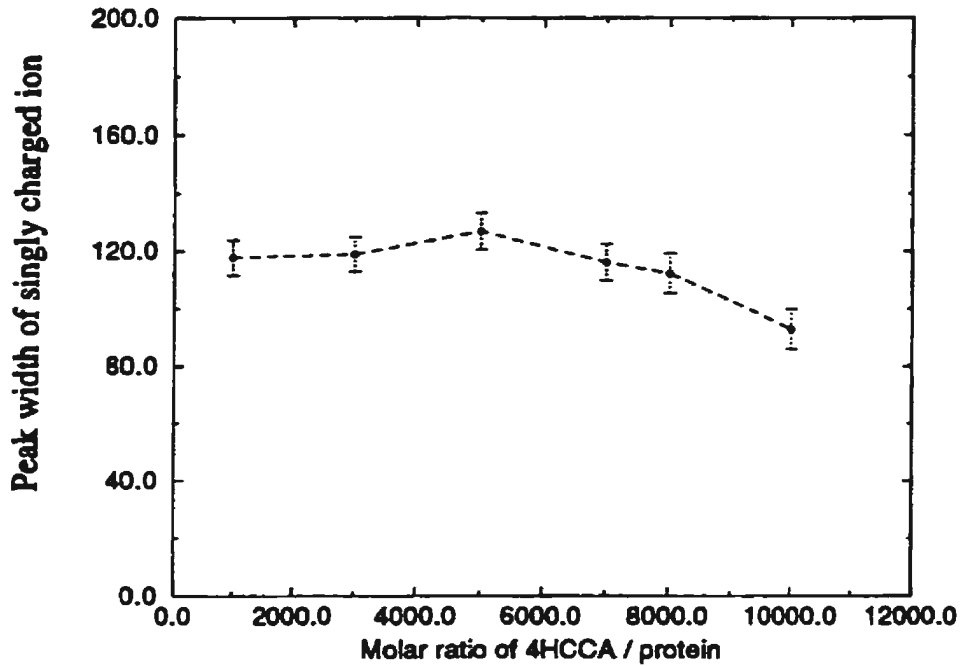


(a)

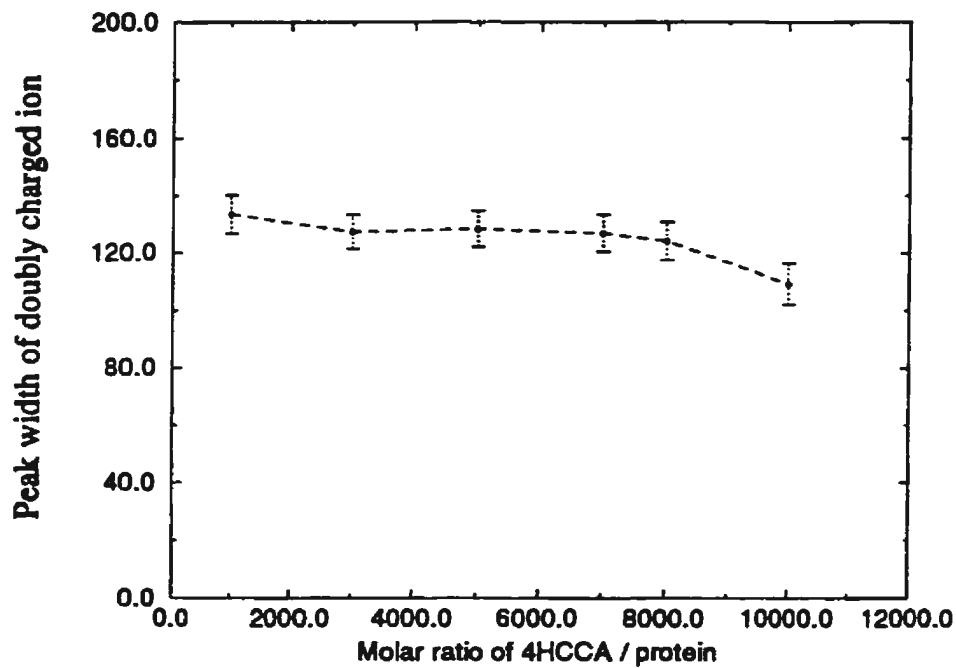


(b)

Figure 4.7: Plots of the measured peak widths (FWHM) versus molar ratio of 2,5DHB to myoglobin for singly (a) and doubly (b) charged molecular ions. Spectra were obtained from 6-9 spots on each of the samples, then peak widths (FWHM) were measured for each of the spectra, and averaged.

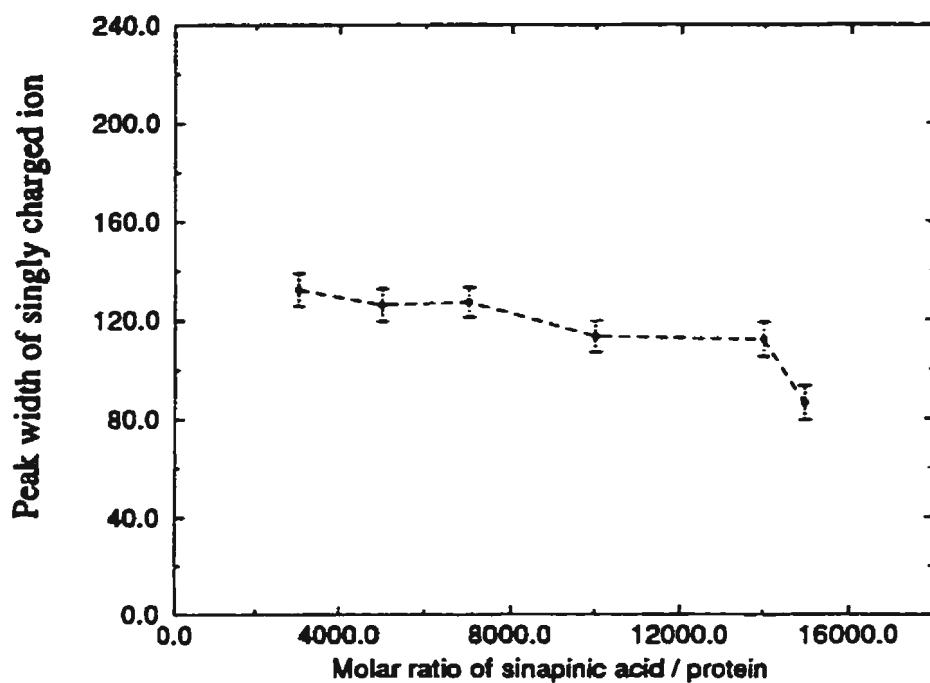


(a)

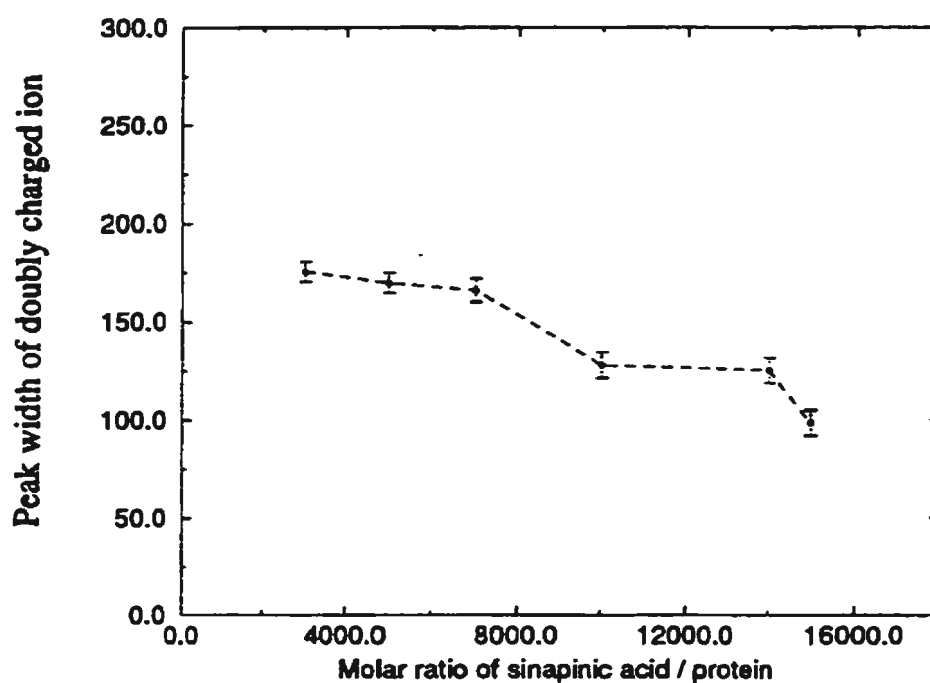


(b)

Figure 4.8: Plots of the measured peak widths (FWHM) versus molar ratio of 4HCCA to myoglobin for singly (a) and doubly (b) charged molecular ions. Spectra were obtained from 6-9 spots on each of the samples, then peak widths (FWHM) were measured for each of the spectra, and averaged.



(a)



(b)

Figure 4.9: Plots of the measured peak widths (FWHM) versus molar ratio of sinapinic acid to myoglobin for singly (a) and doubly (b) charged molecular ions. Spectra were obtained from 6-9 spots on each of the samples, then peak widths (FWHM) were measured for each of the spectra, and averaged.

and by Perera *et al.* [71], with bovine insulin (5733.5 u) in coumarin 152.

The deposit produced using ferulic acid as the matrix showed morphology similar to that obtained with 2,5DHB. The results were similar to those for sinapinic acid, and are not shown here because they only repeat those shown in Figures 4.3, 4.6 and 4.9.

4.3 Discussion

On the basis of the results presented above, two categories of matrix effects can be identified, based on the influence of increasing matrix concentration on analyte ion yield [72].

The first category, essentially physical effects, involves the energy deposition and redistribution processes. The matrix molecules dominate the process of energy deposition. The process is known to be a bulk process rather than a monolayer event [46]. The number of matrix molecules in the heated crystal layers, N_s , in Equation 4.6, can be an important factor in the process of matrix sublimation. The number of matrix molecules absorbing the laser energy depends on the film thickness and the concentration ratio of matrix to analyte. Film thicknesses were determined from the concentration and volume of solution deposited. With this knowledge, and the assumption of uniform film distribution, plus matrix density estimates of $\sim 1 \text{ g cm}^{-3}$, average film thicknesses were estimated to vary from several hundred nanometers to several micrometers in this study. By combining the calculations of the film thickness and the results shown in Figures 4.4-4.6 it is believed that, as the concentration of matrix solution and thus the film thickness increased, more matrix material was ejected into the gas phase by a laser pulse. This hypothesis is fairly well supported

by the recent qualitative study of MALDI desorption by means of the associated acoustic signal [38].

In addition to the effect of matrix solution concentration (i.e. of total quantity of matrix in the MALDI sample) on energy deposition, it is also necessary to discuss its effect on energy redistribution. As the ratio of matrix to analyte in a sample increased, the rates of energy transfer for host-guest and lattice-guest, α_{HG} and α_{LG} defined in Equations 4.15-4.16, are reduced. Consequently the efficiency of the energy transfer into the crystal lattice is raised, and the rate of matrix sublimation is increased as well.

The second category, chemical effects, includes co-crystallization of the matrix and analyte, and photochemical ionization. Detailed studies of single crystals of sinapinic acid have recently shown that proteins are incorporated into the matrix crystal structure by preferential interaction with specific hydrophobic crystal faces [55]. Both hydrophobic and hydrophilic interactions between matrix and analyte molecules are undoubtedly affected by the relative concentrations of the matrix and analyte. In this hypothesis, it can be assumed that the number of matrix incorporation sites decreases as matrix solution concentration (and thus total quantity of matrix) decreases, resulting in a reduced density of proteins bonded to these planes of the crystal [55].

There is an unanswered question in the discussion thus far. How does matrix solution concentration (and thus matrix:analyte ratio) affect analyte ion formation, a prerequisite for mass analysis and detection in mass spectrometry? It is assumed that analyte ion formation takes place in the gas phase, in particular in the dense gas plume above the sample surface. Thermal ion formation is not likely in the case of large molecules because the required temperature would certainly destroy these molecules. However, photoionization of matrix molecules is feasible because

two photons of the most commonly used laser radiation in MALDI together provide enough energy to ionize many organic molecules. This photoionization process could also be more effective in the gas phase. In the clouds of ions and neutrals derived from matrix molecules and neutral analyte molecules, the photoionized matrix molecules become agents for chemical ionization of analyte molecules, and the latter behave as proton traps. In other words, analyte ionization takes place in the gas phase by proton transfer from matrix-derived ions or electronically excited matrix molecules to neutral analyte molecules. An investigation of the mechanism for proton transfer reactions in MALDI was recently conducted by Russell et al. [73]. They concluded that MALDI involves proton transfer reactions between excited states of matrix molecules and ground states of the analyte. If this picture is correct, it can be further hypothesized that, as the content of matrix in the sample increases, more matrix ions are produced in the gas phase. If the number of analyte molecules in the gas phase is constant, the increased abundance of matrix ions will increase the proton attachment reaction rate, and consequently enhance the analyte ion yield. The plateaus in Figures 4.4 and 4.6 can be explained by the saturation of the proton transfer process.

The decrease of the analyte ion intensities at very high matrix content is likely caused by the ejection of the matrix vapor plume from the front surface of the crystal. Studies of arrival-time distribution measurements for protonated ions clearly show that ions are formed over microsecond time periods following the initial laser pulse [74]. In the case of high concentration of matrix, the evaporated material could form a dense gas plume as indicated before. The particles ejected at early times could attenuate the laser radiation reaching the sample surface and thus minimize the energy deposition and photoionization processes.

It is observed in MALDI experiments that both analyte peak widths and intensities are dependent upon the laser fluence [36, 71, 75]. However, there may be many

other factors that influence the peak width and intensity. For instance, the width of the protonated ion signal for analyte was found to depend on the nature of the matrices [73]. Alternatively, the peak widths may be broadened as the result of unresolved ions, e.g. $[M + H]^+$ and $[M + Na]^+$, or matrix adducts [13, 70]. Based on the energy deposition and gas phase ionization model discussed before, it is believed that the present observations are related to the total energy deposited to the sample as well as the density of the material ejected by the laser irradiation. The results shown in Figures 4.7 - 4.9 can be explained by attachment of matrix molecules to analyte ions, since the analyte ion could experience a high density matrix plume at higher matrix concentrations, resulting in increased possibility of the attachment.

Chapter 5

Influence of Matrix Additives on MALDI

In MALDI, detection sensitivity, selectivity, mass resolution and other performance indicators are strongly dependent on the sample/matrix preparation. The crystallization of the mixture of the matrix and the analyte is the basic process of the sample preparation. In this chapter the control of crystal growth by additives will be discussed. Experiments involving 2,5-dihydroxybenzoic acid mixed with its isomers and other benzoic acid derivatives are described. The performance of the mixtures in MALDI MS is evaluated. Initial results indicate that use of additives possessing various properties can serve as a general means of improving the MALDI MS performance for certain matrices.

5.1 Influence of Additives on the Growth of a Crystal

The overall shape of a crystal is determined by the relative rates of deposition of particles on its various faces, the general rule being that faces which grow slowest appear as large, developed faces. The growth rates are determined primarily by a combination of structurally related factors, such as intermolecular bonds and dislocations, and external factors such as temperature, degree of supersaturation, solvent and impurities. Although strictly speaking the solvent itself has to be considered as an impurity, the term "impurity" (or "additive") used in this chapter is restricted to

compounds other than solute and solvent.

For molecular crystals, quantitative measurement of relative face growth rates was initially introduced by Hartman and Perdok [76]. They proposed that the attachment energy E_{att} , defined as the energy per molecule released when a new layer is attached to the surface of the crystal, is a controlling parameter for the growth rate R normal to a face, so that faces with higher E_{att} grow faster [77]. Early attempts to use the Hartman-Perdok theory for molecular crystals were thus qualitative, with bond chains identified and their relative strengths assessed [78]. The increasing access to powerful computers through the 1980s has led to quantitative predictions of crystal morphology. Initially these studies involved a direct extension of the Hartman-Perdok method by calculating the energies of specific bonds. More recently, direct calculations of slice energy E_{sl} , defined as the energy per molecule released when a slice is formed, and attachment energy E_{att} for specific crystal planes, have used crystal structure data together with interatomic potential functions describing the interaction energies between pairs of non-bonded atoms [79, 80]. Several calculations of crystal morphology based on the Hartman-Perdok method have been published, and are in good agreement with observed forms [81, 82, 83].

The presence of impurities in a system can have a profound effect on the growth of a crystal. Some impurities can suppress growth entirely; some may enhance growth, while others may exert a highly selective effect, acting only on certain crystallographic faces and thus modifying the crystal habit. Some impurities can exert an influence at very low concentrations, whereas others need to be present in fairly large amounts. The extensions of the Hartman-Perdok model have shown how additives as impurities exert an influence on attachment energies and hence on morphology [79, 84]. To do this, additive molecules are substituted for substrate molecules in the growth slice taking each lattice site in turn. This assumption gives new values for slice (E_{sl}) and

attachment (E_{att}) energies. It has been shown that the binding energy E_b at a surface site is [79]:

$$E_b = E_{sl} + E_{att} \quad (5.1)$$

for a substrate molecule so that it is possible to calculate the change in binding energy due to the inclusion of an additive in the slice. The faces most likely to be influenced by an additive are those for which this change, ΔE_b , is minimized.

By making use of the model discussed above, Roberts and Docherty have shown a good example, for the first time, of calculations of morphological change of a crystalline substance (benzamide) due to the presence of an additive (benzoic acid) [85]. The results of the calculations were found to be consistent with the available experimental data [86]. In the benzamide crystal, hydrogen-bonded cyclic dimers are interlinked along the *b* axis to form hydrogen-bonded ribbons. These ribbons are stacked along the *a* axis to give (001) layers held together by weaker van der Waals bonds, as shown in Figure 5.1. Retardation of growth, primarily along the *b* axis, was achieved by adding benzoic acid as impurity. The addition of benzoic acid disrupts growth in the *b* direction by interfering with the -N-H...O=C- hydrogen bonds. As shown in Figure 5.2, at the growing end of the ribbon motif an attractive -N-H...O=C- bond is replaced by a repulsive O...O interaction. Retardations of growth along the *a* axis and *c* axis were achieved by adding *o*-toluamide and *p*-toluamide, respectively [86].

2,5-dihydroxybenzoic acid (2,5-DHB) is a widely used matrix for matrix-assisted laser desorption/ionization mass spectrometry at 337 and 355 nm [23, 87]. In the standard preparation for MALDI ("dried droplet" method), 2,5-DHB forms a rather nonhomogeneous sample structure. It shows two distinct regions, i.e. a rim with

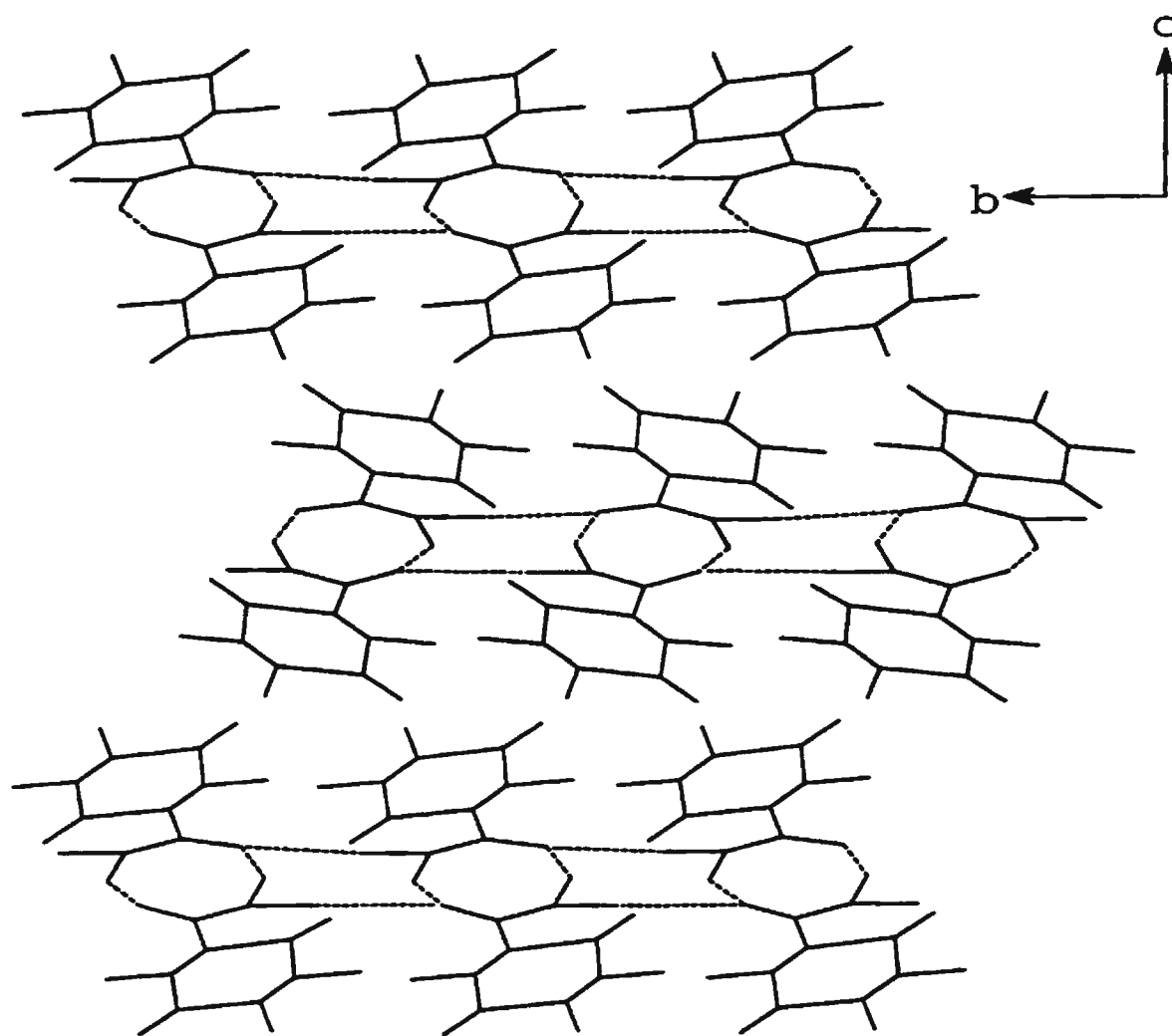


Figure 5.1: Molecular packing in benzamide as viewed along the a axis.

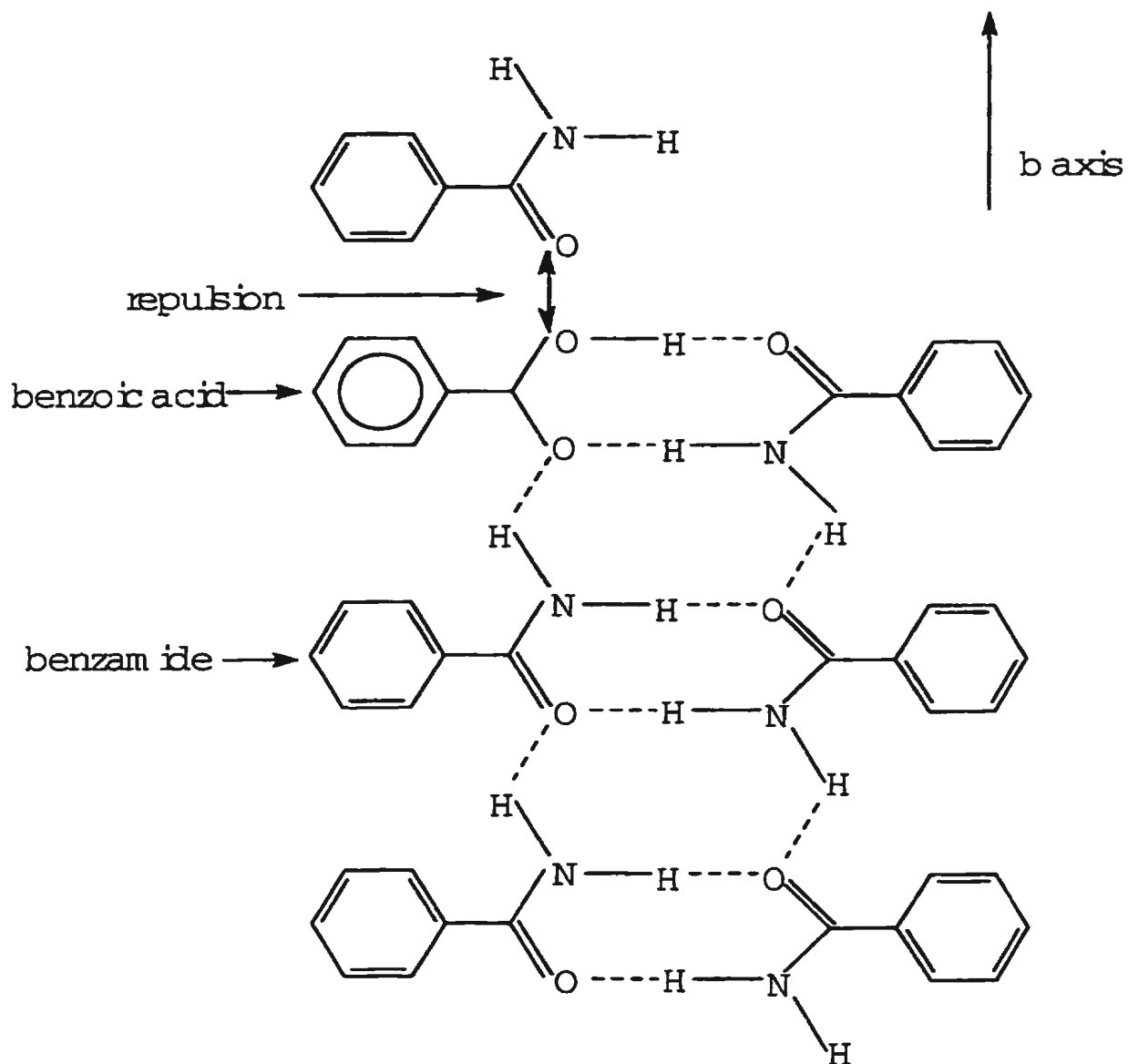
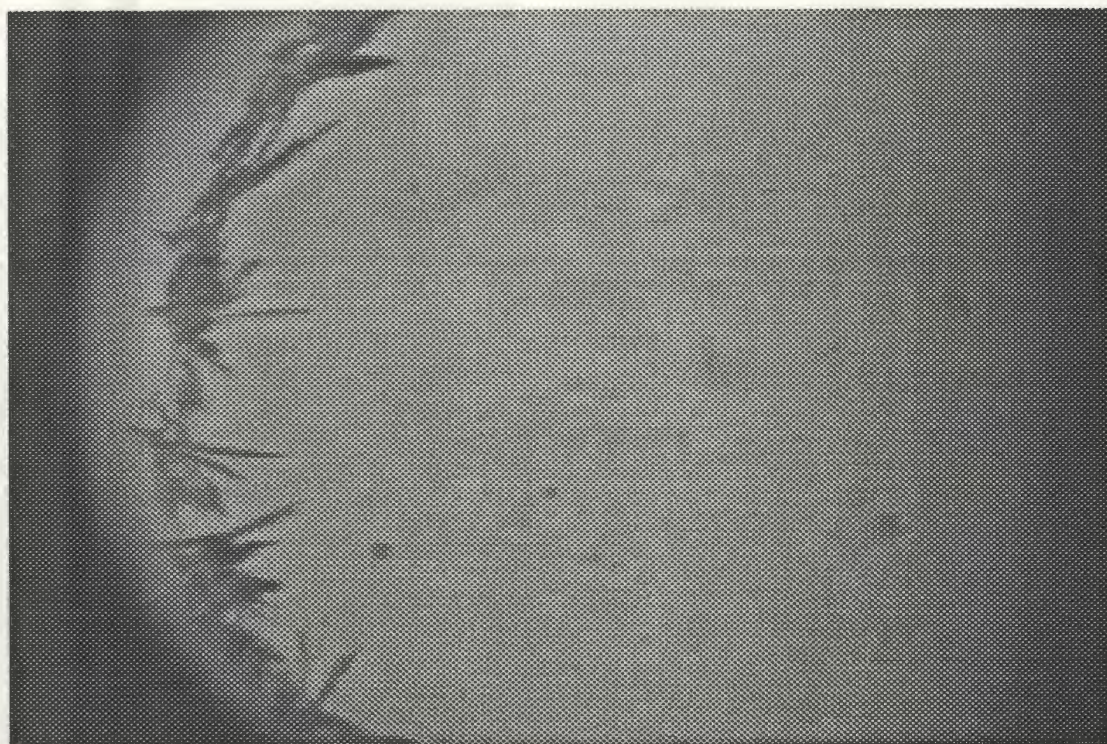


Figure 5.2: Chain formed by the hydrogen-bonds of benzamide. An additive benzoic acid molecule, which replaces a benzamide molecule, is shown.

crystal needles protruding towards the inside and a thin polycrystalline inner region (see Figure 5.3). Spectra with the highest analyte signal intensity are obtained from the crystal needles at the rim, in particular from the tips of the needles. A more recently developed sample preparation method, the poly-crystalline thin film method [44, 57] (see Chapter 3 of this thesis), has led to improved results in some matrices, but it was not generally useful for 2,5-DHB. 2,5-DHB is more soluble in water and most organic solvents than other common matrices, so that the second drop and washing procedure described in Section 3.2 completely redissolve the matrix surface. The characteristics of the crystalline deposit formed by 2,5-DHB create a problem. It is somewhat difficult to form a homogeneous mixture of matrix and analyte, resulting in poor shot-to-shot, point-to-point and sample-to-sample reproducibility. This problem has impaired the application of 2,5-DHB in MALDI quantitative analysis [31, 32]. However, other characteristic features of 2,5-DHB, such as tolerance towards common reagents and contaminants, and high sensitivity for many analytes, make it a desirable matrix for biomolecular mass analysis. Therefore, it is of considerable practical importance to find a method for modifying the morphology of 2,5-DHB crystalline deposits, based on the theory and experiments presented above. In this chapter we present the first investigation focuses on the improvement of the MALDI sample morphology using additives.

5.2 Experimental and Results

The following matrix materials were used in this study: 2,5-dihydroxybenzoic acid was used as the substrate, while its positional isomers and two other benzoic acid derivatives were used as additives (see Table 5.1 for their abbreviations as used here).



(a)



(b)

Figure 5.3: Photomicrograph showing crystals of 2,5-DHB prepared by dried droplet method at concentration of 10g/L. (a) Rim with crystal needles protruding towards the centre of the deposit (magnification: 85x) (b) Thin crystals in central region (magnification: 730x).

Table 5.1: List of additives used in the experiment

Abbreviation	Name of Additives
2,3-DHB	2,3-dihydroxybenzoic acid (lot# LF14112MX)
2,4-DHB	2,4-dihydroxybenzoic acid (lot# JG02530TF)
2,6-DHB	2,6-dihydroxybenzoic acid (lot# EF10430MZ)
3,4-DHB	3,4-dihydroxybenzoic acid (lot# PF02229MF)
3,5-DHB	3,5-dihydroxybenzoic acid (lot# LF01028EZ)
4A3MB	4-amino-3-methoxybenzoic acid (lot# MZ01116MY)
3ATFB	3-amino-2,5,6-trifluorobenzoic acid (lot# KZ01514HX)

All the matrix materials were purchased from Aldrich Chemical Company, Inc. and used without further purification. All the solvents used were obtained from the same sources as stated in the previous chapter.

Initial solutions of the individual matrices were prepared at a concentration of 10g/L by dissolving in 2:1 (v/v) 0.1% aqueous trifluoroacetic acid:acetonitrile. The solutions of 4A3MB and 3ATFB were heated briefly to 40° C to remove any undissolved material. Each of the initial solutions was then cleared by centrifugation before mixing. Each of the additive solutions was added to 2,5-DHB solution in the appropriate ratios. Details of solution composition are indicated in the appropriate figure captions.

Matrix solutions were stirred using a vortex-mixer for more than four minutes, followed by two minutes in an ultrasonic bath. The solution was then stirred again and

allowed to equilibrate for several hours. The analyte samples used in the experiments were bovine insulin and myoglobin. They were dissolved in 0.1% aqueous TFA at 10 μM concentration.

The final sample was prepared by using the dried-droplet method. The protein solution was stirred with the matrix at a typical ratio of 1:10 using a vortex mixer (3 min.). Aliquots of 0.5 - 1 μL of the mixture were deposited onto a stainless steel probe tip and allowed to air-dry at room temperature.

MALDI-MS was performed using a linear time-of-flight instrument, a description of which can be found in Chapter 2. Background pressure within the instrument, measured by an ion gauge located below the flight tube, was lower than 3×10^{-7} torr for all measurements. The instrument was not equipped to permit the microscopic observation of the irradiated sample. The laser spot on the sample surface could, however, be monitored by sight through a window on the top of the ion source. Ion desorption was initiated by a nitrogen laser emitting at 337 nm with a pulse duration of 3 ns. The laser irradiance was 30% above the threshold for each of the samples. The desorbed ions were accelerated to 30 keV energy.

In the crystals of dihydroxybenzoic isomers, the structures consist of centrosymmetric dimers linked together by hydrogen bonds between the carboxylic groups [88, 89]. However, the modes of packing of the dimers turn out to be quite different in the isomeric compounds, despite their common tendency to form hydrogen-bonded pairs. The interactions of the phenolic hydroxy groups play an important role in determining the structure, and result in the different morphologies. For instance, the unit cells of 2,4-DHB and 2,5-DHB are quite different (Table 5.2), the former being triclinic and the latter monoclinic.

In situ photomicrographs of 2,5-DHB isomer crystals were taken in order to understand their structure and morphology. All samples were prepared by applying

Table 5.2: The crystal data for 2,4DHB and 2,5DHB

	a	b	c	α	β	γ	Z	Space group
2,4DHB[90]	9.67	11.56	7.05	105°38'	91°43'	79°55'	4	$P\bar{1}$
2,5DHB[89]	23.95	4.91	5.62		100°59'		4	$P2_1/a$

1 μ L of the initial solutions onto the probe tip, and were allowed to air-dry at room temperature. Under microscopic inspection a rather similar sample structure was revealed for 2,3-DHB, 2,4-DHB and 2,6-DHB crystals, as shown in Figures 5.4 - 5.6. The crystal needles start to grow at the edge of the droplet, extend towards the inside, and distribute over nearly the whole sample area upon droplet drying. Crystals of 3,4-DHB and 3,5-DHB form the same structure as 2,5-DHB with two regions, i.e. crystal needles near the rim and polycrystalline material in the center. Light micrographs of the other isomers, 3,4-DHB and 3,5-DHB samples, are shown in Figures 5.7 and 5.8, respectively.

The mixture of 2,5-DHB with its isomers changed the resulting crystal structures and morphologies. Figures 5.9 - 5.13 show the photomicrographs of 2,5-DHB mixed with its five isomers individually. The sample solutions were prepared by adding the additive solution into the 2,5-DHB solution in a 1:1 ratio. In the mixture of 2,5-DHB with 2,3-DHB, shown in Figure 5.9 (a)-(b), it can be seen that the dense crystal grains distribute homogeneously over the central region. The same crystal distribution and morphology could be observed in the sample of α -cyano-4-hydroxycinnamic acid (4HCCA) prepared by the dried-droplet method (shown in Figure 5.9(c)). The crystal morphology obtained for the mixture of 2,5-DHB:2,6-DHB (shown in Figure 5.10) was analogous to that for the 2,5-DHB:2,3-DHB mixture. The mixture of 2,5-DHB with

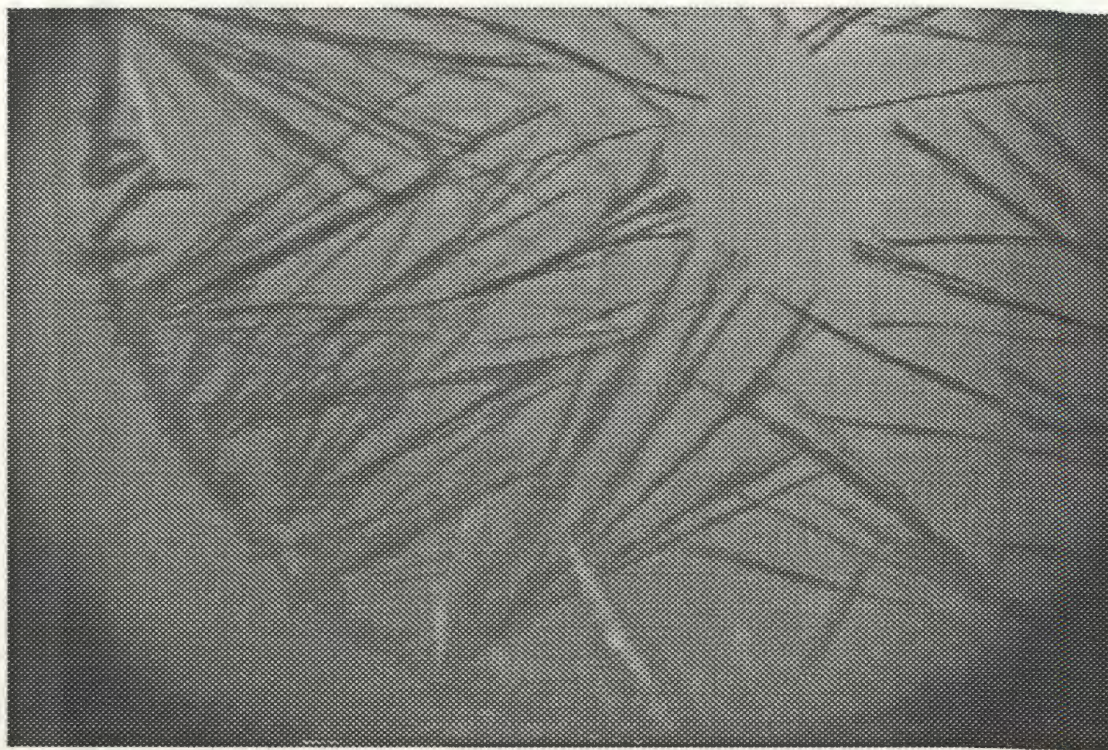


Figure 5.4: Photo microscope image demonstrating the crystal type of 2,3-DHB prepared by dried droplet method at a concentration of 10g/L (magnification: 85x).

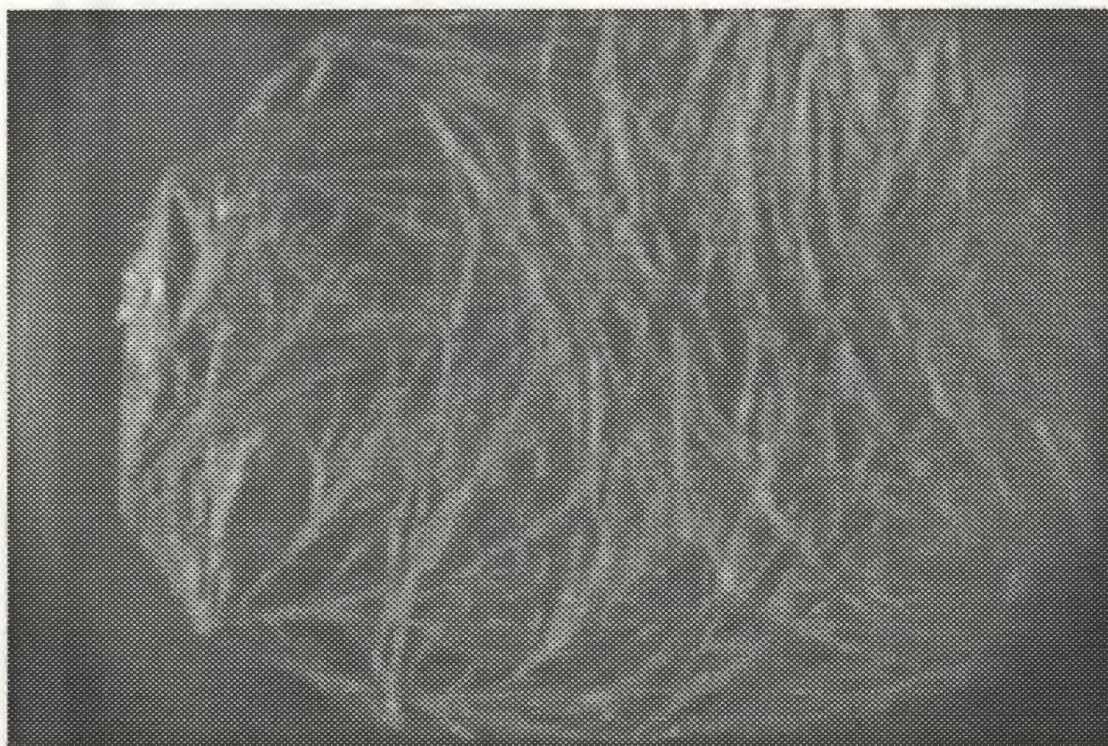


Figure 5.5: Photo microscope image demonstrating the crystal type of 2,4-DHB prepared by dried droplet method at a concentration of 10g/L (magnification:85x).

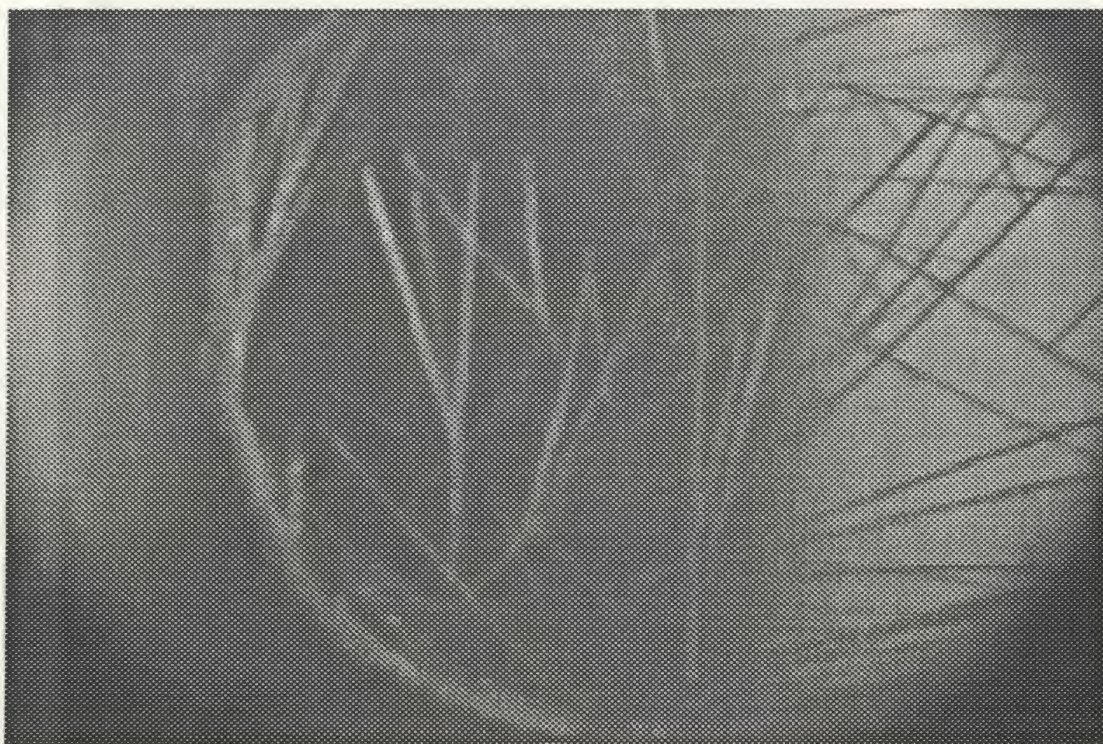
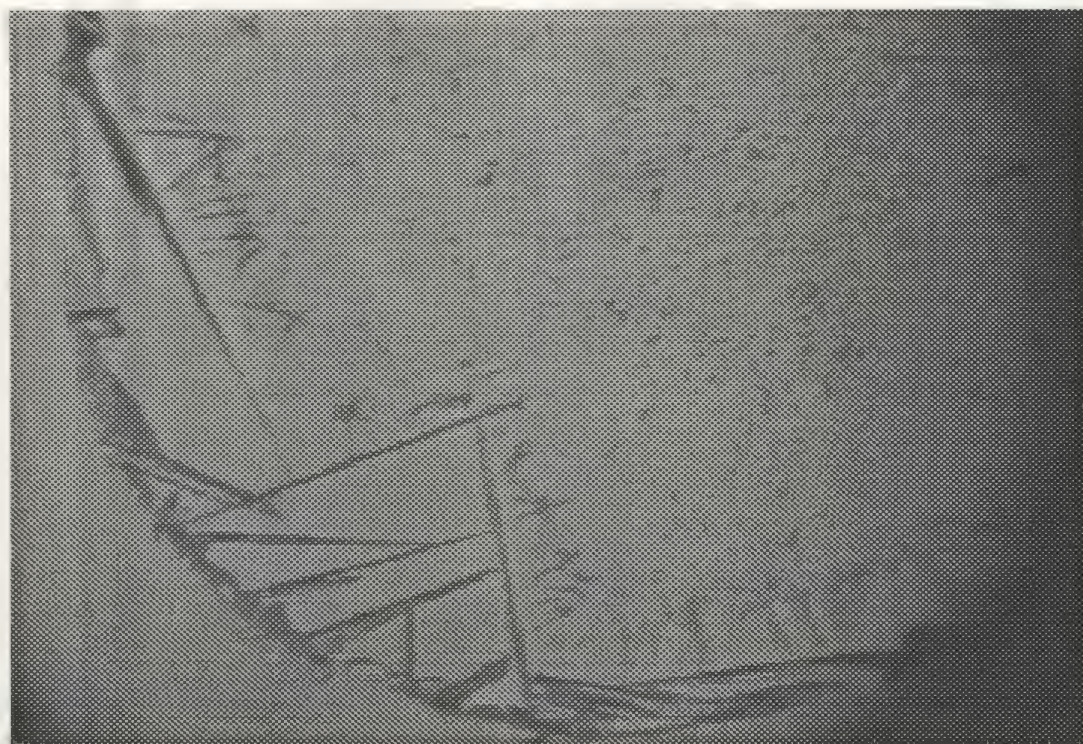
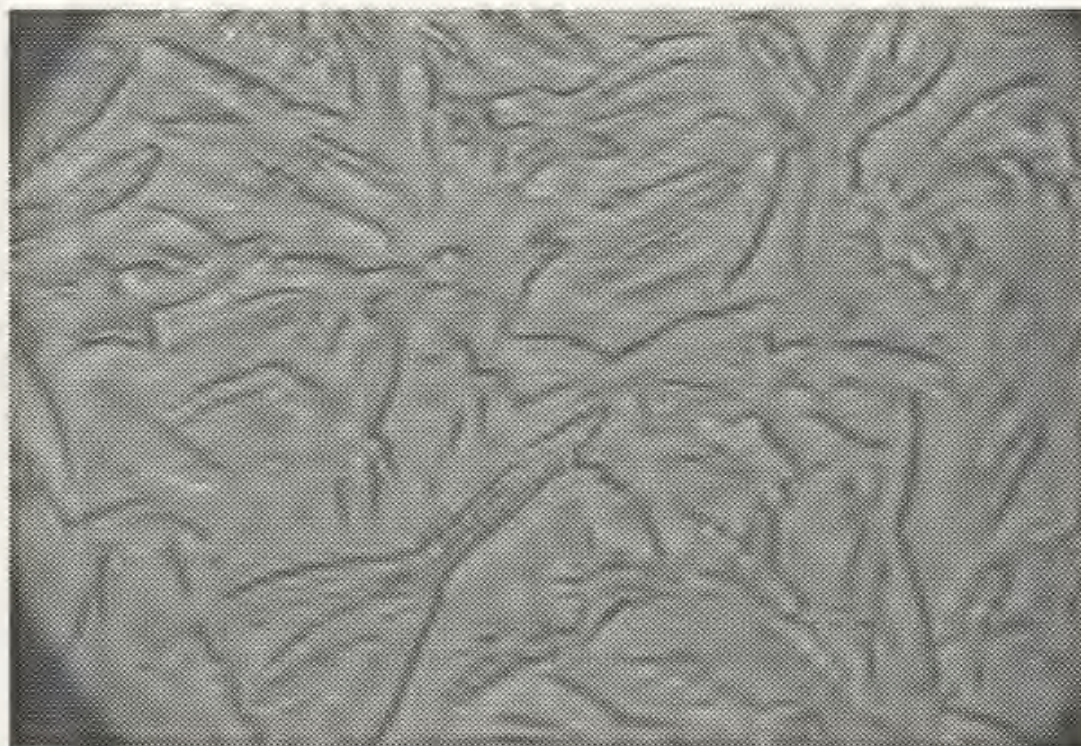


Figure 5.6: Photo microscope image demonstrating the crystal type of 2,6-DHB prepared by dried droplet method at a concentration of 10g/L (magnification:85x).

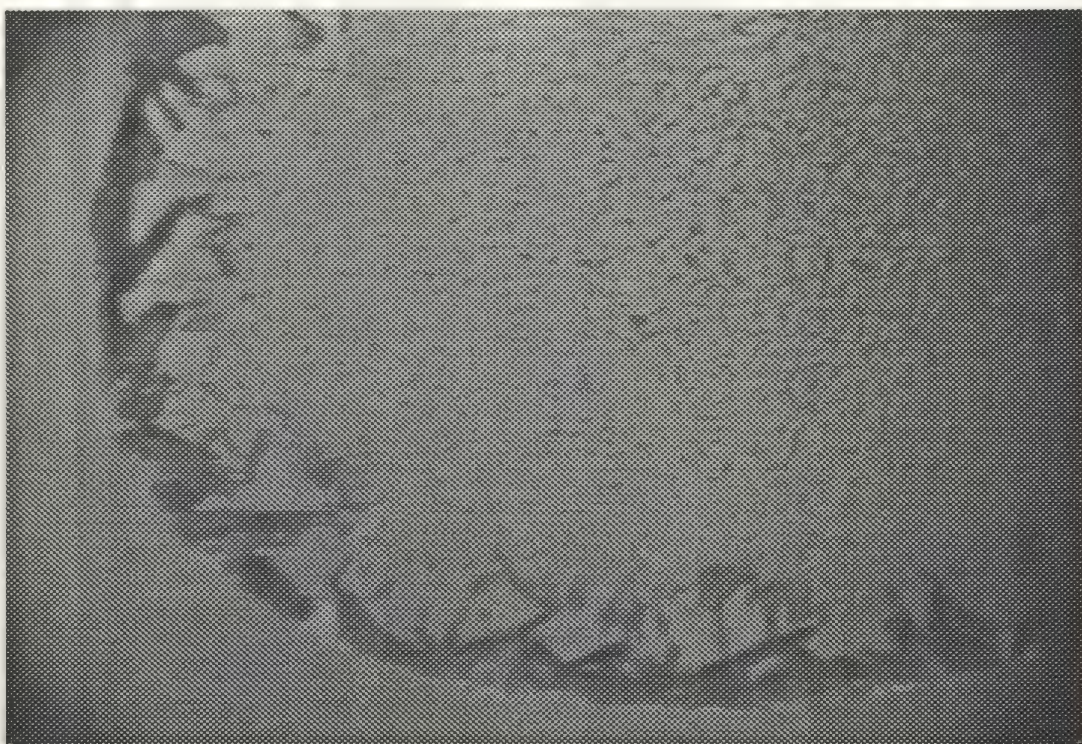


(a)



(b)

Figure 5.7: Photomicrograph showing crystals of 3,4-DHB prepared by dried droplet method at a concentration of 10g/L. (a) Rim with crystal needles protruding towards the centre of the deposit (magnification: 85x) (b) Thin polycrystalline in central region (magnification: 730x).



(a)

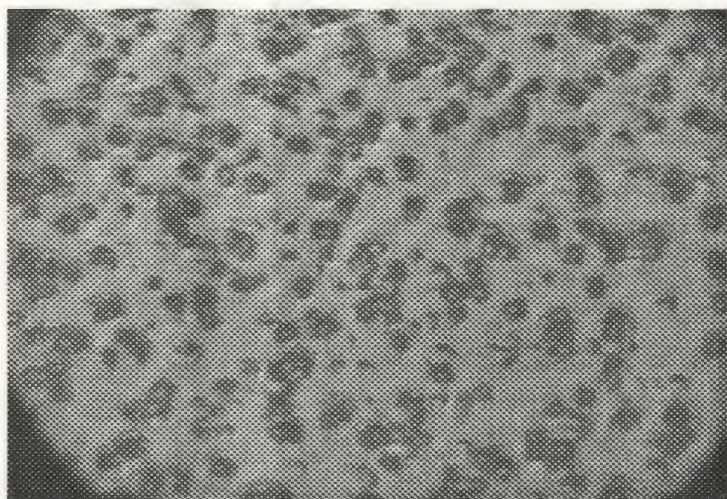


(b)

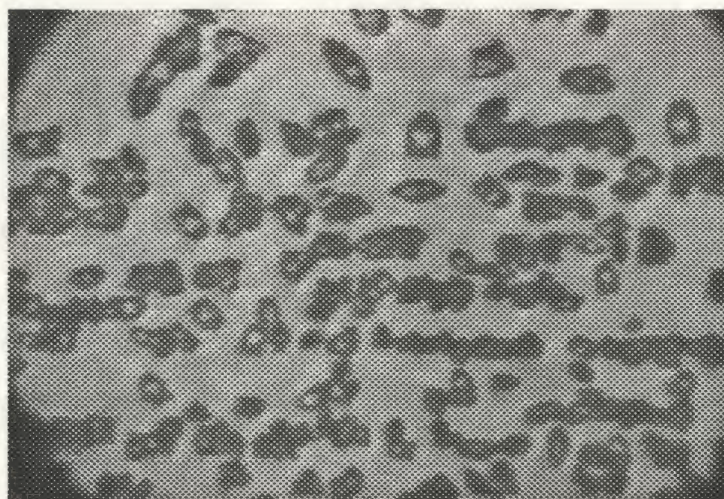
Figure 5.8: Photomicrograph showing crystals of 3,5-DHB prepared by dried droplet method at a concentration of 10g/L. (a) Rim with crystal needles protruding towards the centre of the deposit (magnification: 85x) (b) Thin polycrystalline in central region (magnification: 730x).



(a)

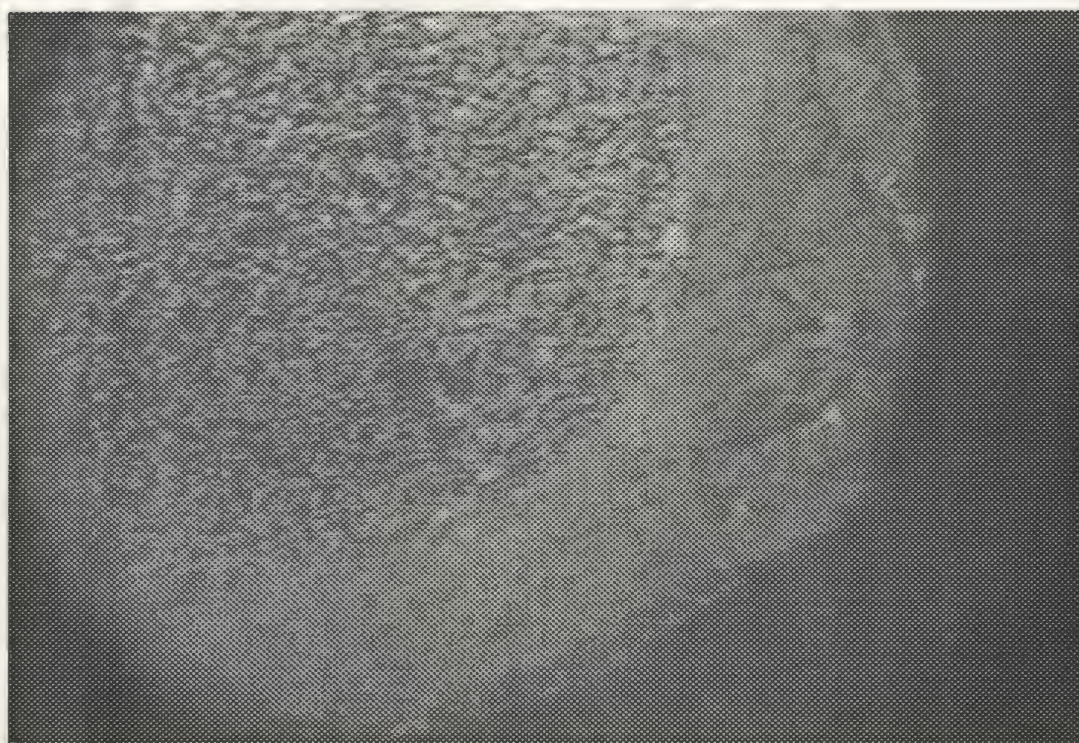


(b)

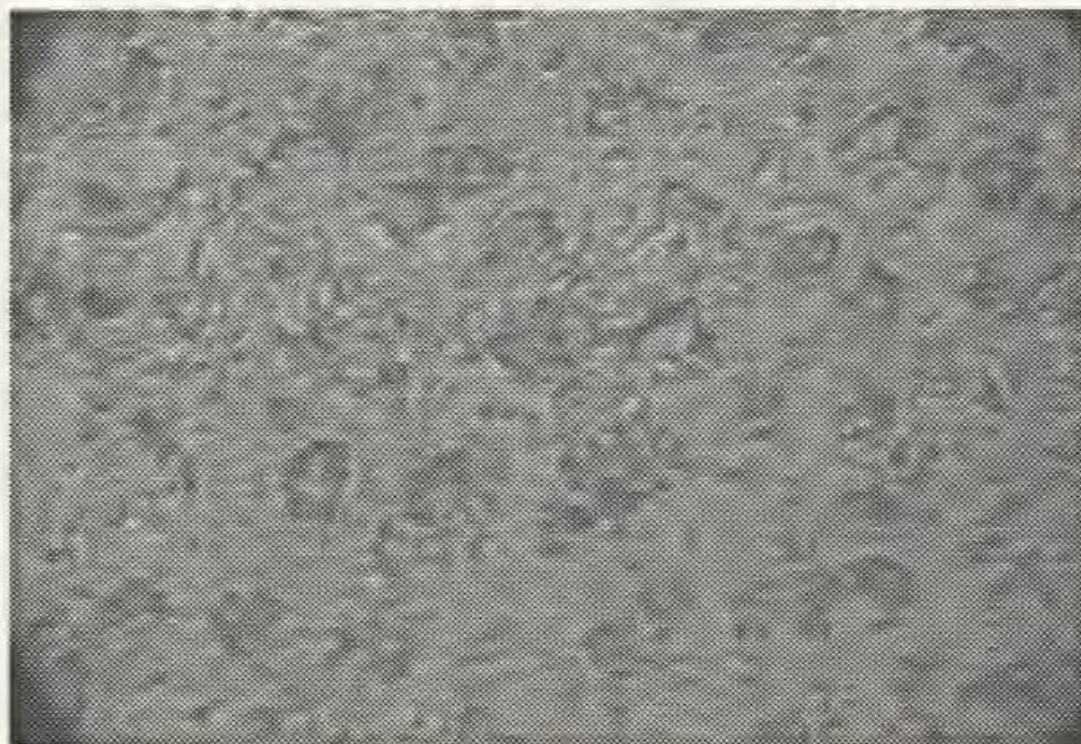


(c)

Figure 5.9: Photomicrograph showing crystals of 2,3-DHB:2,5-DHB mixed in 1:1 (v:v) ratio, prepared by dried droplet method, (a) magnification: 55x, (b) magnification: 500x; (c) photo microscope image of crystals of 4HCCA with the same magnification as in (b), for comparison.

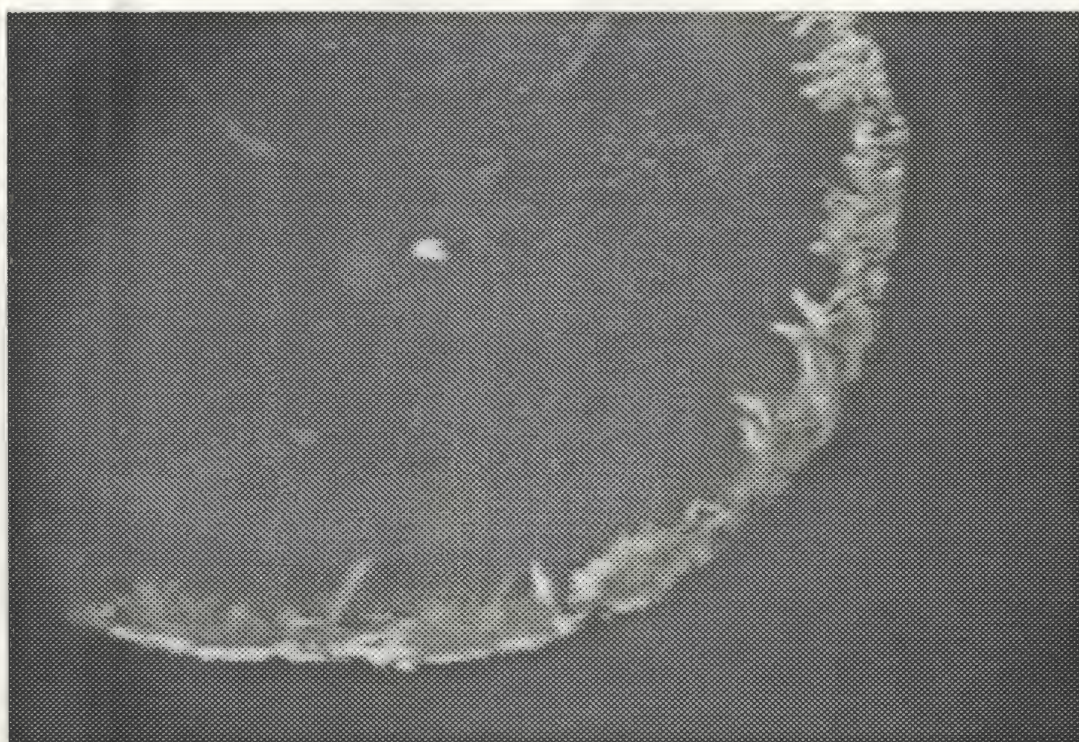


(a)

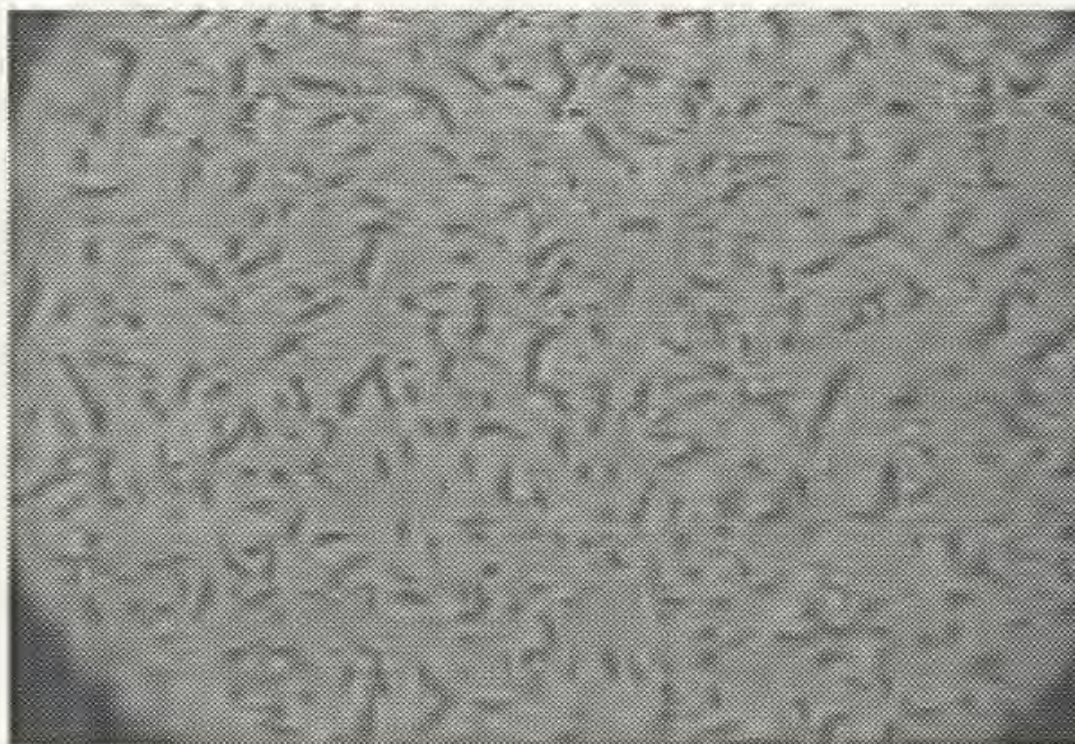


(b)

Figure 5.10: Photomicrograph showing crystals of 2,6-DHB:2,5-DHB mixed in 1:1 (v:v), prepared by dried droplet method, (a) magnification: 85x, (b) magnification: 730x.

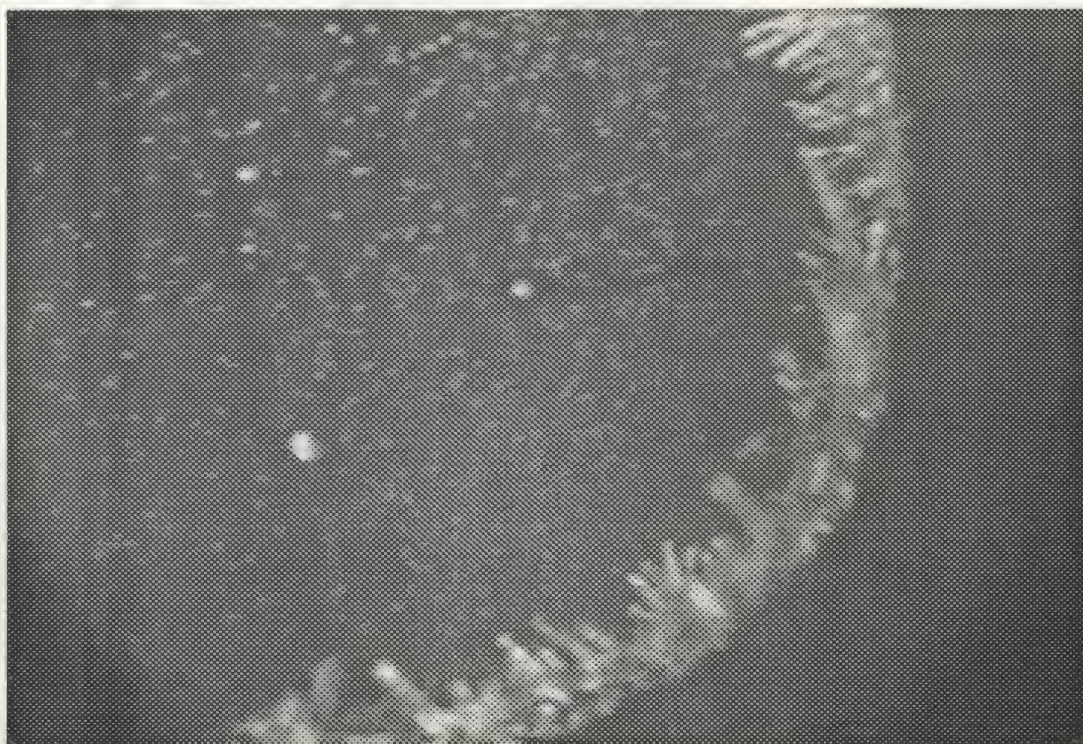


(a)

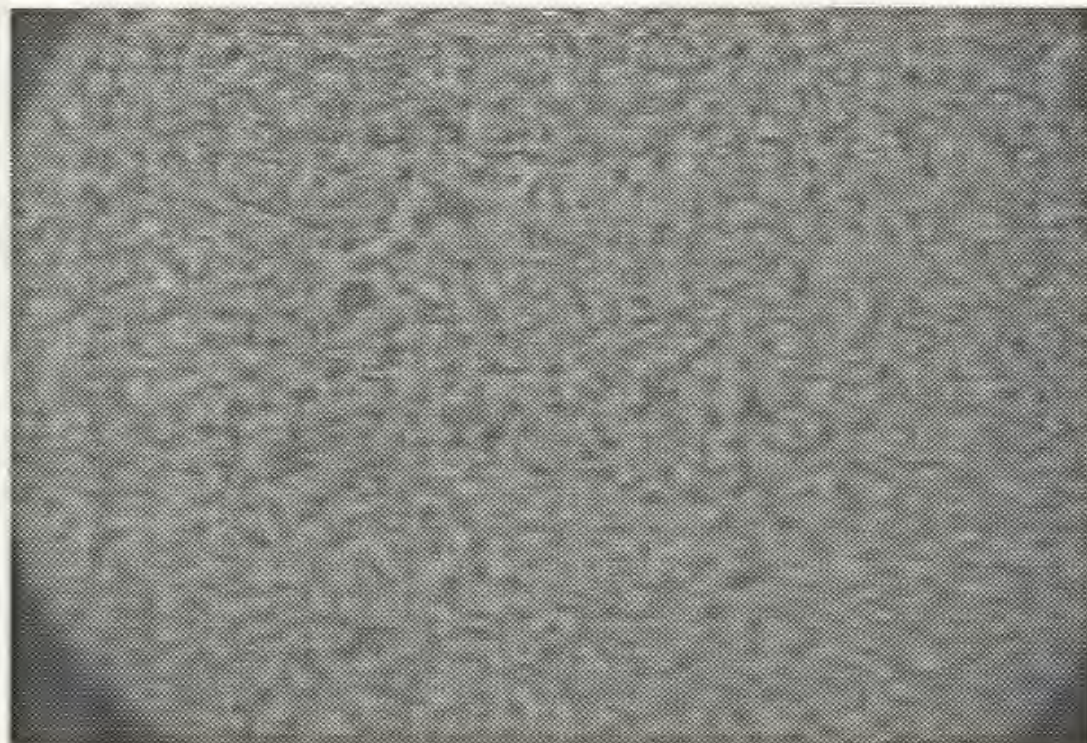


(b)

Figure 5.11: Photomicrograph showing crystals of 2,4-DHB:2,5-DHB mixed in 1:1 (v:v), prepared by dried droplet method, (a) magnification: 85x, (b) magnification: 730x.

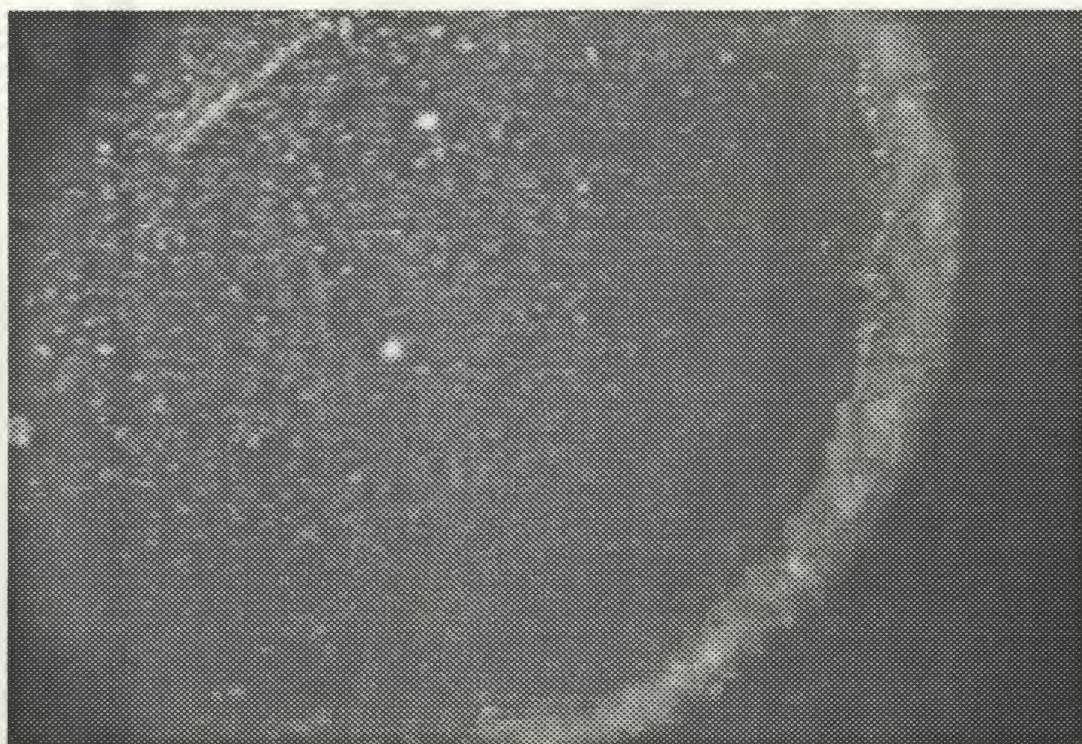


(a)

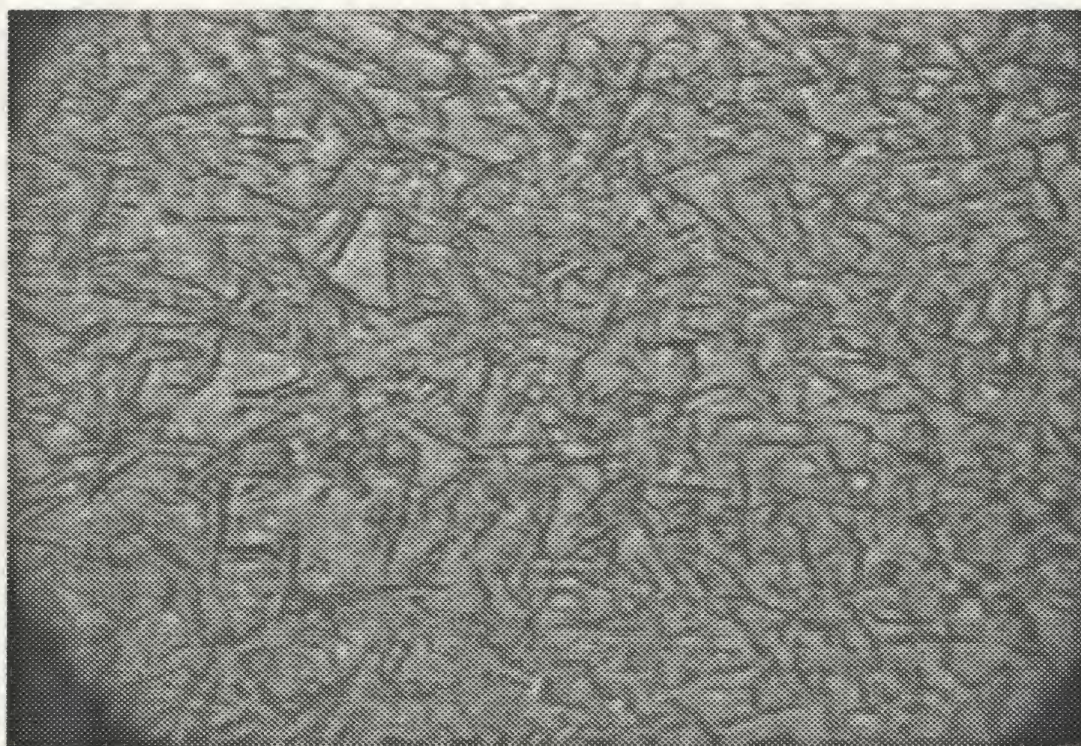


(b)

Figure 5.12: Photomicrograph showing crystals of 3,4-DHB:2,5-DHB mixed in 1:1 (v:v), prepared by dried droplet method, (a) magnification: 85x, (b) magnification: 730x.



(a)



(b)

Figure 5.13: Photomicrograph showing crystals of 3,5-DHB:2,5-DHB mixed in 1:1 (v:v), prepared by dried droplet method, (a) magnification: 85x, (b) magnification: 730x.

the other three isomers, 2,4-DHB, 3,4-DHB and 3,5-DHB, presented an accumulation of the crystal on the rim and very thin tablets covering the center (see Figures 5.11 - 5.13).

The mixture of 2,5-DHB:2,3-DHB was particularly interesting. In the central area of the sample the crystals all produced good ion currents when irradiated. The signal intensity of analyte ions did not vary measurably over the different spots. This observation demonstrates that analyte molecules were incorporated into matrix crystals homogeneously, and the crystals distributed evenly over the central region. A typical TOF mass spectrum of myoglobin in the mixture of 2,5-DHB:2,3-DHB is shown in Figure 5.14.

Another observation was that the mixture of 2,5-DHB:2,3-DHB had a low tendency for adduct ion formation (between analyte and matrix), in comparison with 2,5-DHB alone. Bovine insulin mass spectra from 2,5-DHB, and from its mixture with 2,3-DHB, are shown in Figure 5.15. The concentration of bovine insulin and the ratio of analyte to matrix were identical in the two samples. The main difference between the two spectra is the adduct peak of the singly charged molecular ion at $m/z=5733$, which is apparent for 2,5-DHB and obscure for 2,3-DHB:2,5-DHB mixture. To test the detection limit using the 2,3-DHB:2,5-DHB mixture, the protein solution was mixed with the matrix at the ratio 1:20, so that the amount of the analyte included in a dried sample was reduced to half of the original amount. The result for myoglobin at low concentration in the mixed matrix is displayed in Figure 5.16. The protonated molecule peaks were still clearly observed (compare Figure 5.14) with only 0.5 pmol of protein loaded on the probe. The limit of detection was approximately 0.1 picomole, under these experimental conditions.

The MALDI performance of 2,5-DHB with its other isomers was also examined. For 2,5-DHB:2,4-DHB and 2,5-DHB:2,6-DHB the analyte ions were ejected by laser

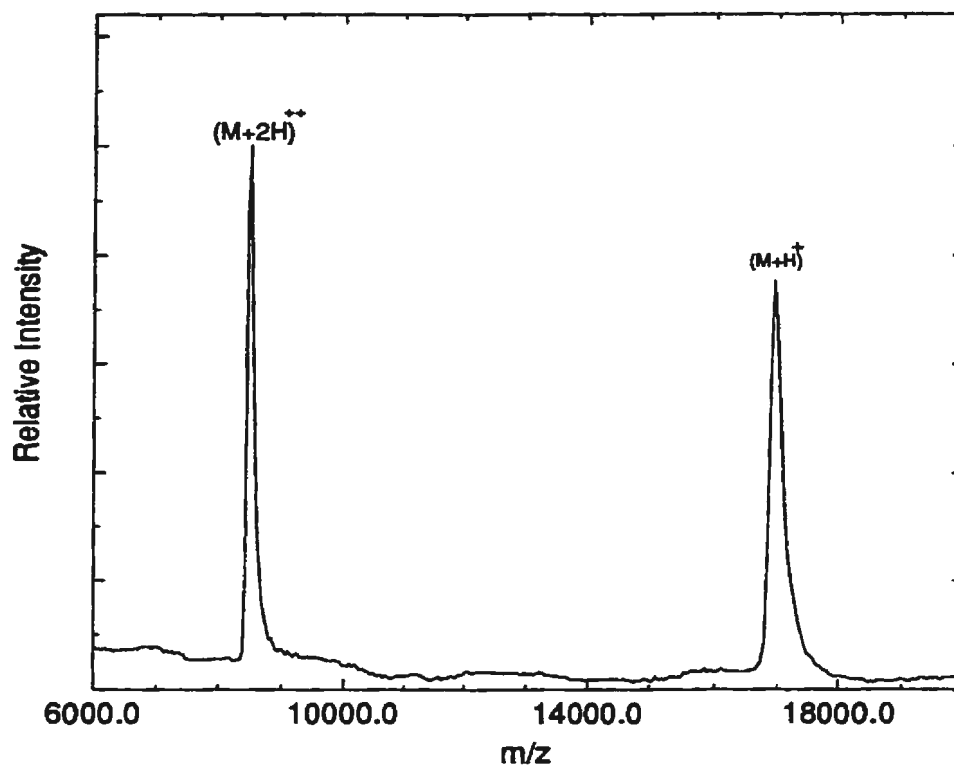


Figure 5.14: A laser desorption TOF mass spectrum of horse skeletal muscle myoglobin (mol. mass = 16951 u) taken from 2,3-DHB:2,5-DHB. The singly and doubly charged ion species are shown. Sample solution was prepared as a mixture of 1:10 (v:v), 10 μ M myoglobin:co-matrix at 10g/L. 1 μ L of sample solution was dropped on the probe tip. This spectrum represents the sum of transients recorded for 20 consecutive laser shots.

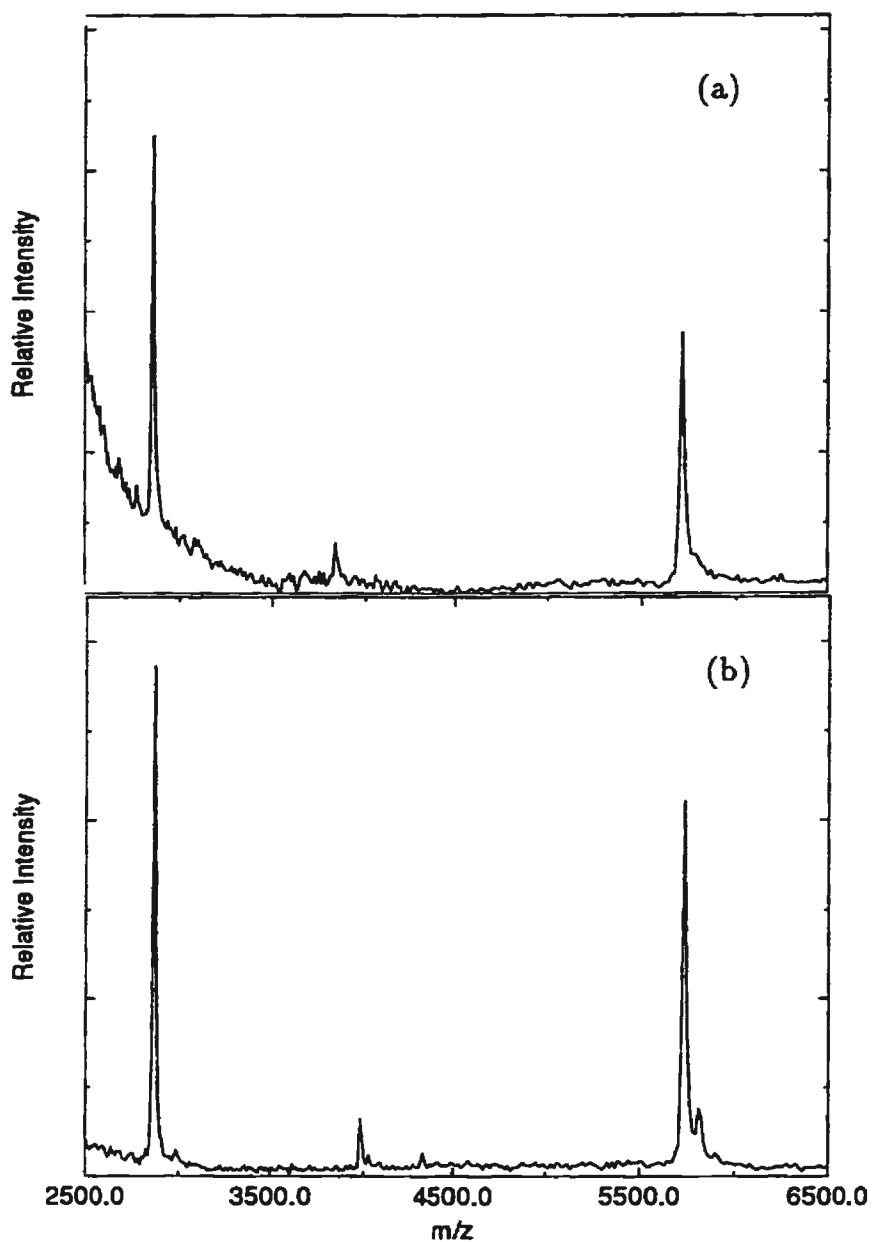


Figure 5.15: Laser desorption TOF mass spectra of bovine insulin (mol. mass = 5733.5 u) taken from (a) 2,3-DHB:2,5-DHB, (b) neat 2,5-DHB. The matrix adduct peak of the singly charged molecular ion is apparent for neat 2,5-DHB.

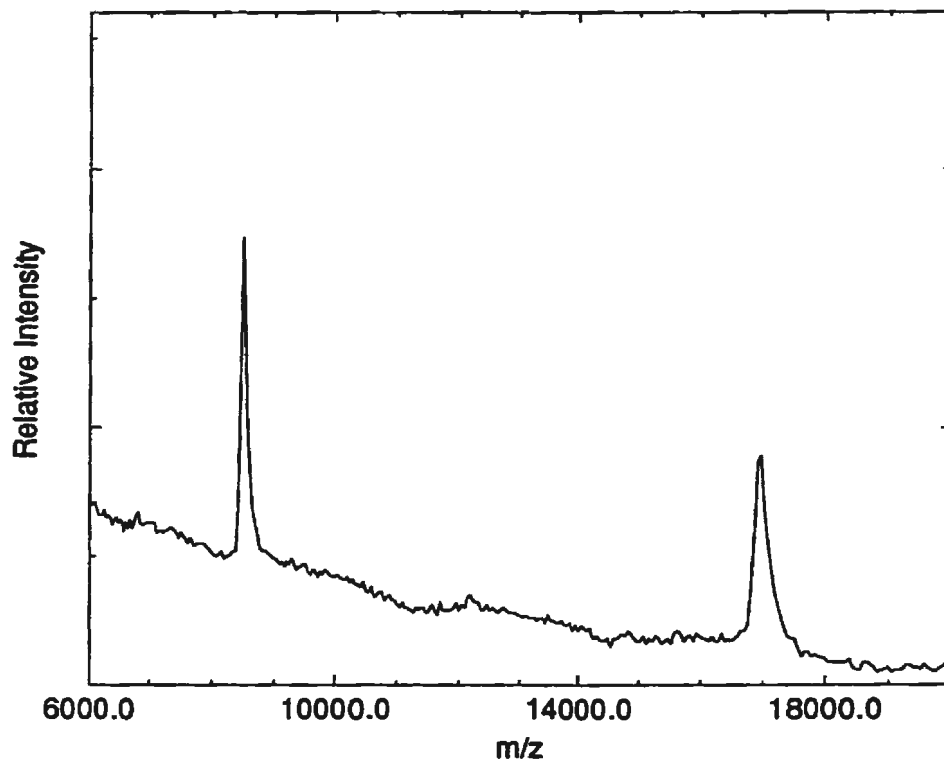


Figure 5.16: A laser desorption TOF mass spectrum of horse skeletal muscle myoglobin (mol. mass = 16951 u) taken from 2,3-DHB:2,5-DHB. The singly and doubly charged ion species are shown. Sample solution was prepared as a mixture of 1:20 (v:v), 10 μ M myoglobin:co-matrix at 10g/L. 1 μ L of sample solution was dropped on the probe tip. Amount of myoglobin in dried sample was 0.5 picomole. This spectrum represents the sum of transients recorded for 20 consecutive laser shots.

light from the rim of a sample. None were obtained from the central area. Figure 5.17 shows a spectrum of myoglobin in 2,5-DHB:2,4-DHB. The sample used for this spectrum was prepared in the same way as used for 2,5-DHB:2,3-DHB. A spectrum of myoglobin from 2,5-DHB:2,6-DHB was shown in Figure 5.18. Analyte ion signals did not change significantly as laser fluence increased. No analyte ion signals could be detected from the mixtures of 2,5-DHB with 3,4-DHB and 3,5-DHB even at high analyte concentration.

4A3MB and 3ATFB as additives with 2,5-DHB were also investigated. As shown in Figure 5.19 pure 4A3MB forms long crystal needles, distributed over nearly the whole sample area. There are no crystalline deposits in the center. However, 3ATFB forms the same structure as 2,5-DHB with two regions: crystal needles near the rim and polycrystallines in the center as shown in Figure 5.20. Analyte molecular ions were produced from both mixtures. A 3ATFB:2,5-DHB mixture showed better performance in MALDI-MS than a 4A3MB:2,5-DHB mixture. Figure 5.21 shows the photomicrograph of mixture of 2,5-DHB:4A3MB. As the concentration of 3ATFB in mixture solution increased, crystals became more closely packed and smaller. Figure 5.22 shows the photomicrographs of 2,5-DHB mixed with 3ATFB at different ratios. A homogeneous crystal distribution at 1:1 ratio improved spot-to-spot reproducibility. Figure 5.23 presents a typical mass spectrum obtained from the mixture of 2,5-DHB:3ATFB at 1:1 ratio. The appearance of multiply protonated analyte ions in the spectrum indicates that the addition of 3ATFB improves protonation in MALDI.

5.3 Discussion

The principles and the experimental results presented in Sections 5.1 and 5.2 have

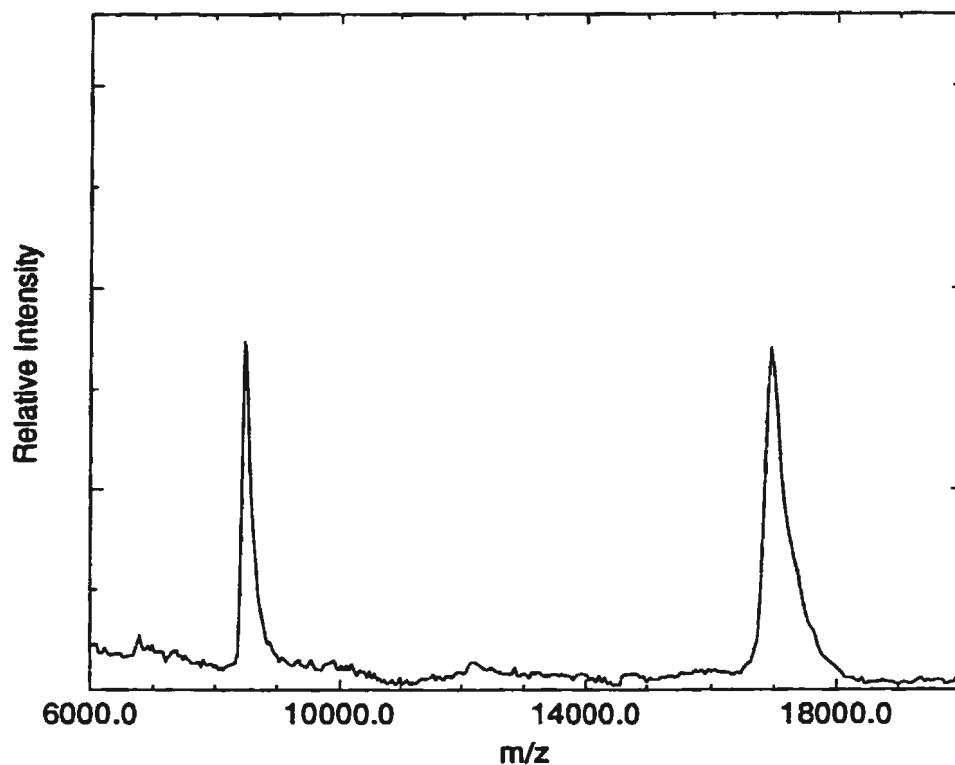


Figure 5.17: A laser desorption TOF mass spectrum of horse skeletal muscle myoglobin (mol. mass = 16951 u) taken from the rim of a 2,4-DHB:2,5-DHB deposit. The singly and doubly charged ion species are shown. Sample solution was prepared as a mixture of 1:10 (v:v), 10 μ M myoglobin:co-matrix at 10g/L. 1 μ L of sample solution was dropped on the probe tip. This spectrum represents the sum of transients recorded for 20 consecutive laser shots.

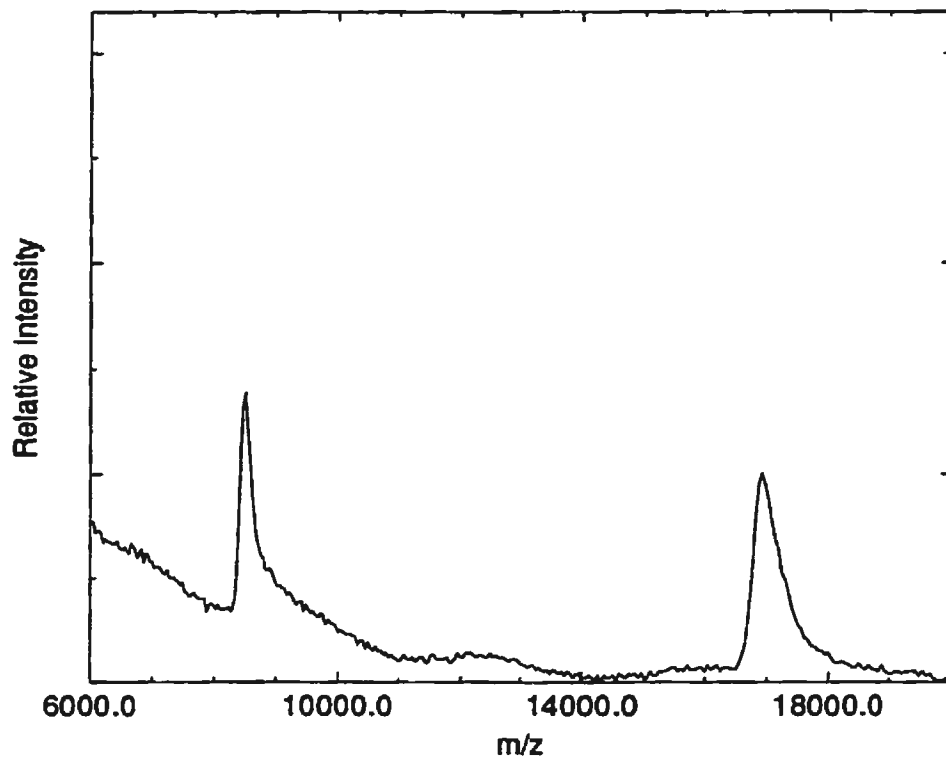


Figure 5.18: A laser desorption TOF mass spectrum of horse skeletal muscle myoglobin (mol. mass = 16951 u) taken from the rim of a 2,6-DHB:2,5-DHB deposit. The singly and doubly charged ion species are shown. Sample solution was prepared as a mixture of 1:10 (v:v), 10 μ M myoglobin:co-matrix at 10g/L. 1 μ L of sample solution was dropped on the probe tip. This spectrum represents the sum of transients recorded for 20 consecutive laser shots.

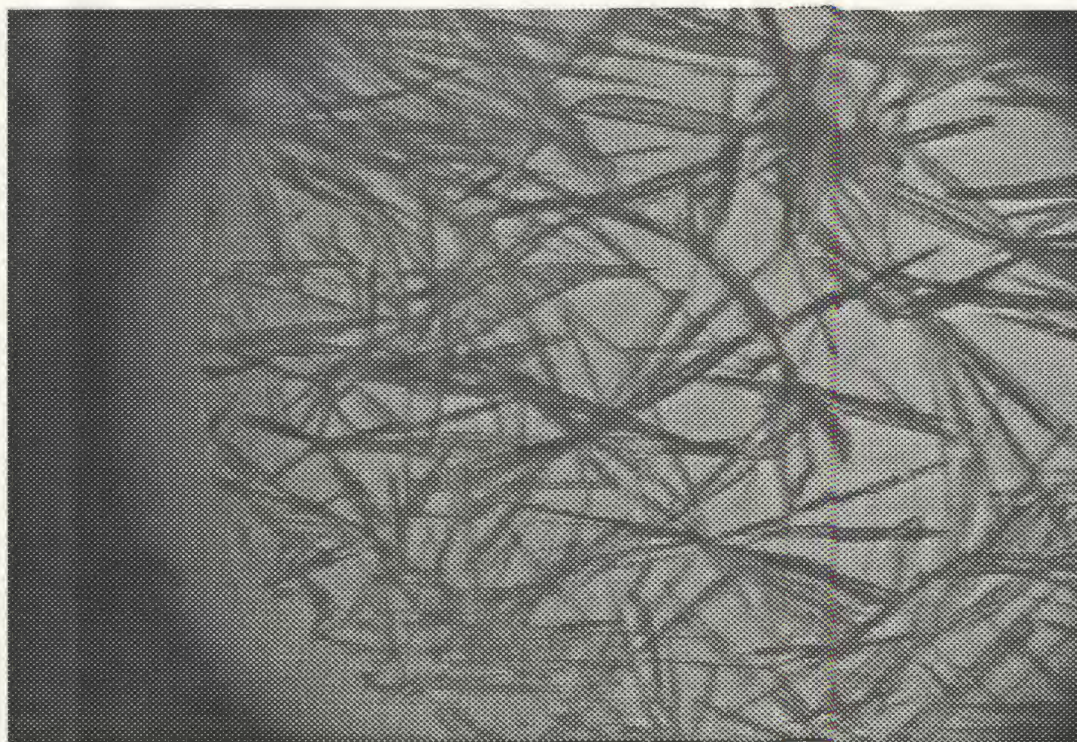


Figure 5.19: Photo microscope image demonstrating the crystal type of 4A3MB prepared by the dried droplet method at a concentration of 10g/L (magnification: 85x).

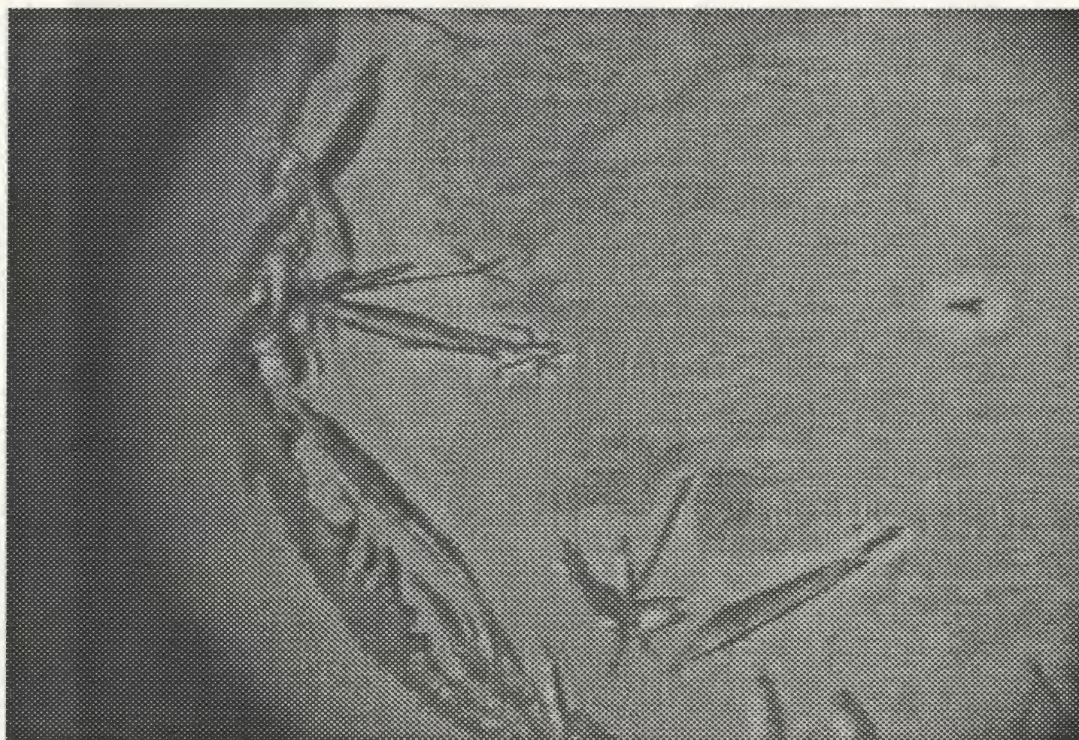


Figure 5.20: Photo microscope image demonstrating the crystal type of 4ATFB prepared by the dried droplet method at a concentration of 10g/L (magnification: 85x).

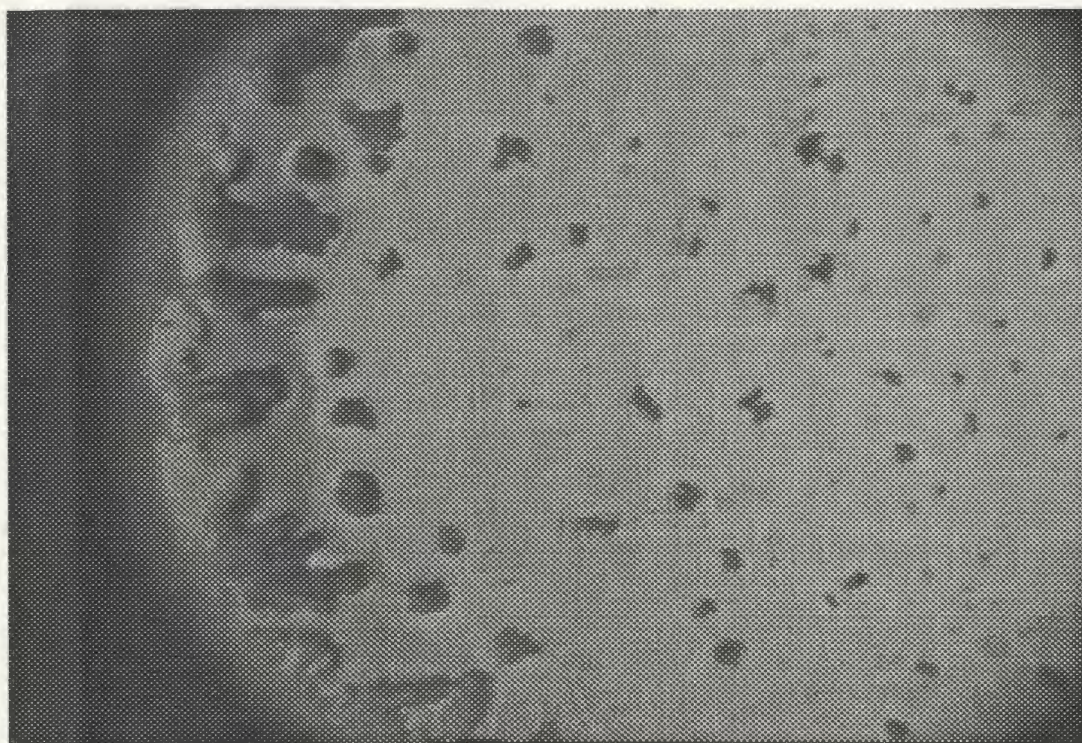


Figure 5.21: Photo microscope image demonstrating the crystal type of 4A3MB:2,5-DHB prepared by the dried droplet method at a concentration of 10g/L (magnification: 85x).

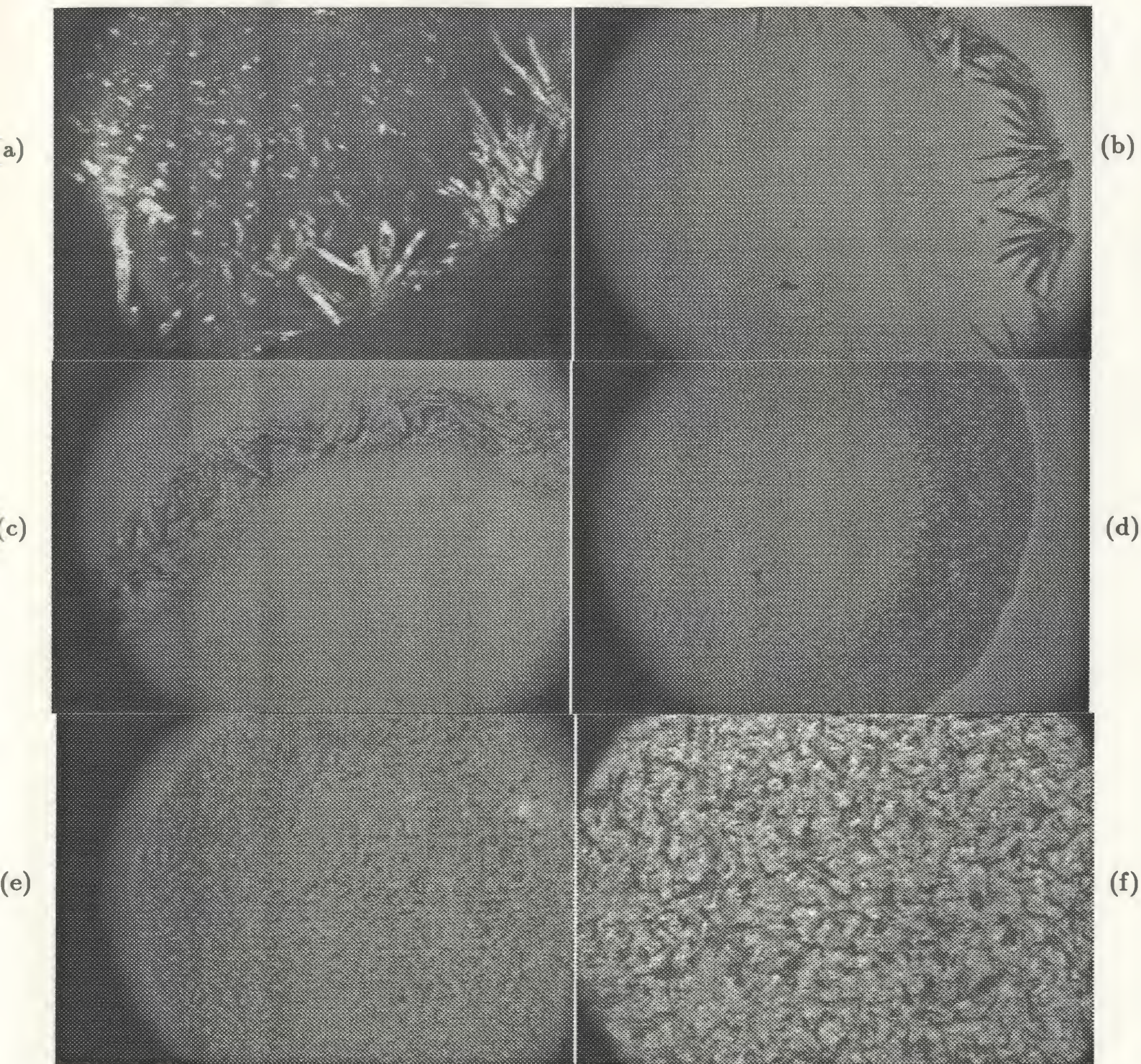


Figure 5.22: Photomicrographs showing crystals of 3ATFB:2,5-DHB (v:v), v=solution volume, mixed at different ratios. (a) 1:5, (b) 2:5, (c) 3:5, (d) 4:5, (e) 5:5 (magnification: 55x) and (f) 5:5 (magnification: 500x).

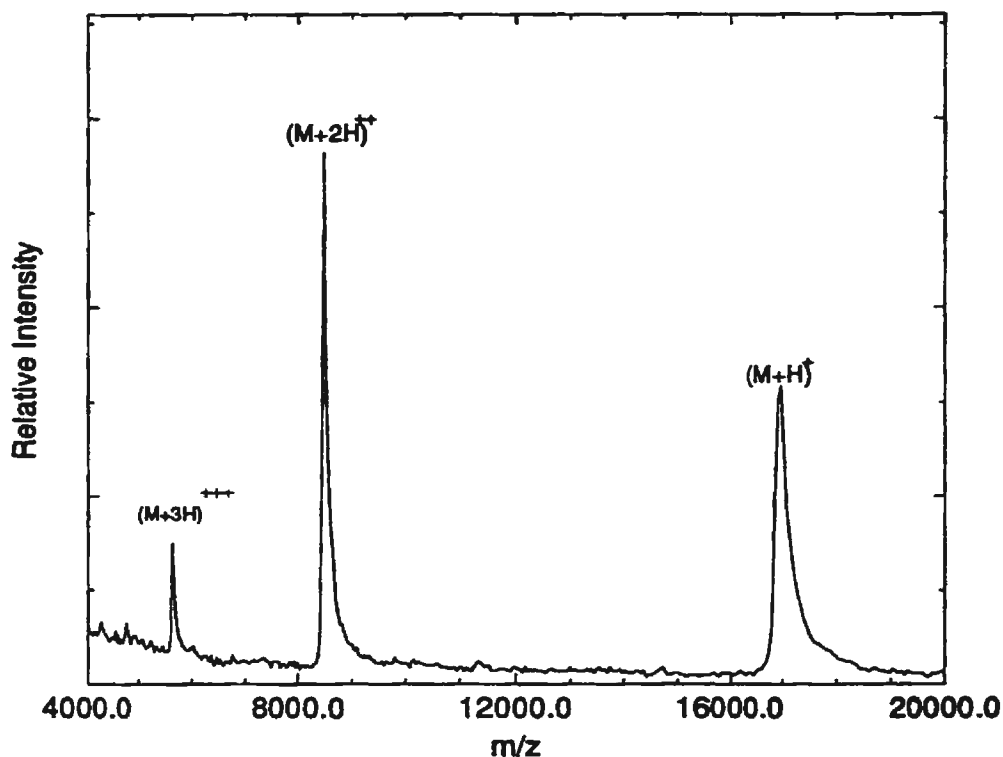


Figure 5.23: A laser desorption TOF mass spectrum of horse skeletal muscle myoglobin (mol. mass = 16951 u) taken from the mixture of 3ATFB:2,5-DHB at 5:5 ratio. The singly, doubly and triply charged ion species are shown. Sample solution was prepared as a mixture of 1:10 (v:v), 10 μ M myoglobin:co-matrix at 10g/L. 0.5 μ L of sample solution was dropped on the probe tip. This spectrum represents the sum of transients recorded for 10 consecutive laser shots.

shown that the presence of additives in a matrix has a profound effect on MALDI ion production. Few investigations directed at the different physical and chemical properties of matrix mixtures have been reported. One approach tested the effect of a carbohydrate such as glucose or fructose, with 2,5-DHB. The result reported by Köster et al. [91] demonstrated that the resolution was thereby increased significantly for MALDI coupled to Fourier transform mass spectrometry. A different approach has been tested by the Münster group [92, 93], who showed that the addition of a low concentration of 2-hydroxy-5-methoxybenzoic acid to 2,5-DHB reduced the intensity of matrix background ions, and resulted in more intense and narrower molecular ion signals in the spectrum. This effect was postulated to be due to a disorder in the 2,5-DHB, caused by the presence of 2-hydroxy-5-methoxybenzoic acid in the lattice, resulting in reduced lattice energy and enhanced ion desorption. Another approach explored is the use of a laser dye in combination with 2,5-DHB to increase the efficiency of energy absorbance [94]. This technique was similar to initial experiments in MALDI development [9, 95], which involved the use of an ultra fine metal powder to promote energy transfer. These approaches, however, did not concentrate on the improvement of the MALDI sample distribution, and did not show a significant change of sample morphology. It was observed that 2,5-DHB crystals do not uniformly distribute on the sample target, nor does the analyte distribute uniformly among the crystals [56]. The MALDI MS spectra from inhomogeneous samples showed dramatic variations in terms of resolution, intensity, and signal profiles as the laser spot was scanned over the probe tip. Therefore, one has less confidence evaluating MALDI performance when forced to compare MALDI mass spectra taken from different spots or samples. The present work emphasizes homogenization of MALDI samples by introducing additives into the matrix crystal. The best results were obtained from the co-matrices of 2,5-DHB:2,3-DHB and 2,5-DHB:3ATFB.

The crystal structure of pure 2,5-DHB consists of pairs of molecules linked by hydrogen bonds between the carboxylic groups, as shown in Figure 5.24. The dimers are stacked along the *b* axis by van der Waals bonds to form a chain. In addition, the chains are held with respect to one another by the hydrogen bonding of the phenolic hydroxylic groups in position 5 and by van der Waals interactions.

Formation of a column by parallel stacking of hydrogen bonded dimers is frequently observed in the crystal structures of benzoic acid derivatives. Therefore, it is assumed that as 2,5-DHB mixed with its isomers at high fractions of 2,5-DHB there were two types of dimers formed in sample crystals, namely, mono-component dimer (m-dimer), which consists of two 2,5-DHB molecules, and dual-component dimer (d-dimer), which consists of one 2,5-DHB molecule and one molecule of its isomer. The hydrogen bonds and van der Waals interactions among the dimers, which play an important role in determining the structure, were thus modified in direction and amplitude. These changes certainly exert an influence on binding energy and result in different crystal morphology as was demonstrated. It is expected that further investigation of the structures of such systems could be fruitful in the future.

Homogeneity of a mixture sample was also related to molar ratio of co-matrix in the sample. As the molar ratio of 2,3-DHB:2,5-DHB increased from 1:5 to 5:5, the appearance of the co-matrix film gradually changed from the 2,5-DHB type distribution to the morphology shown in Figure 5.9. The same trend was observed for the mixture of 3ATFB:2,5-DHB in Figure 5.22. This transition could be attributed to dominance of the m-dimers in the crystal structure at lower molar ratios, and the d-dimers at higher molar ratios.

The differences in the MALDI responses of 2,5-DHB mixtures with its isomers could also reflect in part the different ultraviolet absorption spectra of dihydroxybenzoic acids. The UV absorption spectra of some substituted benzoic acids have

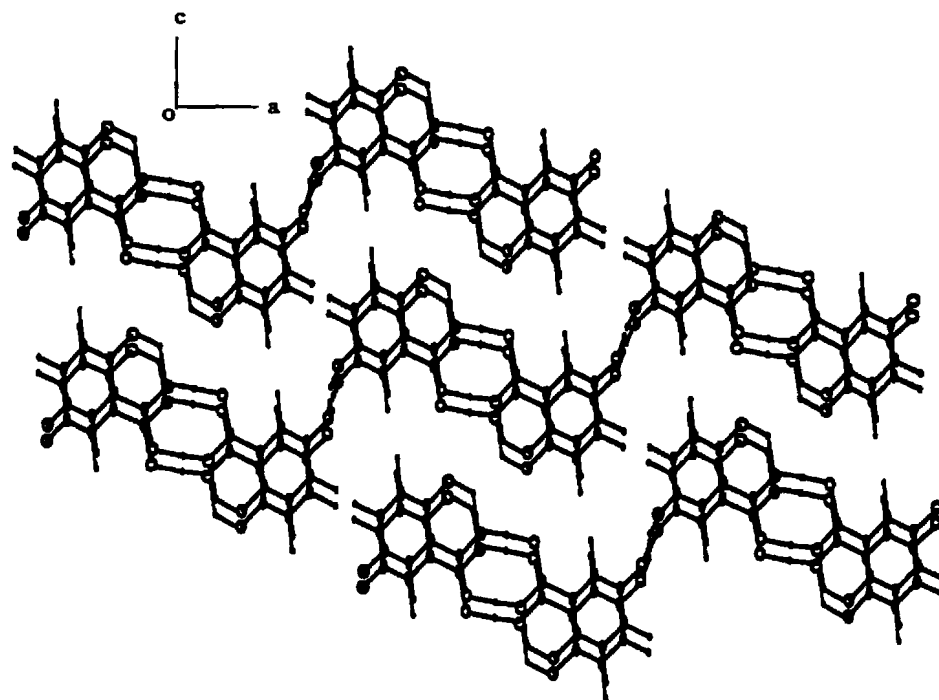


Figure 5.24: Projection of 2,5-DHB crystal structure, showing dimers stacked along b axis.

been studied in water or aqueous dioxan over a pH range of about 1-8 by Kamath *et al.* [96]. The relevant properties of absorption spectra of dihydroxybenzoic acids, selected from their study, are listed in Table 5.3. However, it was observed that in the MALDI film the absorbance maximum is shifted ≈ 20 nm to higher wavelengths, and a long absorption tail extends towards higher wavelengths [38]. Taking the above facts into consideration, it is likely that 2,3-DHB affects laser energy absorption more than other isomers when mixed with 2,5-DHB.

The results presented in this chapter have shown that the use of additives to matrices may provide a general and simpler means of improving the current matrix systems. This method is of considerable significance to quantitative study of MALDI application. The promising results of this investigation have recently stimulated much interest among users of MALDI [97]. In the future, new matrix molecules with new additives will broaden the field of applications of this still relatively new technique.

Table 5.3: Properties of UV absorption of dihydroxybenzoic acids

Matrix	λ_{max} (nm)	Solution ϵ ($mol^{-1}cm^{-1}$)
2,3-DHB	317	3162
2,4-DHB	295	5248
2,5-DHB	330	4073
2,6-DHB	316	3630
3,4-DHB	293	5623
3,5-DHB	306	2951

Chapter 6

Summary

In this thesis, the effects of sample preparation on matrix-assisted laser desorption/ionization of proteins have been described. A time of flight mass spectrometer was used to identify the masses of the generated ions.

In chapter 3, a new method of preparing the sample probes for MALDI experiments was described. The dried-droplet method of preparing matrix-embedded protein samples for MALDI-MS is a simple one-step process, but high concentrations of involatile solvents such as glycerol, urea, DMSO, and other protein stabilizers can reduce or eliminate the intensity of protein ion signals. In the new approach, a tightly adhered crystal nucleation layer was formed on the surface of the sample holder, resulting in a more uniform crystal nucleation surface for the matrix/analyte solution as it dried. The resulting film did not wash off in room-temperature water. The experiments presented in this chapter show that additions of glycerol or salt to the matrix-protein solution do not appear to affect laser ionization efficiency for myoglobin, if this improved methodology is used. The films are more uniform than dried-droplet deposits with respect to ion production, and this represents a major advantage. The new method has been recognized as a major development of MALDI sample preparation. The important features of this method have also led to the substantial use of the MALDI technique in biomolecule mass analysis. The paper describing this method has been cited 34 times till the end of 1996 since it was

published in 1994.

In chapter 4, the energy deposition and redistribution processes for MALDI were described phenomenologically. The matrix plays an essential role in this description. The influence of matrix concentrations on both the analyte ion yield and on the mass resolution of the molecular ion signals was investigated. MALDI time-of-flight mass spectra of protein mixed with different concentrations of matrix solution, for each of 2,5-DHB, 4HCCA and sinapic acid, were presented. The results show that the intensities of the analyte ion peaks increase gradually with an increase in concentration of matrix solution at fixed laser fluence, and then decrease slightly as the concentration of matrix solution continues to increase. The analysis of the spectra also shows that the molecular ion peaks are broadened, that is the mass resolution decreases, as the matrix concentration increases. The results of the investigations are important because they provide more evidence to support the model proposed to describe the laser ablation of the matrix and energy redistribution. Another significance of the results is to show us that the ratio of matrix/analyte in MALDI samples is a critical parameter in MALDI performance.

The characteristics of the crystalline deposit formed by 2,5-DHB create a problem for MALDI. It is somewhat difficult to find a mixture of matrix and analyte which is homogeneous in terms of shot-to-shot, point-to-point and sample-to-sample reproducibility. This problem has limited the use of 2,5-DHB in MALDI quantitative analysis. In chapter 5, a strategy to alleviate this problem was presented. The technique of controlling crystal growth by additives was discussed first. Controlled amounts of additives present in solution during crystallization may have a pronounced effect on the crystallization process, in particular on the morphology of the deposited crystals. Experiments on 2,5-DHB mixed with its isomers and other benzoic acid derivatives were described, and the performance of the resulting crystals for MALDI

MS was evaluated. The results show that mixtures of 2,5-DHB with 2,3-DHB or 3-amino-2,5,6-trifluorobenzoic acid have a more homogeneous crystal morphology, and consequently improved MALDI MS performance. While 2,5-DHB is still used as a favorable matrix, the results presented in this chapter show a significant development of using 2,5-DHB for quantitative analysis by MALDI. The presentation of this work on 1997 ASMS conference has triggered much interest among practitioners of MALDI. More than 200 requests for a reprint of the presentation have been sent to author. In the future, this relatively new technique could be applied to new matrix molecules with new additives.

While this thesis was being finally revised, two recently published papers were brought to the author's attention. Knochenmuss et al. [98] presented an investigation of matrix ion suppression effects in MALDI. The matrix ion suppression effect is a remarkable phenomenon noted in the literature [99, 100, 101]: at appropriate matrix:analyte mixing ratios (10:1 to about 2000:1) small to moderate sized analyte ions (1000 - 20000 u) can fully suppress positively charged matrix ions in MALDI mass spectra. From the results of their investigation they proposed a general model for prompt MALDI ion creation processes. In this model excited, but not ionized, matrix molecules are the common precursors for all subsequent ion products. The simultaneous neighboring presence of two such excitations is required for ionization. The proposed model further supports the discussion of matrix concentration effects on analyte ion formation presented in Section 4.3 of this thesis.

In their report describing a new liquid matrix for MALDI, Kolli et al. [102] presented a binary mixture of α -cyano-4-hydroxycinnamic acid and 3-amino-quinoline. The major benefit of this matrix is that it is a viscous liquid with a self-healing surface. These properties provide very long-lasting and reasonably constant ion currents from only a few pmol of analyte without refocusing the laser/mass spectrometer.

This behavior allows MALDI spectra to be obtained on magnetic sector instruments with point detectors. The current results obtained using new matrices will stimulate practitioners of MALDI to further efforts to develop new matrices. Those new matrices would be expected to have specific functions for analyzing different samples and for working on different kind of mass spectrometers.

Bibliography

- [1] D. F. Thorgerson, R. P. Skowronski, and R. D. Macfarlane. *Biochem. Biophys. Res. Commun.*, **60**:616, 1974.
- [2] M. Barber, R. S. Bordoli, R. S. Sedgwick, and A. N. Tyler. *J. Chem. Soc. Chem. Commun.*, page 325, 1981.
- [3] W. T. Moore and R. M. Caprioli. Continuous flow fast atom bombardment mass spectrometry in analytical biochemistry. In M. L. Gross, editor, *Mass Spectrometry in the Biological Sciences: A Tutorial*, page 229. Kluwer Academic Publishers, 1990.
- [4] P. Roepstorff and W. J. Richter. *Int. J. Mass Spectrom. Ion Processes*, **118119**:789, 1992.
- [5] M. Barber and B. N. Green. *Rapid Commun. Mass Spectrom.*, **1**:80, 1987.
- [6] P. C. Andrews and J. E. Dixon. *Methods Enzymol.*, **168**:72, 1989.
- [7] E. Bernal G., L.P. Levine, and J. F. Ready. *Rev. Sci. Instr.*, **37**:938, 1966.
- [8] M. A. Posthumus, P. G. Kistemaker, H. L. C. Meuzelaar, and M. C. Ten Noever de Brauw. *Anal. Chem.*, **50**:985, 1978.
- [9] K. Tanaka, H. Waki, Y. Ldo, S. Akita, Y. Yoshida, and T. Yoshida. *Rapid Commun. Mass Spectrom.*, **2**:151, 1988.
- [10] M. Karas and F. Hillenkamp. *Anal. Chem.*, **60**:2299, 1988.

- [11] R. C. Beavis and B. T. Chait. *Rapid Commun. Mass Spectrom.*, **3**:432, 1989.
- [12] R. C. Beavis and B. T. Chait. *Rapid Commun. Mass Spectrom.*, **3**:233, 1989.
- [13] R. C. Beavis and B. T. Chait. *Anal. Chem.*, **62**:1836, 1990.
- [14] R. C. Beavis and B. T. Chait. *Proc. Natl. Acad. Sci., USA*, **87**:6873, 1990.
- [15] H. D. Kratzin, J. Wiltfang, M. Karas, V. Neuhoff, and N. Hischmann. *Anal. Biochem.*, **183**:1, 1989.
- [16] F. H. Strobel, T. Solouki, M. A. White, and D. H. Russell. *J. Am. Soc. Mass Spectrom.*, **2**:91, 1991.
- [17] M. Karas, U. Bahr, A. Ingendoh, and F. Hillenkamp. *Angew. Chem. Int. Ed. Engl.*, **28**:760, 1989.
- [18] B. Stahl, M. Steup, M. Karas, and F. Hillenkamp. *Anal. Chem.*, **63**:1463, 1991.
- [19] G. Parr, M. Fitzgerald, and L. Smith. *Rapid Commun. Mass Spectrom.*, **6**:369, 1992.
- [20] K. Tang, S. Allman, and C. Chen. *Rapid Commun. Mass Spectrom.*, **6**:365, 1992.
- [21] P. O. Danis, D. E. Karr, F. Mayer, A. Holle, and C. H. Watson. *Org. Mass Spectrom.*, **27**:843, 1992.
- [22] J. A. Castoro, C. Köster, and C. Wilkins. *Rapid Commun. Mass Spectrom.*, **6**:239, 1992.
- [23] K. Strupat, M. Karas, and F. Hillenkamp. *Int. J. Mass Spectrom. Ion Processes*, **111**:89, 1991.

- [24] R. Caprioli and B. Whaley. In J. J. Willafranca, editor, *Techniques in Protein Chemistry II*, page 479. Academic Press, San Diego, CA, 1991.
- [25] M. Schar, K. O. Bornsen, and E. Gassman. *Rapid Commun. Mass Spectrom.*, 5:319, 1991.
- [26] P. Juhasz, I. A. Papayannopoulos, Ch. Zeng, V. Papov, and K. Biemann. In *Proceedings of the 40th ASMS Conference on Mass Spectrometry and Allied Topic*, page 1913, Washington, DC, 1992. American Society for Mass Spectrometry.
- [27] P. C. Andrews, M. H. Allen, M. L. Vestal, and R. W. Nelson. In R. H. Angeletti, editor, *Techniques in Protein Chemistry III*, page 515. Academic Press Inc., San Diego, CA, 1992.
- [28] B. T. Chait, R. Wang, R. C. Beavis, and S. B. H. Kent. *Science*, 262:89, 1993.
- [29] A. I. Gusev, W. R. Wilkinson, A. Proctor, and D. M. Hercules. *Appl. Spectrosc.*, 47:8, 1993.
- [30] M. W. Duncan, G. Matanovic, and A. Cerpa-Poljak. *Rapid Commun. Mass Spectrom.*, 7:1090, 1993.
- [31] R. W. Nelson and M. A. McLean. *Anal. Chem.*, 66:1408, 1994.
- [32] A. I. Gusev, W. R. Wilkinson, A. Proctor, and D. M. Hercules. *Anal. Chem.*, 67:1034, 1995.
- [33] H. Egge, J. Peter-Katalinic, M. Karas, and B. Stahl. *Pure Appl. Chem.*, 63:491, 1991.

- [34] R. C. Beavis, T. Chaudhary, and B. T. Chait. *Org. Mass Spectrom.*, **27**:156, 1992.
- [35] S. Zhao, K. V. Somayajula, A. G. Sharkey, D. Hercules, F. Hillenkamp, M. Karas, and A. Ingendoh. *Anal. Chem.*, **63**:450, 1991.
- [36] W. Ens, Y. Mao, F. Mayer, and K. G. Standing. *Rapid Commun. Mass Spectrom.*, **5**:117, 1991.
- [37] B. Spengler, D. Kirsch, and R. Kaufmann. *Rapid Commun. Mass Spectrom.*, **5**:198, 1991.
- [38] Theodore W. Heise and E. S. Yeung. *Anal. Chimica Acta*, **299**:377, 1995.
- [39] F. Hillenkamp, M. Karas, R. C. Beavis, and B. T. Chait. *Anal. Chem.*, **63**:1193A, 1991.
- [40] M Salehpour, I. Perera, J. Kyellberg, A. Hedin, M. A. Islamian, P. Håkansson, and B. U. R. Sundqvist. *Rapid Commun. Mass Spectrom.*, **3**:259, 1989.
- [41] R. C. Beavis and B. T. Chait. *Chem. Phys. Lett.*, **181**:479, 1991.
- [42] V. Bokelmann, B. Spengler, and R. Kaufmann. *Eur. Mass Spectrom.*, **1**:81, 1995.
- [43] S. R. Weinberger, K. O. Boernsen, J. W. Finchy, V. Robertson, and B. D. Musselman. In *Proceedings of the 41st ASMS Conference on Mass Spectrometry and Allied Topics*, page 775a, San Francisco, 1993. American Society for Mass Spectrometry.
- [44] O. Vorm, P. Roepstorff, and M. Mann. *Anal. Chem.*, **66**:3281, 1994.

- [45] S. L. Cohen and B. T. Chait. *Anal. Chem.*, **68**:31, 1996.
- [46] Bo. U. R. Sundqvist. *Int. J. Mass Spectrom. Ion Processes*, **118/119**:265, 1992.
- [47] A. Vertes and R. Gijbels. In A. Vertes, R. Gijbels, and F. Adams, editors, *Laser Ionization Mass Analysis*, chapter 3, page 127. John Wiley & Sons, New York, 1993.
- [48] A. Vertes, R. Gijbels, and R. D. Levine. *Rapid Commun. Mass Spectrom.*, **4**:228, 1990.
- [49] A. Vertes, G. Irinyi, and R. Gijbels. *Anal. Chem.*, **65**:2389, 1993.
- [50] A. Vertes and R. Gijbels. *Scanning Microsc.*, **5**:317, 1991.
- [51] A. Vertes. In D. G. Howitt, editor, *Microbeam Analysis*, page 25. San Francisco Press, San Francisco, 1991.
- [52] R. E. Johnson and B. U. R. Sundqvist. *Rapid Commun. Mass Spectrom.*, **5**:574, 1991.
- [53] R. E. Johnson, S. Banerjee, A. Hedin, D. Fenyő, and B. U. R. Sundqvist. Heavy-ion and laser-pulse induced ejection of large organic molecules. In K. G. Standing and W. Ens, editors, *Methods and Mechanisms for Producing Ions from Large Molecules*, page 89. Plenum Press, New York, 1991.
- [54] F. Xiang and R. C. Beavis. *Org. Mass Spectrom*, **28**:1424, 1993.
- [55] R. C. Beavis and J. N. Bridson. *J. Phys. D.:Appl.Phys.*, **26**:442, 1993.
- [56] L. Li, R. Whittal, and Y. Dai. In *Proceedings of the 43rd ASMS Conference on Mass Spectrometry and Allied Topic*, page 1226, Atlanta, Georgia, 1995. American Society for Mass Spectrometry.

- [57] F. Xiang and R. C. Beavis. *Rapid Commun. Mass Spectrom.*, **8**:199, 1994.
- [58] R. C. Beavis. *Chapter 7 in Laser Desorption and Ablation, in the series: Methods in Experimental Physics*,. to be published, Editors: J. C. Miller and R. F. Haglund, Jr.
- [59] T. P. Melia and W. P. Moffitt. *Ind. Engng Chem. Fundam.*, **3**:313, 1964.
- [60] N. W. Cayey and J. Estrin. *Ind. Engng Chem. Fundam.*, **6**:13, 1967.
- [61] M. Lahav and L. Leiserowitz. *J. Phys. D.: Appl. Phys.*, **26**:B22, 1993.
- [62] J. K. Whitesell, R. E. Davis, M. S. Wong, and N. L. Chang. *J. Phys. D.: Appl. Phys.*, **26**:B32, 1993.
- [63] R. C. Beavis and B. T. Chait. In W. Ens and K. G. Standing, editors, *Methods and Mechanisms for Producing Ions from Large Molecules*, page 227. Plenum Press, New York, 1991.
- [64] A. Vertes and R. D. Levine. *Chem. Phys. Lett.*, **171**:284, 1990.
- [65] M. von Allmen and A. Blatter. *Laser-Beam Interactions with Materials: Physical Principles and Applications*. 2nd edition, Springer-Verlag, Berlin, 1995.
- [66] A. N. Shibanov. In V. S. Letokhov, editor, *Laser Analytical Spectrochemistry*, page 353. Adam Hilger, Bristol, 1986.
- [67] H. S. Carslaw and J. C. Jaeger. *Conduction of Heat in Solid*, 2nd. ed. Oxford Univ. Press, Oxford, 1959.
- [68] D. Burgess, Jr., R. Viswanathan, I. Hussla, P. C. Stair, and E. Weitz. *J. Chem. Phys.*, **79**:5200, 1983.

- [69] R. N. Zare and R. D. Levine. *Chem. Phys. Letters*, **136**:593, 1987.
- [70] D. Shannon Cornett, M. A. Duncan, and I. Jonathan Amster. *Anal. Chem.*, **65**:2608, 1993.
- [71] I. K. Perera, S. Kantartzoglou, and P. E. Dyer. *Int. J. Mass Spectrom. Ion Processes*, **137**:151, 1994.
- [72] Fan Xiang and R. C. Beavis. In *Proceedings of the 79th Canadian Society for Chemistry Conference and Exhibition*, St. John's, Newfoundland, Canada, 1996.
- [73] M. E. Gimon, L. M. Preston, T. Solouki, M. A. White, and D. H. Russell. *Org. Mass Spectrom.*, **27**:827, 1992.
- [74] M. A. White, F. H. Strobel, and D. H. Russell. In *Proceedings of the 39th ASMS Conference on Mass Spectrometry and Allied Topics*, page 334, Nashville, TN, 1991. American Society for Mass Spectrometry.
- [75] G. Bolbach, K. Riahi, M. Spiro, A. Brunot, F. Breton, and J. C. Blais. *Analisis*, **21**:383, 1993.
- [76] P. Hartman and W. G. Perdok. *Acta Crystallogr*, **8**:49, 1955.
- [77] P. Hartman and P. Bennema. *J. Cryst. Growth*, **49**:145, 1980.
- [78] P. Hartman. *Crystal Growth: An Introduction*, page 367. North Holland: Amsterdam, 1973.
- [79] Z. Berkovitch-Yellin. *J. Am. Chem. Soc.*, **107**:8239, 1985.
- [80] R. Docherty and K. J. Roberts. *J. Cryst. Growth*, **88**:159, 1988.

- [81] P. Hartman. *J. Cryst. Growth*, **49**:157, 1980.
- [82] R. Hamer, D. Tassoni, J. P. Riquet, and F. Duran. *Ibid*, **51**:493, 1981.
- [83] D. Tassoni, J. P. Riquet, and F. Durand. *Acta Crystallogr., Sect. A*, **36**:420, 1980.
- [84] G. Clydesdale, R. Docherty, and K. J. Roberts. *Comp. Phys. Comm.*, **64**:188, 1991.
- [85] R. Docherty and K. J. Roberts. *Modelling the Morphology of Molecular Crystals*. PhD thesis, University of Strathclyde, 1989.
- [86] Z. Berkovitch-Yellin, L. Addadi, M. Idelson, M. Lahav, and L. Leiserowitz. *Angew. Chem. Suppl.*, page 1336, 1982.
- [87] K. Strupat, M. Karas, and F. Hillenkamp. In *Proceeding of the 12nd International Mass Spectrometry Conference*, page 26, Amsterdam, 1991.
- [88] G. Giacomello, A. M. Liquori, and A. Ripamonti. *Nature*, **177**:944, 1956.
- [89] M. Haisa, S. Kashino, S. I. Hanada, K. Tanaka, S. Okazaki, and M. Shibagaki. *Acta Cryst.*, **B38**:1480, 1982.
- [90] J. D. H. Donnay and H. M. Ondik. *Crystal Data Determinative Tables*, volume I. The U. S. Department of Commerce, National Bureau of Standards, and Joint Committee on Powder Diffraction Standards, third edition edition, 1972.
- [91] C. Koster, J. A. Castoro, and C. L. Wilkins. *J. Am. Chem. Soc.*, **114**:7572, 1992.

- [92] M. Karas, H. Ehring, E. Nordhoff, B. Stahl, K. Strupat, and F. Hillenkamp. *Org. Mass Spectrom.*, **28**:1476, 1993.
- [93] A. Tsarbopoulos, M. Karas, K. Strupat, B. N. Pramanik, T. L. Nagabhushan, and F. Hillenkamp. *Anal. Chem.*, **66**:2062, 1994.
- [94] D. Shannon Cornett, M. A. Duncan, and I. Jonathan Amster. *Org. Mass Spectrom.*, **27**:831, 1992.
- [95] K. Tanaka, Y. Ldo, S. Akita, Y. Yoshida, and T. Yoshida. In *Proceeding of the 2nd Japan-China Symp. on Mass Spec.*, page 185, 1987.
- [96] B. V. Kamath, J. D. Mehta, and S. L. Bafna. *J. appl. Chem. Biotechnol.*, **25**:743, 1975.
- [97] Fan Xiang and R. C. Beavis. In *Proceedings of the 45th ASMS Conference on Mass Spectrometry and Allied Topic*, Palm Springs, California, 1997. American Society for Mass Spectrometry.
- [98] R. Knochenmuss, F. Dubois, M. J. Dale, and R. Zenobi. *Rapid Commun. Mass Spectrom.*, **10**:871, 1996.
- [99] T. W. D. Chan, A. W. Colburn, and P. J. Derrick. *Org. Mass Spectrom*, **26**:342, 1991.
- [100] T. W. D. Chan, A. W. Colburn, P. J. Derrick, D. J. Gardiner, and M. Bowden. *Org. Mass Spectrom*, **27**:188, 1992.
- [101] P. Juhasz, B. H. Wang, and K. Biemann. In *Proceedings of the 40th ASMS Conference on Mass Spectrometry and Allied Topic*, page 372, Wachington, DC, 1992. American Society for Mass Spectrometry.

[102] V. S. K. Kolli and R. Orlando. *Rapid Commun. Mass Spectrom.*, **10:923**, 1996.

[103] J. D. Jackson. *Classical Electrodynamics*. John Wiley & Sons, Inc., New York, 1962.

Appendix

The simplest form of light is a monochromatic, linearly polarized plane wave. This model provides a good approximation to a real laser beam. The dynamic properties of the reflection and refraction of light depend entirely on the specific nature of electromagnetic fields and their boundary conditions.

The notations of the plane wave and the boundary conditions used in this calculation are similar to those used in the text book "Classical Electrodynamics" written by J. D. Jackson [103]. In applying the boundary conditions it is necessary to consider two separate situations, one in which the incident plane wave is linearly polarized with its polarization vector perpendicular to the plane of incidence, and the other in which the polarization vector is parallel to the plane of incidence. A single microscope cover-slip used in the construction of the attenuator has two surfaces, with thickness $d = 0.1175$ mm as shown in Figure 2.5.

First consider the electric field parallel to the plane of incidence. At surface I, $z = 0$, the boundary condition (I)

$$(\vec{E}_0 + \vec{E}_1) \times \vec{n} = (\vec{E}_2 + \vec{E}_3) \times \vec{n} \quad (6.1)$$

gives

$$E_0 \cos i - E_1 \cos i = E_2 \cos r - E_3 \cos r ; \quad (6.2)$$

and the boundary condition (II)

$$(\vec{B}_0 + \vec{B}_1) \times \vec{n} = (\vec{B}_2 + \vec{B}_3) \times \vec{n} \quad (6.3)$$

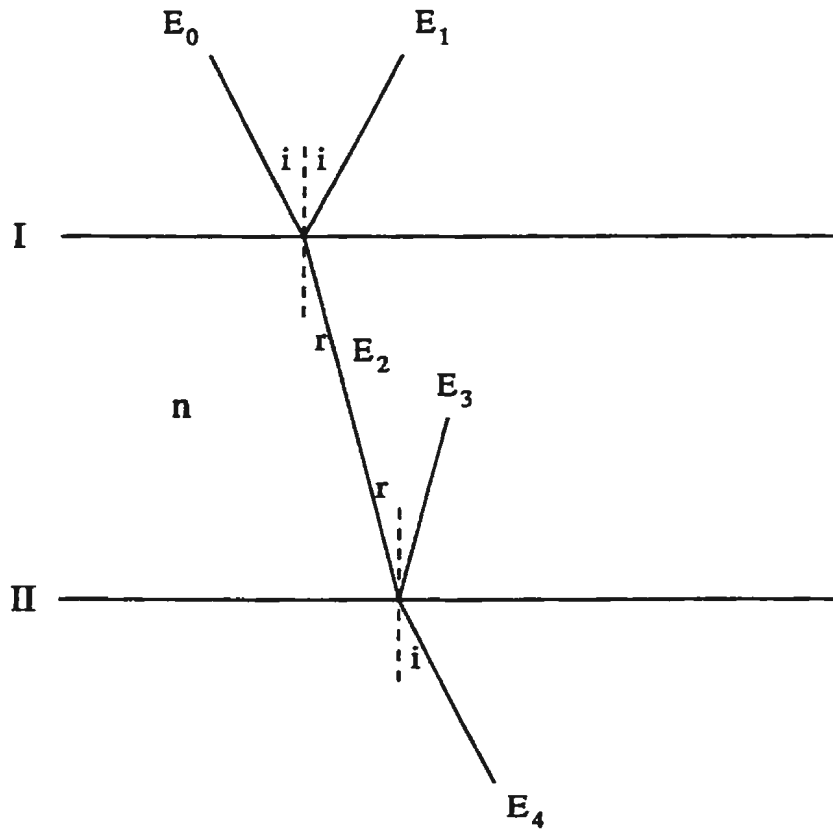


Figure 6.1: Transmission of light through a microscope cover-slip.

$$B_0 + B_1 = B_2 + B_3 \tag{6.4}$$

gives

$$E_0 + E_1 = n(E_2 + E_3) \tag{6.5}$$

At surface II, $z = d$, the boundary condition (I) gives

$$E_2 \cos r e^{ik'd} - E_3 \cos r e^{-ik'd} = E_4 \cos i e^{ikd} \tag{6.6}$$

where $k = \frac{\omega}{c}$, $k' = n\frac{\omega}{c} = \frac{2\pi n}{\lambda}$, and n is the index of the refraction. The boundary condition (II)

gives

$$n(E_2e^{ik'd} + E_3e^{-ik'd}) = E_4e^{ikd} \quad (6.7)$$

It is useful to define a parameter m where

$$m = \frac{\cos i}{\cos r} = \sqrt{\frac{1 - \sin^2 i}{1 - \sin^2 r}} = \sqrt{\frac{1 - \sin^2 i}{1 - \frac{\sin^2 i}{n^2}}} \quad (6.8)$$

From Equations (2.6), (2.9), (2.10), (2.11) and (2.12) one obtains

$$\frac{E_4}{E_0} = \frac{4nm}{(1 + nm)^2 e^{i(k-k')d} - (1 - nm)^2 e^{i(k+k')d}} \quad (6.9)$$

Therefore, the transmittance T of the single cover-slip of thickness d is written as:

$$T = \left| \frac{E_4}{E_0} \right|^2 = \frac{8n^2 m^2}{1 + n^4 m^4 + 6n^2 m^2 - (1 - n^2 m^2)^2 \cos(2dk')} \quad (6.10)$$

If the electric field is perpendicular to the plane of incidence, using the boundary conditions (I) and (II), one can obtain, at surface I ($z = 0$),

$$E_0 + E_1 = E_2 + E_3 \quad (6.11)$$

and

$$(E_0 - E_1) \cos i = n(E_2 - E_3) \cos r \quad (6.12)$$

at surface II ($z = d$),

$$E_2e^{ik'd} + E_3e^{-ik'd} = E_4e^{ikd} \quad (6.13)$$

and

$$n(E_2 - E_3)e^{-ik'd} \cos r = E_4 e^{ikd} \cos i \quad . \quad (6.14)$$

From the equation (2.15) - (2.18) one obtains

$$\frac{E_4}{E_0} = \frac{4nm}{(n+m)^2 e^{i(k-k')d} - (n-m)^2 e^{i(k+k')d}} \quad . \quad (6.15)$$

Therefore, the transmittance T of the single cover-slip of thickness d is written as:

$$T = \left| \frac{E_4}{E_0} \right|^2 = \frac{8n^2 m^2}{n^4 + m^4 + 6n^2 m^2 - (n^2 - m^2)^2 \cos(2dk')} \quad . \quad (6.16)$$

For an attenuator consisting of four slips, the transmittance is

$$T_4 = T^4 \quad (6.17)$$

The plots of transmission versus incident angle are shown in the following Figures 6.2 and 6.3.

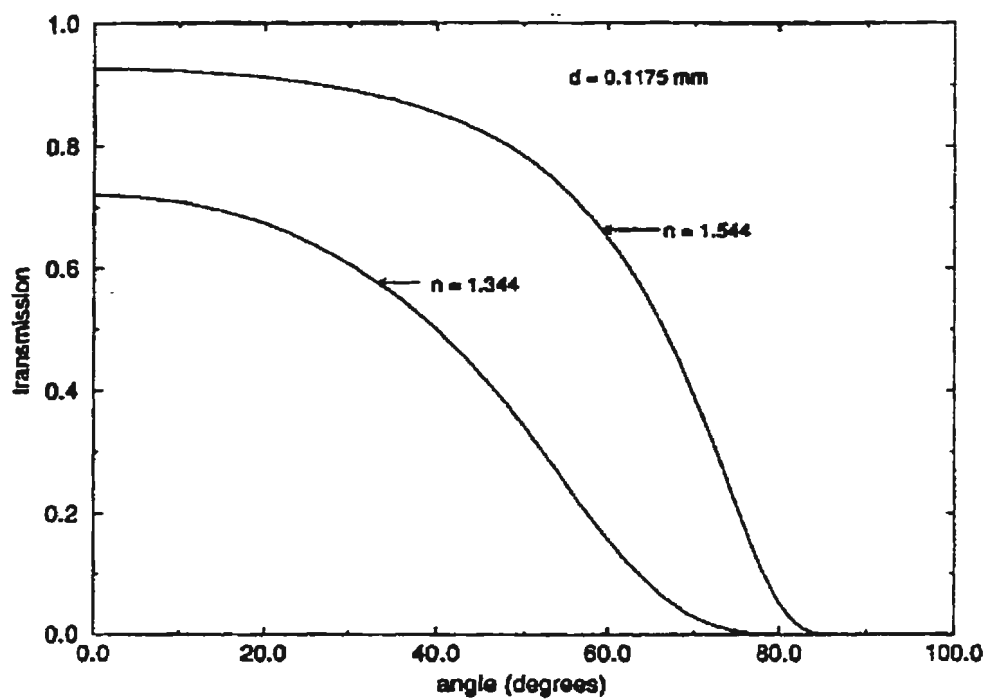


Figure 6.2: Plot of transmittance versus incident angle for TE wave.

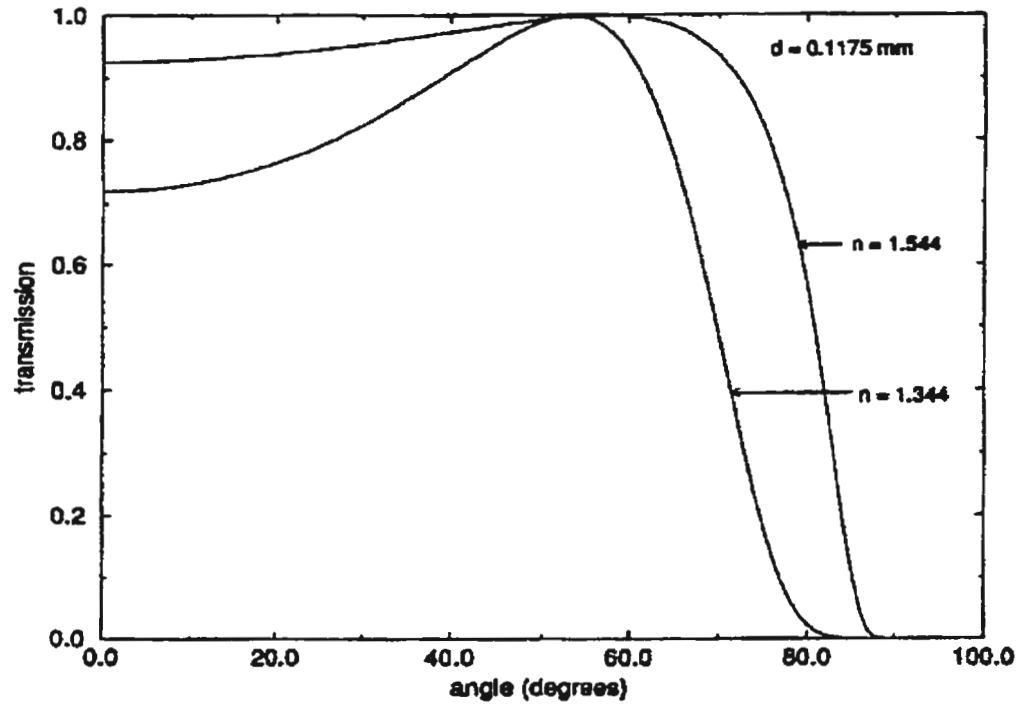
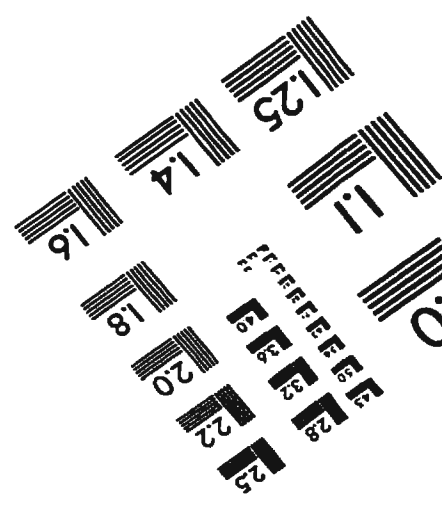
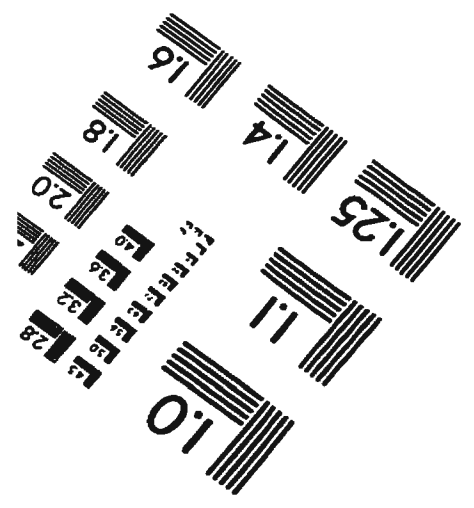
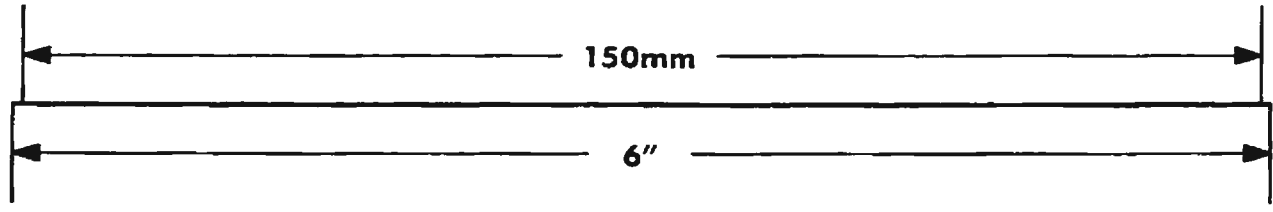
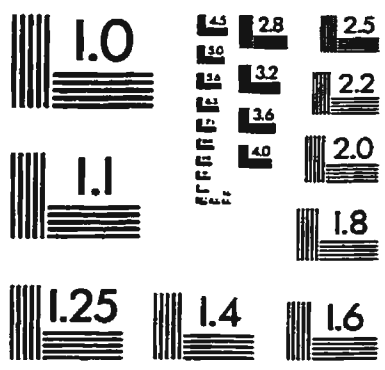
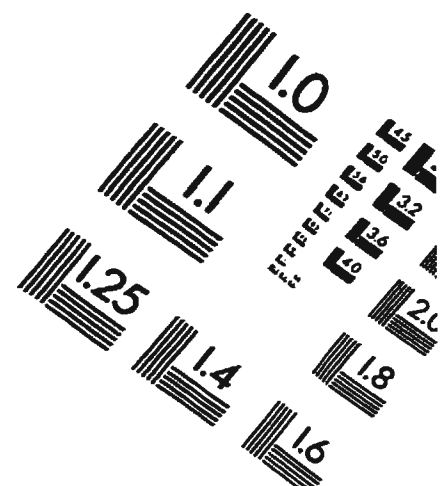
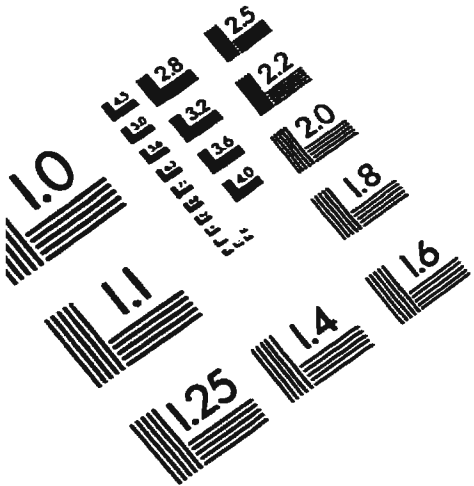


Figure 6.3: Plot of transmittance versus incident angle for TM wave.

IMAGE EVALUATION TEST TARGET (QA-3)



APPLIED IMAGE . Inc
1653 East Main Street
Rochester, NY 14609 USA
Phone: 716/482-0300
Fax: 716/288-5989

© 1993, Applied Image, Inc., All Rights Reserved



